UNIVERSITY OF CALIFORNIA SAN DIEGO

Canonical BAF complex activity licenses effector and memory CD8+ T cell fates

A Dissertation submitted in partial satisfaction of the requirements
for the degree Doctor of Philosophy

in

Biomedical Sciences

by

Bryan McDonald

Committee in charge:

Professor Susan Kaech, Chair
Professor John Chang, Co-Chair
Professor Ananda Goldrath
Professor Bing Ren

2023

The Dissertation of Bryan McDonald is approved, and it is acceptable in quality and form for publication on microfilm and electronically.

University of California San Diego

2023

DEDICATION

I dedicate this thesis to the many mentors that have guided me scientifically and professionally throughout my career.

TABLE OF CONTENTS

LIST OF FIGURES

LIST OF ABBREVIATIONS

TEM	Effector memory T cell
TCM	Central memory T cell
TRM	Tissue-resident memory T cell
TE	Terminal effector
MP	Memory precursor
BAF	BRG1/BRM associated factor
cBAF	Canonical BAF
PBAF	Polybromo BAF
ncBAF	Non-canonical BAF

ACKNOWLEDGEMENTS

I would like to thank Dr. Susan Kaech for her support as my advisor and for providing an amazing environment to hone my skills as an immunologist and grow as a scientist. I would also like to thank the wonderful past and present folks of the Kaech lab for driving me to become the best scientist I could be and for making the Salk feel like a home away from home.

Chapter 1 contains unpublished material. McDonald B, Kaech SM. The dissertation author was the primary investigator.

Chapter 2 contains material submitted for publication at *Yale Journal of Biology and Medicine* in July 2023. McDonald B, Chick BY, Hargreaves DC, Kaech SM. The dissertation author was the primary investigator and author of this paper.

Chapter 3, in full, is a reprint of the material as it appears in *Immunity* 2023. McDonald B, Chick BY, Ahmed NS, Burns M, Ma S, Casillas E, Chen D, Mann TH, O'Connor C, Hah N, Hargreaves DC, Kaech SM. The dissertation author was the primary investigator and author of this paper. We thank the Kaech lab for helpful discussion; N. Claffey, M. Liem at the Salk Flow Cytometry core. This work was supported by NIH grants F31HL158235 and F99CA274688 (B.M.), 5T32GM133351 (B.Y.C), 2T32CA009370 (N.S.A.), R37 AI066232 (to S.M.K.) and AI151123 (to D.C.H.), the Pew-Stewart Scholars for Cancer Research (D.C.H.), and the American Cancer Society Research Scholar Award (D.C.H.) as well as fellowships from the Cancer Research Institute (S.M.), Damon Runyon Cancer Research Foundation (T.M.), and the NOMIS Center (D.C.). Additional support came from the Flow Cytometry Core Facility of the Salk Institute with funding from NIH-NCI CCSG: P30

014195 and Shared Instrumentation Grant S10-OD023689 (Aria Fusion cell sorter) and by the NGS Core Facility of the Salk Institute with funding from NIH-NCI CCSG: P30 014195, the Chapman Foundation and the Helmsley Charitable Trust.

Chapter 4 contains unpublished material. McDonald B, Kaech SM. The dissertation author was the primary investigator and author of this material.

VITA

2014 Bachelor of Science in Human Biology, University of California San Diego

2023 Doctor of Philosophy in Biomedical Sciences, University of California San Diego

PUBLICATIONS

Picarda G, Ghosh R, **McDonald B**, Verma S, Thiault N, El Morabiti R, Griffith TS, Benedict CA. Cytomegalovirus Evades TRAIL-Mediated Innate Lymphoid Cell 1 Defenses. *J Virol*. 2019;93(16):e00617-19. doi:10.1128/JVI.00617-19

Milner JJ, Toma C, He Z, Kurd NS, Nguyen QP, **McDonald B**, Quezada L, Widjaja CE, Witherden DA, Crowl JT, Shaw LA, Yeo GW, Chang JT, Omilusik KD, Goldrath AW. Heterogenous Populations of Tissue-Resident CD8+ T Cells Are Generated in Response to Infection and Malignancy. *Immunity*. 2020;52(5):808-824.e7. doi:10.1016/j.immuni.2020.04.007

Chung HK, **McDonald B**, Kaech SM. The architectural design of CD8+ T cell responses in acute and chronic infection: Parallel structures with divergent fates. *Journal of Experimental Medicine*. 2021;218(4):e20201730. doi:10.1084/jem.20201730

Farsakoglu Y*, **McDonald B***, Kaech SM. Motility Matters: How CD8+ T-Cell Trafficking Influences Effector and Memory Cell Differentiation. *Cold Spring Harb Perspect Biol*. Published online May 17, 2021:a038075. doi:10.1101/cshperspect.a038075

Campbell JR*, **McDonald BR***, Mesko PB, Siemers NO, Singh PB, Selby M, Sproul TW, Korman AJ, Vlach LM, Houser J, Sambanthamoorthy S, Lu K, Hatcher SV, Lohre J, Jain R, Lan RY. Fc-Optimized Anti-CCR8 Antibody Depletes Regulatory T Cells in Human Tumor Models. *Cancer Res*. 2021;81(11):2983-2994. doi:10.1158/0008-5472.CAN-20-3585

Sydney C Morgan, Stefan Aigner, Catelyn Anderson, Pedro Belda-Ferre, Peter De Hoff, Clarisse A Marotz, Shashank Sathe, Mark Zeller, Noorsher Ahmed, Xaver Audhya, Nathan A Baer, Tom Barber, Bethany Barrick, Lakshmi Batachari, Maryann Betty, Steven M Blue, Brent Brainard, Tyler Buckley, Jamie Case, Anelizze Castro-Martinez, Marisol Chacón, Willi Cheung, LaVonnye Chong, Nicole G Coufal, Evelyn S Crescini, Scott DeGrand, David P Dimmock, J Joelle Donofrio-Odmann, Emily R Eisner, Mehrbod Estaki, Lizbeth Franco Vargas, Michele Freddock, Robert M Gallant,

Andrea Galmozzi, Nina J Gao, Sheldon Gilmer, Edyta M Grzelak, Abbas Hakim, Jonathan Hart, Charlotte Hobbs, Greg Humphrey, Nadja Ilkenhans, Marni Jacobs, Christopher A Kahn, Bhavika K Kapadia, Matthew Kim, Sunil Kurian, Alma L Lastrella, Elijah S Lawrence, Kari Lee, Qishan Liang, Hanna Liliom, Valentina Lo Sardo, Robert Logan, Michal Machnicki, Celestine G Magallanes, Clarence K Mah, Denise Malacki, Ryan J Marina, Christopher Marsh, Natasha K Martin, Nathaniel L Matteson, Daniel J Maunder, Kyle McBride, **Bryan McDonald**, Daniel McDonald, Michelle McGraw, Audra R Meadows, Michelle Meyer, Amber L Morey, Jasmine R Mueller, Toan T Ngo, Julie Nguyen, Viet Nguyen, Laura J Nicholson, Alhakam Nouri, Victoria Nudell, Eugenio Nunez, Kyle O'Neill, R Tyler Ostrander, Priyadarshini Pantham, Samuel S Park, David Picone, Ashley Plascencia, Isaraphorn Pratumchai, Michael Quigley, Michelle Franc Ragsac, Andrew C Richardson, Refugio Robles-Sikisaka, Christopher A Ruiz, Justin Ryan, Lisa Sacco, Sharada Saraf, Phoebe Seaver, Leigh Sewall, Elizabeth W Smoot, Kathleen M Sweeney, Chandana Tekkatte, et al. Automated, miniaturized, and scalable screening of healthcare workers, first responders, and students for SARS-CoV-2 in San Diego County. *medRxiv*. Published online January 1, 2021:2021.06.25.21257885. doi:10.1101/2021.06.25.21257885

Xu S, Chaudhary O, Rodríguez-Morales P, Sun X, Chen D, Zappasodi R, Xu Z, Pinto AFM, Williams A, Schulze I, Farsakoglu Y, Varanasi SK, Low JS, Tang W, Wang H, **McDonald B**, Tripple V, Downes M, Evans RM, Abumrad NA, Merghoub T, Wolchok JD, Shokhirev MN, Ho PC, Witztum JL, Emu B, Cui G, Kaech SM. Uptake of oxidized lipids by the scavenger receptor CD36 promotes lipid peroxidation and dysfunction in CD8+ T cells in tumors. *Immunity*. 2021;54(7):1561-1577.e7. doi:10.1016/j.immuni.2021.05.003

Chung HK, Liu C, Casillas E, Chick B, **Mcdonald B**, Wang J, He P, Sun M, Ma S, Yang Q, Chen D, Hoffmann F, Varanasi SK, Tripple V, Hang Y, Cho UH, Ho J, Williams A, Wang Y, Hargreaves D, Kaech SM, Wang W. Multiomics atlas-assisted discovery of transcription factors enables specific cell state programming. Published online January 13, 2023:2023.01.03.522354. doi:10.1101/2023.01.03.5223541.

McDonald B*, Chick BY*, Ahmed NS, Burns M, Ma S, Casillas E, Chen D, Mann TH, O'Connor C, Hah N, Hargreaves DC, Kaech SM. Canonical BAF complex activity shapes the enhancer landscape that licenses CD8+ T cell effector and memory fates. *Immunity*. 2023;56(6):1303-1319.e5. doi:10.1016/j.immuni.2023.05.005

Chen D, Varanasi SK, Hara T, Traina K, Sun M, **McDonald B**, Farsakoglu Y, Clanton J, Xu S, Garcia-Rivera L, Mann TH, Du V, Chung HK, Xu Z, Tripple V, Casillas E, Ma S, O'Connor C, Yang Q, Zheng Y, Hunter T, Lemke G, Kaech SM. CTLA-4 blockade induces CD4+ T cell IFNγ-driven microglial phagocytosis and anti-tumor function in glioblastoma. *Immunity*. Published online August 11, 2023. doi:10.1016/j.immuni.2023.07.015

ABSTRACT OF THE DISSERTATION

Canonical BAF complex activity licenses effector and memory CD8+ T cell fates

by

Bryan McDonald

Doctor of Philosophy in Biomedical Sciences

University of California San Diego, 2023

Professor Susan Kaech, Chair
Professor John Chang, Co-Chair

CD8$^+$ T cells provide host protection against pathogens by differentiating into distinct effector and memory cell subsets. Though many of the key transcription factors that govern effector and memory differentiation have been identified, our understanding of how differentiation is transcriptionally and epigenetically regulated is incomplete. In particular how chromatin is site-specifically remodeled during their differentiation is unclear. Given its critical role in regulating chromatin and enhancer accessibility through its nucleosome remodeling activities, we investigated the role of the canonical BAF (cBAF) chromatin remodeling complex in antiviral CD8$^+$ T cells during infection. ARID1A, a subunit of cBAF, was recruited early after activation and established *de novo* open chromatin regions at enhancers. *Arid1a* deficiency impaired the opening of thousands of activation-induced enhancers, leading to loss of TF binding, dysregulated proliferation, gene expression, and failure to undergo terminal effector differentiation. While *Arid1a* was dispensable for circulating memory cell formation *per se*, functionality and recall capacity was strongly impaired in the absence of *Arid1a*. Furthermore, tissue-resident memory formation was strongly impaired in *Arid1a*-deficient cells. Inducible deletion of *Arid1a* several days after priming *in vivo* also led to strongly diminished terminal effector differentiation, indicating that terminal fate determining events require continuous cBAF activity in order for terminal effector cells to form. *Arid1b, Pbrm1* (PBAF-specific), and *Brd9* (ncBAF-specific) deletions had minimal impact on effector cell differentiation. Thus, ARID1A-containing cBAF governs the enhancer landscape of activated CD8$^+$ T cells that orchestrates TF recruitment and activity and the acquisition of specific effector and memory differentiation states.

INTRODUCTION

$CD8^+$ T cells provide host protection against pathogens and cancer through their ability to recognize and kill infected or malignant cells. A key feature of T cells is the ability to form long-lasting immunological memory after primary infections or vaccination which is critical for protection against recurrent infections. The pool of pathogen-specific effector and memory $CD8^+$ T cells that form in response to acute infection are remarkably diverse with regards to their gene expression programs, epigenetic states, as well as their effector functions and anatomical distribution[1]. In particular, memory T cells can be distinguished by their trafficking patterns—some circulate in the vasculature and secondary lymphoid organs whereas others rather dwell long-term within peripheral tissues[2]. Coordinated differentiation into heterogeneous cellular states is crucial for the effective control of pathogens while preventing overt host pathology. In the context of chronic infection, activated $CD8^+$ T cells establish host-pathogen détente but can also mediate tissue damage at sites of inflammation and in extreme cases leads to host demise[3–5], thus necessitating an intricate balance of effector mechanisms and negative regulatory systems to ensure host survival. Moreover, T cell function and differentiation can be therapeutically manipulated as seen in the revolutionary treatment of immune checkpoint blockade in cancer. Thus, understanding the types of T cells that form, where they traffic and how their functions are regulated or tolerated is critical to host defense to cancer and infection and tissue and organismal health.

After initial activation, T cells undergo a rapid proliferative burst that is accompanied by significant alterations to chromatin structure and transcriptional output, which allows the T cells to differentiate into different types of effector and memory cells.

Activated effector cells exhibit transcriptional and epigenetic heterogeneity, display diverse modes of tissue homing patterns and memory-forming potential, and are distinguished by expression of markers like IL7R (CD127), KLRG1 and CX_3CR_1[6]. Memory precursor (MP) cells express higher levels of CD127 and preferentially give rise to the long-lived circulating memory cell pool[7]. High inflammatory conditions typical of systemic viral infections promote the formation of short-lived terminal effector (TE) cells expressing KLRG1 and CX_3CR_1 that exhibit potent cytotoxic potential but preferentially die following the resolution of infection[8–10]. Early effector cells (EEC) express low levels of CD127, KLRG1, and CX_3CR_1, and can give rise to both TE and MP cells[10–12]. Following the resolution of infection, a diverse array of long-lived memory cells form. Central memory (T_{CM}; $CD127^{hi}CD62L^{+}$) and effector memory (T_{EM}; $CD127^{hi}CD62L^{-}$) cells preferentially inhabit lymphoid organs and can rapidly expand in response to secondary infection. Tissue-resident memory (T_{RM}) cells reside permanently in barrier and non-barrier non-lymphoid tissues like the small intestine, salivary gland, liver, and many others[13]. Significant progress has been made to outline the extrinsic (e.g. cytokines[8,10], hypoxia[14]) and intrinsic (e.g. transcription factors) mechanisms that govern the spectrum of effector and memory $CD8^{+}$ T cell differentiation, but little is known mechanistically how these cell fates are epigenetically imprinted via chromatin modulation. Defining these mechanisms will be imperative for understanding how to better tailor $CD8^{+}$ T cell-based vaccines and for optimizing antitumor responses in the context of immune checkpoint blockade, adoptive cell therapy (ACT), or *in vivo* T cell reprogramming.

Several models exist to explain how diverse effector cell fates arise. Importantly, it is well accepted that one single T cell can give rise to many different types of effector and

memory cell fates, also known as the 'one cell, multiple fates' model[15]. However, the mechanistic basis for this model has not been fully elucidated, especially with respect to *when* during the proliferative response this heterogeneity arises. MP and TE cells can be readily identified within about 7-8 days after acute infection[7,16], though the initial imprinting of each of these specialized effector fates are proposed to occur much earlier in progenitor populations[17,18]. Notably, CD25 expression on early effector precursors potentially identifies cells that are strongly biased toward TE fates[19,20]. Extrinsic factors including IL-12 and IFN-1, which are induced within the first days following certain infections, are essential for promoting TE cell fates[8,10,21] by sustaining CD25 expression and thus allowing for prolonged IL-2 sensing and cell division[22]. Sensing of these extrinsic factors must occur concurrently or shortly after antigen recognition in order for TE cells to form[8], further supporting the notion that effector cell fates are imprinted within the first days of infection.

Spatial positioning of T cells within sites of priming strongly influences effector cell fates[23]. For example, during LCMV infection, CXCR3 (a T-BET-dependent chemokine receptor[24]) positions T cells within CXCL9/10- and LCMV-rich peripheral regions in lymph nodes; *Cxcr3* deficient T cells have reduced exposure to both antigen and extrinsic cues in peripheral regions of lymph nodes, which consequently shifts the balance of effector cells towards a more MP-like phenotype at the expense of KLRG1$^+$ terminal effectors[25,26]. Several lines of evidence support this model: T-bet overexpression induces preferential migration of effector P14 cells to the red pulp in the spleen of LCMV-infected mice; conversely, *Prdm1* KO cells preferentially reside in the T cell zones[27]. Secondly, forced sequestration of T cells in the T cell zone by CCR7 overexpression favors the adoption

of MP fates over TE fates[26,28]. Mechanistically, *Cxcr3* deficient T cells more rapidly downregulate CD25 expression within the first 2 days of infection, and fail to migrate to- and form clusters in DC-abundant, IFN-1 enriched marginal zones[29]. Altogether, these data point to a model where T cell intrinsic mechanisms (TCR-dependent activation induced transcription factors, e.g. T-bet) induce molecules like CXCR3, or suppress others like CCR7, and thus promote trafficking to specific regions of lymphoid organs that are rich in antigen and extrinsic inflammatory cues that help drive terminal differentiation in a subset of effector cells. However, these data imply that cell fates are deterministic, and cannot fully explain how such vast heterogeneity arises within a clonal pool of effector cells.

Asymmetric division of T cells, particularly in the first cell division, is one proposed mechanism to generate heterogeneous progeny via unequal inheritance of certain intracellular components, including c-Myc, mTORC1, proteasome, cBAF, as well as the surface protein CD25[17,30–35]. Given that IL-12/IFN-1 sustains CD25 expression, and that CD25 is needed for terminal effector fates, this asymmetric inheritance helps to explain how one cell can stochastically give rise to multiple cell fates. Asymmetric cell division (ACD) is reported to occur in already-differentiated exhausted LCMV-specific T cells[35–37], suggesting that this mechanism is not restricted to the first division and may underly one aspect of cell fate diversification throughout the lifetime of any one cell's proliferative history. Whether ACD can only occur in cells that have an active immunologic synapse, or whether it can additionally occur during 'autopilot' programmed proliferation[38,39] is not clearly understood. Furthermore, the extent to which asymmetric division occurs in all responding clones, and in what fraction of mitotic events also remains elusive. Altogether,

the field still lacks a comprehensive model to precisely identify at what time an individual T cell and its progeny commit to adopt certain effector cell fates, and the mechanisms involved in generating those cell fate decisions.

Towards this goal, a key focus of the field in recent decades has been the identification of key transcription factors (TFs) and chromatin modifiers that regulate the spectrum of effector and memory differentiation states that form[16,40–61]. While the identities of TFs that promote effector (*Id2*, *Tbx21*, *Batf*), tissue-residency (*Runx3*, *Zfp683*, *Bhlhe40*), and memory $CD8^+$ T cell fates (*Eomes*, *Tcf7*, *Id3*, *Myb*) are well described[1,62–65], the underlying biological processes that regulate the binding and activity of these TFs are largely undefined. Indeed, individual TFs exert overlapping and distinct roles across many cell states (e.g., *Tbx21* and *Eomes* in memory versus exhausted T cells[66]) highlighting the need to better understand how TF binding site accessibility is regulated to control the behavior of TFs and the differentiation states they specify. More specifically, major gaps remain in our knowledge as to how the TFs are targeted to their specific loci in a concentration- or signal-dependent manner to control how T cells adopt one cell fate, but not another. Polycomb Repressive Complex 2 (PRC2) establishes heterochromatin regions that are generally inaccessible to TF binding[67], and preferentially silences naïve and memory cell-associated genes in order for more terminally differentiated effector cells to form, but is dispensable for memory cell formation[18,68]. Deficiencies for *Suv39H1*, an H3K9 methyltransferase, or *Tet2*, which catalyzes 5-methylcytosine to 5-hydroxymethylcytosine, similarly impair TE formation during LCMV infection through repressive epigenetic mechanisms that are distinct from PRC2[69,70]. However, while these studies illuminated key mechanisms by which genes expression

programs become silenced to restrict certain cell fates, we still lack an understanding of how other gene programs become epigenetically activated.

Cis-regulatory elements (e.g. promoters and enhancers) on chromatin act as platforms for *trans*-factors (e.g. TFs) to assemble and regulate transcription[71–73]. In particular, TFs and transcriptional co-activators are concentrated and cluster at enhancer regions[72] that primarily act to positively increase the amplitude and/or frequency of transcriptional bursts of linked genes[74,75]. In most cases, binding site availability (i.e. accessibility) of promoters and enhancers is necessary for TFs to bind and exert function, thus necessitating nucleosome remodeling machinery to both *initiate* and *maintain* chromatin accessibility for TF activity. The majority of this dissertation focuses on the Mammalian SWItch/Sucrose Non-Fermentable (SWI/SNF a.k.a. BRG/BRM associated factor, or **BAF**) nucleosome remodeling complex which utilizes ATP to physically slide or eject nucleosomes to alter chromatin accessibility and control TF binding[76,77]. There are three variants: canonical BAF (cBAF), Polybromo-associated BAF (PBAF), and non-canonical BAF (ncBAF), each composed of many shared subunits (e.g. SMARCA4), but distinguishable by inclusion of unique subunits, including ARID1A/ARID1B (cBAF), PBRM1/ARID2/BRD7 (PBAF), and GLTSCR1/GLTSCR1L/BRD9 (ncBAF)[78–80]. Enhancer accessibility is particularly sensitive to the loss of ARID1A, a key subunit of the cBAF complex[81–83]. Deletion of either *Arid1a* or *Smarca4* during murine hematopoiesis eliminates the formation of essentially all leukocyte lineages[84–86]. ARID1A mutations lead to dysregulated gene expression and differentiation patterns and are commonly found in human cancers[87,88], including T cell lymphomas[88–90]. Given the importance of cBAF in regulating cellular differentiation in diverse contexts, we reasoned that cBAF could play a

critical role in regulating the differentiation and functional diversification of activated T lymphocytes, a process that involves extensive chromatin remodeling[91,92]. Recently, we and others have begun to unravel the complex roles of ARID1A in the differentiation of effector and memory $CD8^+$ T cells[32,93–96].

In this dissertation, I present my findings in four chapters. In Chapter 1, I investigate transcriptional regulation of memory cells with particular focus on the transcription factor ZEB1. In Chapters 2-4, which constitute the main findings of my research, I primarily focus on the following key questions:

1. *How are chromatin landscapes shaped by cBAF over time in activated $CD8^+$ T cells?*

2. *How does the evolving chromatin landscape govern the activity of key transcription factors to give rise to diverse effector and memory cell fates?*

Briefly, we found that ARID1A profoundly regulates chromatin remodeling at sites that rapidly become accessible in response to antigen recognition *in vitro* and *in vivo*. Temporal control of *Arid1a* deletion revealed that cBAF actively shapes and maintains open chromatin regions in activated T cells, such that deletion of *Arid1a* either at early or late timepoints similarly impair the acquisition of terminal effector fates. These findings identify the cBAF complex as key factor in determining effector and memory cell fates following LCMV infection in mice.

CHAPTER 1: ZEB1 regulates central memory CD8+ T cell homeostasis

1.1 Introduction

We previously demonstrated that ZEB1 was important for memory CD8+ T cell survival and function[97]. However, how different populations of memory T cells are affected by the loss of *Zeb1* have not been described in great detail. Similarly, while TGFβ was proposed to promote *Zeb1* expression[40], we lack a comprehensive view of what other signals and transcription factors help to promote *Zeb1* expression. In this study, we utilized public transcriptomic data to map the transcriptional networks that govern memory and effector $CD8^+$ T cell populations, and identify that *Zeb1* is tightly co-regulated with *Bach2* and *Foxo1*, but is only loosely co-regulated with *Tcf7*. When *Zeb1* was deleted early using a *Gzmb*-cre genetic model, T_{CM} formation was strongly impaired in lymphoid organs and in the liver, but was entirely dispensable for T_{RM} formation in the small intestine. However, when *Zeb1* was deleted using an inducible *CreERT2* model, T_{CM} formation was not affected, suggesting that early *Zeb1* activity may be critical for promoting the formation of T_{CM} precursors, a subset of memory precursors that directly give rise to the initial pool of T_{CM} cells[98,99]. Interestingly, *Zeb1* deletion resulted in the upregulation of the epithelial marker EPCAM, suggesting that in addition to its role in promoting epithelial mesenchymal transition in cancer cells[100], *Zeb1* may similarly act to suppress epithelial gene programs and maintain mesenchymal gene programs in $CD8^+$ T cells.

1.2 Results

1.2.1 Transcriptional networks identify *Zeb1* as a key naïve and T_{CM} transcription factor.

To more broadly characterize transcriptional regulators of memory cell development and/or maintenance, public available RNA-seq data naïve, memory precursor, terminal effector, effector memory, and central memory cells[101] were re-analyzed. Pearson correlations for all transcription factor expression values were calculated, and then hierarchical clustering was performed on the correlation coefficients (**Figure 1.1 A**) which revealed that *Zeb1* clustered along with a class of mostly naïve-associated TFs including *Foxo1*, *Lef1*, *Bach2*. These findings suggest that these TFs may be transcriptionally co-regulated. Interestingly, *Tcf7* clustered separately from these TFs in a group of TFs more broadly expressed in naïve, T_{EM}, and T_{CM} cells. Further interrogation via scale-free undirected network analysis highlighted the fact that *Tcf7* is co-regulated with a group of TFs that are distinct from the *Zeb1*, *Foxo1* cluster (**Figure 1.1 B**). Given the importance of *Tcf7* in orchestrating memory T cell responses, we then constructed a "*Tcf7*-centric" network, which revealed that while *Zeb1* is contained within <3 degrees of interaction with *Tcf7*, the two TFs are not strictly co-regulated (i.e. 1 degree of interaction). Thus, relatively speaking, *Zeb1* may play an important but relatively minor role in memory cell development and function compared to *Tcf7*.

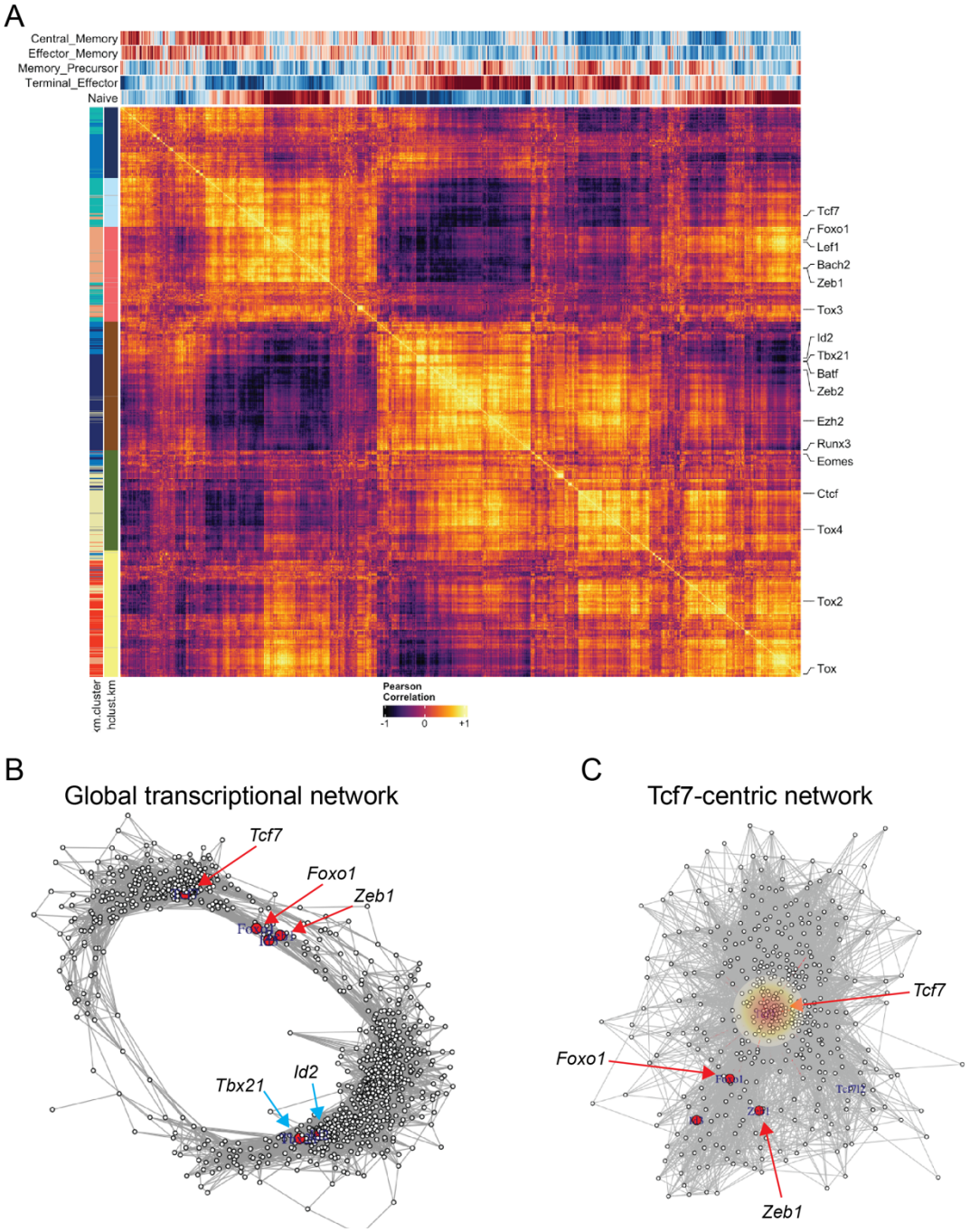

Figure 1.1 **Transcriptional network analysis identifies *Zeb1* as a key naïve and T_{CM}-associated transcription factor.** (**A**) Hierarchical clustering of gene-by-gene Pearson correlations from RNA-seq data from Hudson et al. (**B**) Undirected, scale-free network analysis of transcription factor correlation. ρ>0.8 was set as the pairwise interaction threshold. 4 degrees of interaction are permitted. (**C**) Undirected scale-free network with *Tcf7* as the central node. 2 degrees of interaction are permitted.

1.2.2 Early *Zeb1* deletion specifically impacts T_{CM} formation.

To specifically test whether ZEB1 regulates memory cell formation without affecting its function in naïve cells, we utilized conditional *Zeb1* KO mice crossed with *Gzmb-cre* which is conditionally activated after T cell activation[102]. *Zeb1*$^{fl/fl}$ *Gzmb-cre*+ (*Zeb1* KO) or littermate control (WT) P14 cells were transferred into congenic C57BL/6 mice that were subsequently infected with LCMV Armstrong. Sixty to seventy days post-infection (d.p.i.), memory cell formation of donor P14 cells was assessed by flow cytometry. *Zeb1* KO P14 cells formed fewer long-lived memory cells as WT P14 cells in lymphoid organs (spleen and mesenteric lymph nodes (mesLN)) and in the liver, but formed similar frequencies of T_{RM} in the small intestine intraepithelial layer (**Figure 1.2 A**). In particular, the T_{CM} population was strongly diminished (**Figure 1.2 B,C**) in the spleen, mesLN, and liver. Surprisingly, given the importance of the transcription factor TCF1 in the formation of memory CD8+ T cell populations, we did not identify measurable differences in TCF1 protein expression in WT and *Zeb1* KO memory cells (**Figure 1.2 D**). Finally, we observed similar numbers of T_{RM} (data not shown) and equivalent expression levels of CD69 and CD103 (canonical T_{RM} markers on CD8αβ IELs) on both WT and *Zeb1* KO IELs (**Figure 1.2 E**). Together these data indicate that ZEB1 specifically acts to promote T_{CM} formation, but not T_{RM} or other memory cell populations in $CD8^+$ T cells following acute LCMV Armstrong infection.

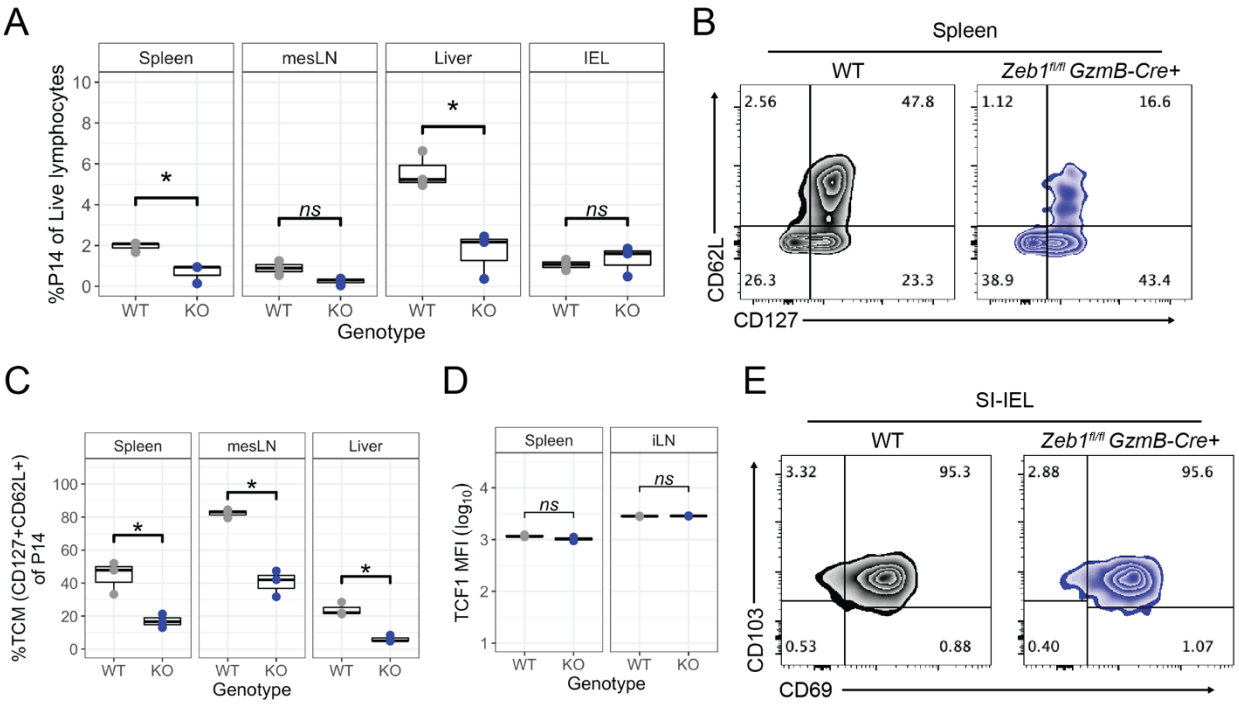

Figure 1.2 **Early *Zeb1* deletion specifically impacts T_{CM} formation.** (**A**) Frequency of WT or *Zeb1* KO Thy1.1$^+$ donor P14 cells in indicated organs at d60 p.i. (**B**) Representative flow plot of memory P14 cells in the spleen at 60 d.p.i. (**C**) Frequency of CD127$^+$CD62L$^+$ T_{CM} P14 cells in indicated organs at d60 p.i. (**D**) Representative flow plot of SI-IEL T_{RM} phenotypes at d70 p.i.

1.2.3 Induced Zeb1 deletion does not strongly impair T_{CM} formation.

To investigate the temporal requirement for ZEB1 in promoting T_{CM}, we generated inducible *Zeb1* KO mice by crossing *Zeb1*$^{fl/fl}$ P14 mice with *CreERT2*+ mice. As outlined in **Figure 1.3 A**, WT and *Zeb1*$^{fl/fl}$ *CreERT2*+ (*Zeb1* iKO) were co-transferred in equal ratios into naïve C57BL/6 congenic recipient mice and then infected with LCMV Armstrong. Groups of 3 mice each were treated with tamoxifen at early (d1-d5), peak effector (d7-11), contraction/early memory (d21-25), or late (d40-d44) timepoints to induce *Zeb1* deletion before analyzing donor cells in various tissues at d54 p.i. Early *Zeb1* deletion slightly increased the ratio of WT to *Zeb1* iKO cells. Later deletions did not strongly impact donor ratios across all organs (**Figure 1.3 B**). Interestingly, while there was a trend toward reduced T_{CM} population in later induced *Zeb1* deletion groups, *Zeb1* deletion at any of the indicated timepoints failed to recapitulate the strong reduction of the T_{CM} population (**Figure 1.3 C, D**) that was observed using the *Gzmb-Cre* model (**Figure 1.2 B**).

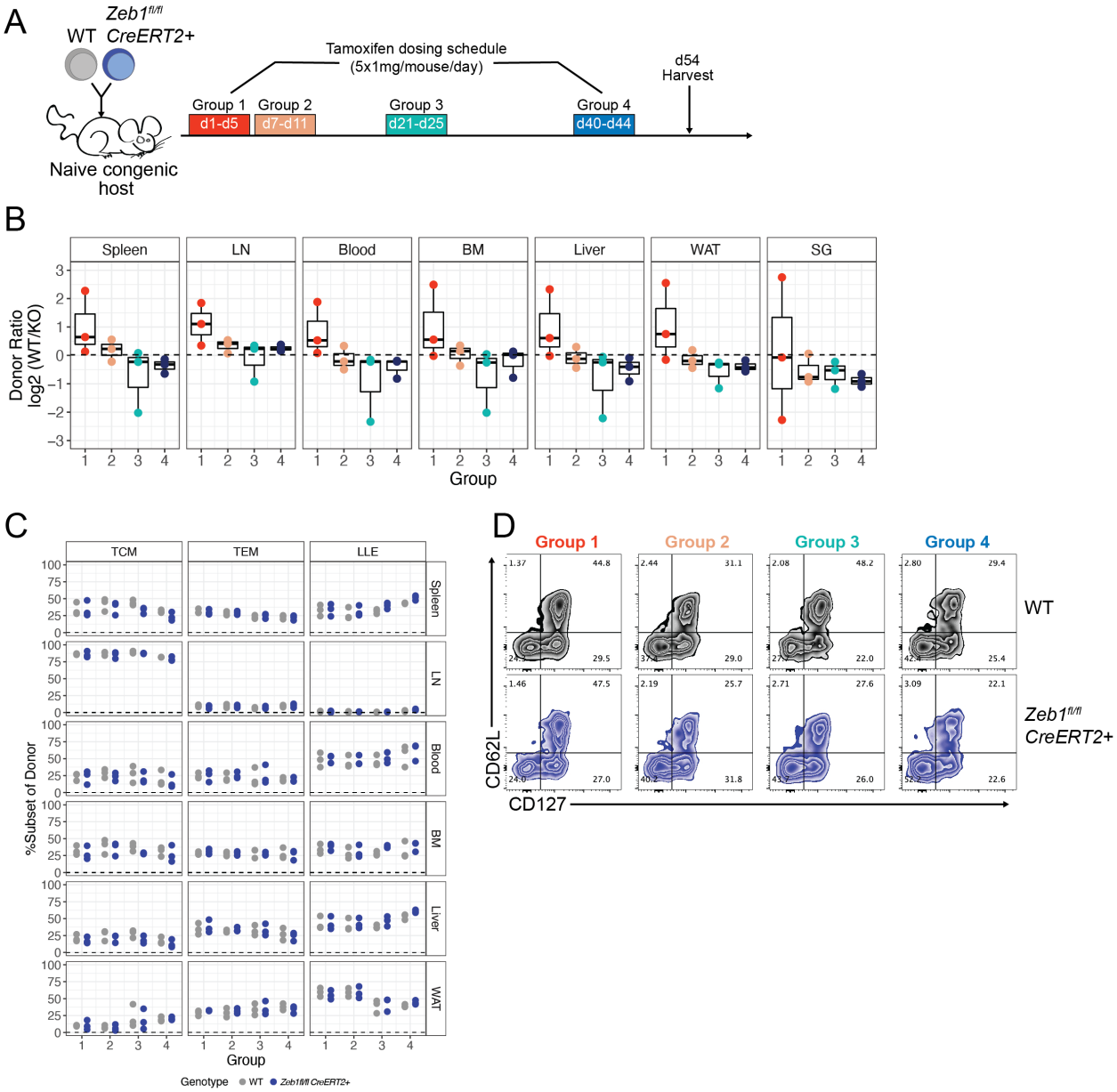

Figure 1.3 **Induced *Zeb1* deletion does not strongly impair T_{CM} formation.** (**A**) Experimental schematic of tamoxifen treatment schedule (**B**) WT:iKO donor P14 ratios across multiple organs at d54 p.i. (**C**) Frequency of T_{CM}, T_{EM}, and LLE ($CD127^-$) P14 cells in indicated organs at d54 p.i. (**D**) Representative flow plot of memory phenotypes at d54 p.i.

1.2.4 Early *Zeb1* deletion induces aberrant EpCAM expression.

Zeb1 is a critical regulator of epithelial-to-mesenchymal (EMT) differentiation *in vivo*[103]. I hypothesized that *Zeb1* may act in virus-specific $CD8^+$ T cells to repress epithelial- and promote mesenchymal-associated gene programs. Indeed, early induced deletion of *Zeb1* strongly increased the expression of the prototypic epithelial marker protein EpCAM[104] in memory cells (**Figure 1.4 A**). Interestingly, salivary gland (SG) T_{RM} cells exhibited basal EpCAM expression that was further enhanced by early *Zeb1* deletion. EpCAM induction was less pronounced in cells with later induced *Zeb1* deletions, indicating that ZEB1 likely acts within the first week of T cell activation to suppress the epithelial gene program. EpCAM was most strongly induced in T_{CM} cells, followed by T_{EM} cells, while long-lived effector cells (LLE) exhibited minimal EpCAM expression (**Figure 1.4 B,C**).

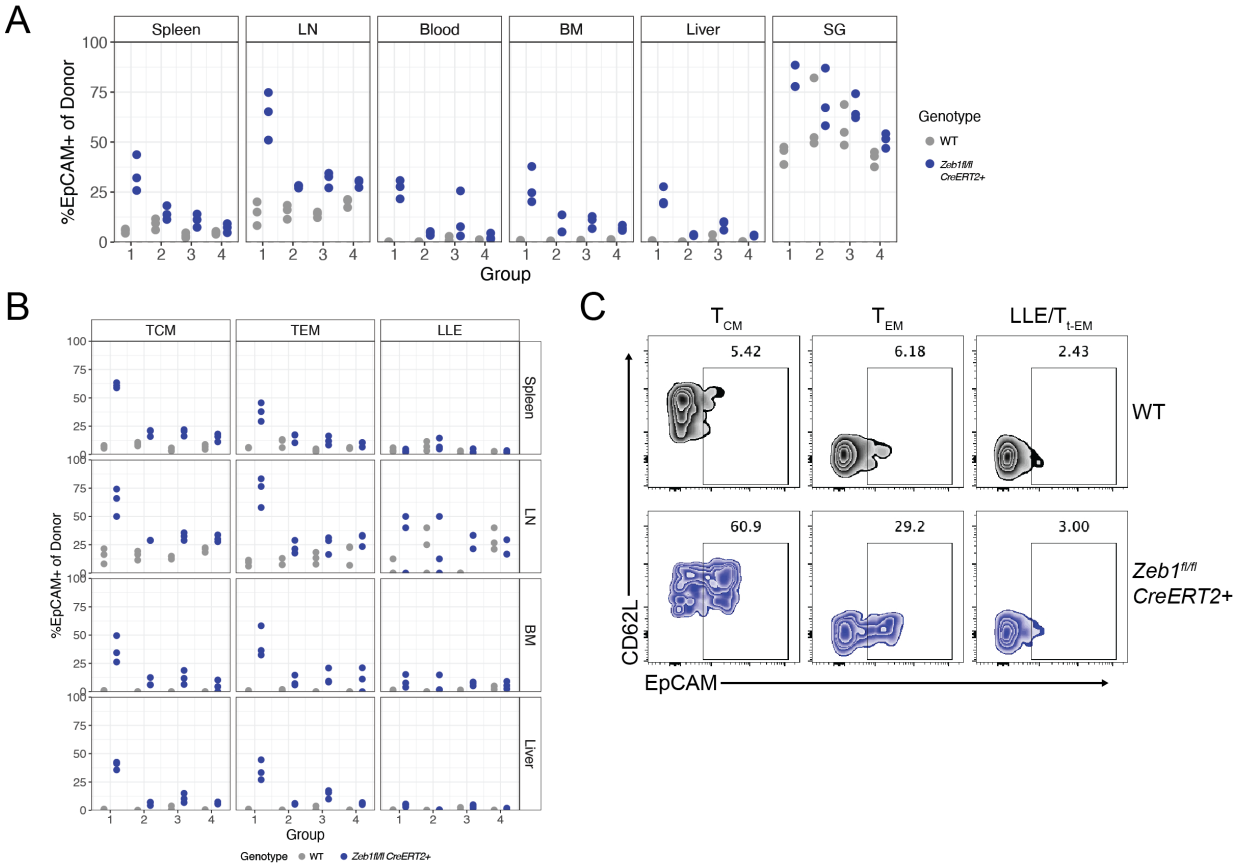

Figure 1.4 **Early *Zeb1* deletion induces aberrant EpCAM expression.** (**A**) Frequency of EpCAM+ WT or iKO donor P14 cells 54 d.p.i. (**B**) Frequency of EpCAM+ WT or iKO donor P14 T_{CM}, T_{EM}, and LLE cells 54 d.p.i. (**C**) Representative flow plot of EpCAM expression in indicated memory cell subtypes from Group 1.

1.4 Discussion

These studies reveal that *Zeb1* activity during the first few days of LCMV-specific $CD8^+$ activation and differentiation. Early *Zeb1* deletion using a truncated human *GZMB* promoter driving Cre recombinase expression[102], in which Cre expression is rapidly activated, strongly impaired the formation of the T_{CM} pool, resulting in an overall decrease in total memory cells. However, deletion via tamoxifen-induced CreERT2 activity at early or late timepoints was largely inconsequential for T_{CM} formation *per se*. These results suggest that ZEB1 activity is most critical during the first 2-3 days after T cell activation, when the dynamics of chromatin remodeling are most active[93]. Early tamoxifen-induced deletion (d0-d4) did not phenocopy the effects of *Gzmb-cre* mediated deletion, possibly due to delayed kinetics of CreERT2 relative to GZMB-Cre.

Transcriptomic analysis indicated that *Tcf7*, a key global regulator of T cell memory[105,106], clustered separately from *Zeb1* and other known memory-related genes including *Foxo1* and *Bach2*. Indeed, *Foxo1* deletion impairs the generation of $Tcf7^+$ effector cells at d4-d5 after LCMV infection[107], and *Bach2* deletion entirely eliminated the $CD62L^+$ T_{CM} precursor population[108]. However, unlike *Zeb1* which had no impact on memory cell numbers or phenotypes when deleted later via inducible CreERT2, induced late *Foxo1* deletion diminished the MCMV-specific memory CD8+ T cell pool and led to TCF7 downregulation[109]. Together these data establish a relative hierarchy of transcription factors that regulate memory formation and homeostasis with TCF7, FOXO1, and BACH2 playing critical and nonredundant roles in both of these functions, while ZEB1 may only be necessary for aiding in the formation of a T_{CM} precursor

population while additionally serving other functions such as the suppression of epithelial gene programs during the initial stages of effector programming.

Zeb1 deletion in early effector cells led to increased EPCAM expression that was sustained for at least 50-60 days. EpCAM is a prototypic epithelial cell marker[104] that is not typically expressed on $CD8^+$ T cells. Given the critical role of ZEB1 in promoting EMT in other contexts[100], these findings suggest that ZEB1 was acting early during effector cell development to suppress aberrant epithelial characteristics. However, a more comprehensive transcriptional profiling effort would be needed to determine whether *Zeb1* deletion led to global epithelial gene program upregulation or if this effect was specific to EPCAM alone. EPCAM expression was also observed in WT salivary gland T_{RM} cells, which was further elevated in *Zeb1* deleted cells. Interestingly, salivary gland $CD8^+$ T_{RM} have been previously shown to express E-cadherin, another epithelial cell marker[110]. Together these findings suggest that salivary gland $CD8^+$ T_{RM} in particular may harbor latent epithelial cell-like gene programs that act to promote tissue residency, and these epithelial characteristics are further bolstered by the absence of mesenchymal-promoting ZEB1 activity. In support of this, *Zeb1* deleted P14 T_{RM} were more abundant than WT cells in the salivary gland (**Figure 1.3B**).

1.5 Methods

1.5.1 Mice and infections

C57BL/6J were purchased from Jackson Laboratories. P14 *Zeb1*$^{fl/f}$ *Gzmb-cre* mice have been previously described[40]. Both female and male mice were used for all studies. Animals were housed in specific-pathogen-free facilities at the Salk Institute. All

experimental studies were approved and performed in accordance with guidelines and regulations implemented by the Salk Institute Animal Care and Use Committee. Mice were infected with $2x10^5$ PFU LCMV-Armstrong by intraperitoneal injection. LCMV-Armstrong stocks were prepared as previously described[111].

1.5.2 Cell Isolation

Spleens, lymph nodes, and livers were mechanically dissociated with 1mL syringe plungers over a 70um nylon strainer. Livers were resuspended in 8mL 40% isotonic percoll and centrifuged at 800g for 12 minutes at 20C. Spleens and livers were incubated in ammonium chloride potassium (ACK) buffer for 5 minutes. For isolation of small intestinal IEL, Peyer's patches were first removed by dissection. Intestines were longitudinally cut and then cut into 1cm pieces and washed in PBS. Pieces were incubated in 30mL HBSS with 10% FBS, 10mM HEPES, and 1mM dithioerythritol with vigorous shaking at 37C for 30 minutes. Supernatants were collected, washed, and further isolated using a 40/67% discontinuous percoll density centrifugation for 20 minutes at room temp with no brakes. Salivary glands were minced with scissors and incubated in RPMI with 5% FBS and 0.5mg/mL Collagenase IV, 0.1mg/mL DNAse1, and 2mM CaCl2 for 30 minutes at 37C with gentle shaking, and then strained over 70um nylon strainers.

1.5.3 Flow Cytometry

Cell suspensions were first incubated with eBioscience Fixable Viability Dye eFluor 780 for 5 minutes at room temp. Cells were stained with primary surface antibodies in PBS with 2% FBS, 0.1% NaN3 for 20 minutes on ice. For intracellular staining, cells were first fixed with eBioscience Foxp3/Transcription Factor Staining buffer

fixation/permeabilization buffer for 30 minutes at room temp, and staining was performed in 1X permeabilization buffer for 30 minutes at room temp. Flow cytometry analysis samples were acquired on a BD Symphony A3.

1.5.4 Adoptive T cell transfer

Naive WT, *Zeb1*$^{fl/fl}$ *Gzmb-cre*$^{+}$ or *Zeb1*$^{fl/fl}$ *CreERT2*$^{+}$ CD8^{+} P14 cells were isolated by negative selection with biotinylated antibodies against CD4, CD19, B220, MHCII, CD11b, CD11c, CD49b, and Ter119 in MACS buffer, and MojoSort beads were added at 5% v/v for 5 minutes before placing the cell suspension on a magnet and collecting the supernatant. $2.5x10^4$ P14 cells were injected into recipient mice 18-24 hours before infection.

1.5.5 Acknowledgement

Chapter 1 contains unpublished material. McDonald B, Kaech SM. The dissertation author was the primary investigator.

CHAPTER 2: Early chromatin remodeling events in acutely stimulated $CD8^+$ T cells

2.1 Summary

T cells undergo extensive chromatin remodeling over several days following stimulation through the T cell receptor. However, the kinetics and gene loci targeted by early remodeling events within the first 24 hours of T cell priming to orchestrate effector differentiation have not been well described. We identified that chromatin accessibility is rapidly and extensively remodeled within 1 hour of stimulation of naïve $CD8^+$ T cells, leading to increased global chromatin accessibility at many effector T cell-associated genes that are enriched for AP-1, early growth response (EGR), and nuclear factor of activated T cells (NFAT) binding sites, but this short duration of stimulation is insufficient for commitment to clonal expansion *in vivo*. Sustained 24-hour stimulation led to further chromatin remodeling and was sufficient to enable clonal expansion. These data suggest that the duration of antigen receptor signaling is intimately coupled to chromatin remodeling and activation of genes involved in effector cell differentiation, and highlight a potential mechanism that helps $CD8^+$ T cells discriminate between foreign- and self-antigens.

2.1 Introduction

CD8+ T cells are critical for host defense against intracellular pathogens and against tumors. Following T cell receptor (TCR)-dependent recognition of cognate peptides bound to major histocompatibility complex class I (MHC-1) on antigen presenting cells, naïve $CD8^+$ T cells initiate protein tyrosine kinase signaling cascades, including ZAP-70 (signaling via MAP kinase cascades), and phospholipase Cγ1 (signaling via second messengers to activate protein kinase C (PKC) and regulate intracellular Ca^{2+}

levels)[112]. These signaling pathways convey information to the nucleus via nuclear accumulation of the transcription factors (TFs) NFAT, NFkB, and the AP-1 family of TFs[113,114], leading to activation of biosynthesis pathways, epigenetic remodeling, increased global transcription and translation, rewiring of metabolic pathways to sustain energetic expenditure, activation of cytotoxic and other functional effector genes, and entry into the cell cycle and rapid clonal expansion that gives rise to a large effector cell pool capable of mediating host defense[1,115].

In order to prevent aberrant T cell responses directed against host tissues, peripheral T cells must discriminate between foreign and host antigens, and both TCR signal strength and duration are key factors regulating this discriminatory property. On short timescales (seconds), one proposed underlying mechanism is the 'kinetic proofreading' antigen recognition model: local TCR-proximal signaling events (e.g. tyrosine phosphorylation, signaling complex recruitment, which occur within ~3-4 seconds of TCR-pMHC engagement[116,117]) propagate more slowly than individual TCR-pMHC interaction lifetimes, while dissociation rates of nonspecific complexes are sufficiently rapid as to prevent premature systemic secondary messenger activity, therefore necessitating sustained high affinity (low K_{OFF} rate) TCR-pMHC interactions for successful T cell activation[118,119]. Indeed, ~6 hours of continuous antigenic stimulus are minimally required for $CD8^+$ T cells to enter into programmed, or "autopilot" proliferation[38,39,120]. Similarly, the BAF (BRG/BRM associated factors) chromatin remodeling complex is rapidly recruited to chromatin within minutes of activation by TCR crosslinking or by PKC stimulation[121]. *In vivo,* naïve $CD8^+$ T cells were observed to undergo priming in phases, initially by scanning DCs and forming transient suboptimal interactions for ~8 hours [122], followed by prolonged

~8-20 hour continuous interactions by high affinity TCR-pMHC interactions with DCs[123]. If antigen receptor signaling can induce rapid BAF complex recruitment (and presumably activity, which occurs within minutes of recruitment *in vitro*[124,125]), then what longer timescale mechanisms exist to help naïve T cells discriminate between spurious short-term (<6 hours) and longer (>6 hours) antigen-derived signals to prevent or enable effector cell differentiation and programmed proliferation?

There is mounting evidence that *in vivo* $CD8^+$ effector cell fates are established early during infection, even during the first cell division[30], but the extent to which effector cell fates become epigenetically imprinted during priming prior to the first cell division are not clearly understood. Therefore, to address this gap we investigated how the chromatin landscape is influenced by stimulation signal duration (1 hour versus 24 hour). Chromatin was rapidly remodeled within 1 hour of stimulation, defined by simultaneous *de novo* gain of open chromatin regions (OCRs) enriched for bZIP (AP-1), EGR, and NFAT TF binding motifs that neighbored genes involved in effector functions, cell growth, and Myc-related genes. However, 1 hour stimulated cells could not undergo programmed proliferation when transferred into antigen-free hosts. In summary, these data define early temporal kinetics of chromatin accessibility dynamics of recently activated $CD8^+$ T cells.

2.3 Results

2.3.1 Chromatin is remodeled rapidly after T cell activation.

To better understand the dynamics of T cell chromatin remodeling within short timeframes, we activated purified naïve P14 TCR-transgenic $CD8^+$ T cells with immobilized antibodies directed against CD3 and CD28 with recombinant hIL-2 for either 1 hour or 24 hours, and then isolated nuclei and performed assay for transposable

chromatin with sequencing (ATAC-seq) to assess genome-wide chromatin accessibility profiles. Principal component analysis (PCA) of all replicates revealed that 84.6% of variance within the dataset was explained by the duration of antigenic stimulus (**Figure 2.1 A**). Importantly, this analysis indicated that 1 hour stimulated cells were epigenetically distinct from unstimulated cells, which was further underscored by quantification of differentially accessible regions that showed that ~9500 sites gained *de novo* accessibility, and ~4500 sites lost accessibility following 1 hour of stimulation *in vitro* (**Figure 2.1 B**). Cells stimulated for 24 hours continued to both acquire and lose several thousand OCRs (**Figure 2.1 B**), indicating that chromatin remodeling is a dynamic and evolving process in $CD8^+$ T cells responding to antigenic stimulus over a 24-hour period. In spite of the fact that 1 hour stimulated cells undergo robust chromatin remodeling and upregulate activation markers like CD44, most of these cells failed to divide at all when transferred into congenic C57BL/6 mice, while a small subset underwent a single round of division (**Figure 2.1 C-D**), altogether indicating that this epigenetic rewiring was not sufficient to engage “autopilot” proliferation *in vivo*. Importantly, however, 1 hour stimulated cells that were transferred into mice that were subsequently immunized with GP33 peptide along with CpG-B (ODN-1826) adjuvant successfully underwent multiple rounds of division similar to 24 hour stimulated cells (**Figure 2.1 D**), indicating that acute cessation of antigen signaling after 1 hour does not prevent the cells from responding to antigen at a later time (i.e. the cells do not become anergic).

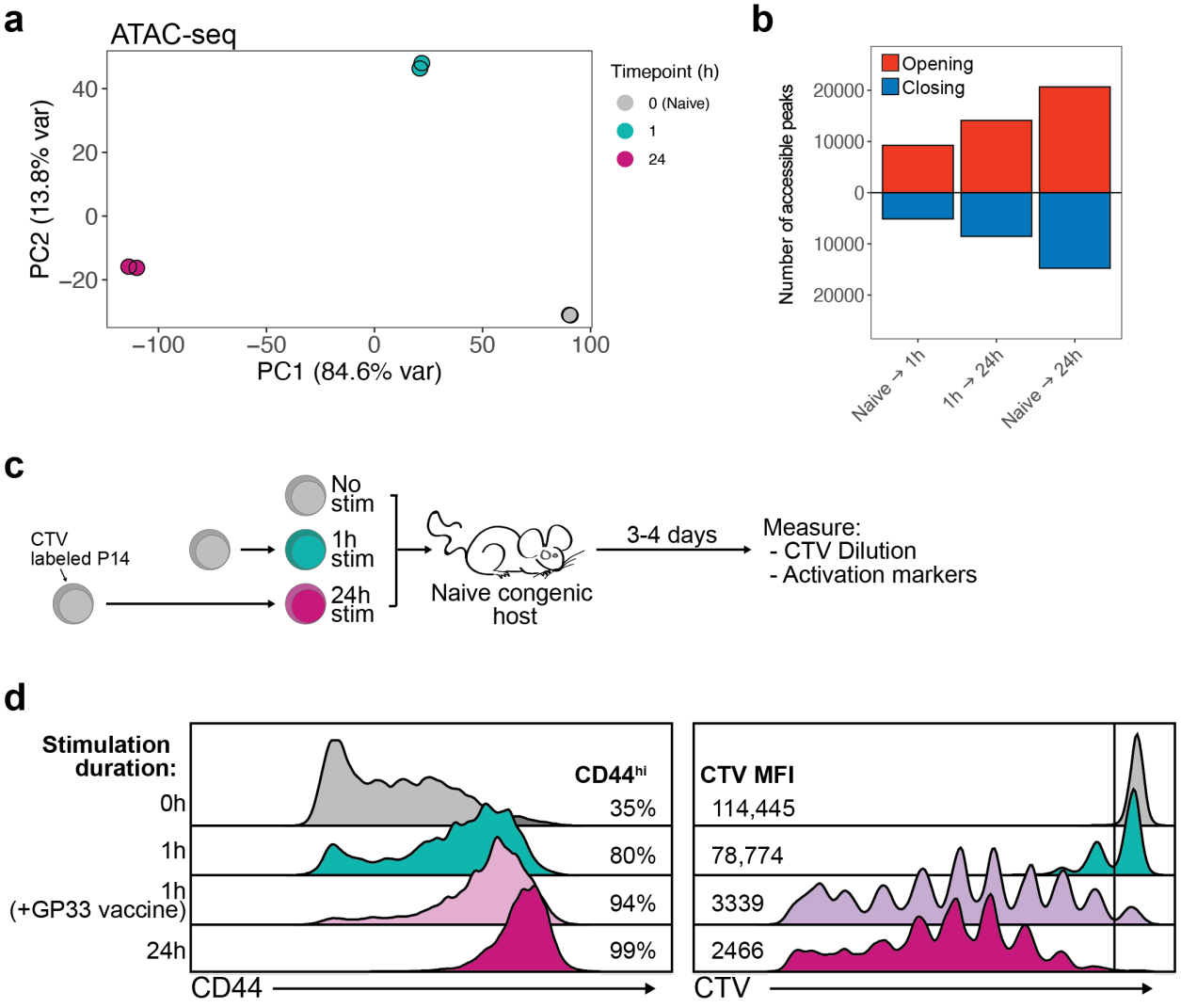

Figure 2.1 **Chromatin is remodeled rapidly after T cell activation.** (**a**) Principal component analysis of ATAC-seq from naïve, 1 hour, or 24 hour stimulated P14 CD8$^+$ T cells. (**b**) Number of OCRs gained and lost following activation. (**c**) Experimental design and (**d**) representative CD44 and CellTrace Violet (CTV) histograms from transferred P14 cells 3 days after adoptive transfer.

2.3.2 Early activated accessible regions are enriched in cell cycle and effector response-associated genes.

To better define the biological processes that are regulated by the changes in chromatin accessibility, we first annotated the genomic positions of OCRs and then clustered the OCRs by temporal dynamics (**Figure 2.2 A**). This revealed various patterns of accessibility dynamics, including I) rapid and progressively closed OCRs, II) slow closing OCRs, III) transient, 1 hour activation-specific OCRs, IV) rapid induced OCRs, and V) late induced OCRs. Clusters I and II were strongly and similarly enriched for ETS, FORKHEAD, LEF1, and TCF7 binding motifs, consistent with the known roles of these TF families in naïve $CD8^+$ T cells. In contrast, all induced clusters (clusters III-V) were strongly enriched for bZIP and NFAT family motifs. Early induced clusters (III-IV) were also enriched in EGR motifs, while late induced cluster V OCRs were enriched for IRF, PRDM1, and T-box binding motifs. All five dynamic OCR clusters were predominantly located in non-promoter (i.e. intronic and intergenic) regions (**Figure 2.2 B**). Genes annotated to early induced OCRs at 1 hour were enriched for Gene Ontology (GO) terms related to transcription and translation, cell development, and nuclear receptor binding (**Figure 2.2 C**), suggesting that cells are preparing to enter the cell growth phase, though no GO terms related to cell division or proliferation were significantly enriched (data not shown).

To more finely resolve the genes that may be regulated by opening and closing of OCRs, we focused on several classes of genes with established roles in regulating T cell responses or cell cycle dynamics and analyzed both chromatin accessibility at each locus as well as corresponding protein abundance[126] (**Figure 2.2 D, 2.2 E**). Genes exhibiting early induced OCRs included functional effector molecule *Ifng* and the high affinity IL-2 receptor *Il2ra*, the critical transcriptional regulator of cell growth *Myc* and its target gene

Slc7a5[127] which is critical for amino acid transport in activated T cells. Several intronic regions at the positive cell cycle regulator *Cdk6* locus increased and maintained accessibility by 1 hour, while the key negative cell cycle regulator *Cdkn1b* ($p27^{Kip1}$) locus exhibited an overall decrease in accessibility over time. *Hk2* (hexokinase 2), a critical regulator of glucose metabolism and the rate limiting factor for aerobic glycolysis[128], increased in accessibility at one intron within 1 hour, and two additional intronic regions by 24 hours. *Ezh2*, a component of polycomb repressive complex 2 (PRC2), showed *de novo* accessibility at an upstream intergenic site. Finally, transcription factor genes *Egr1* and *Nr4a1* exhibited transient locus-wide increases in accessibility which sharply decreased by 24 hours, consistent with the kinetics of protein levels of these factors (**Figure 2.2 E**).

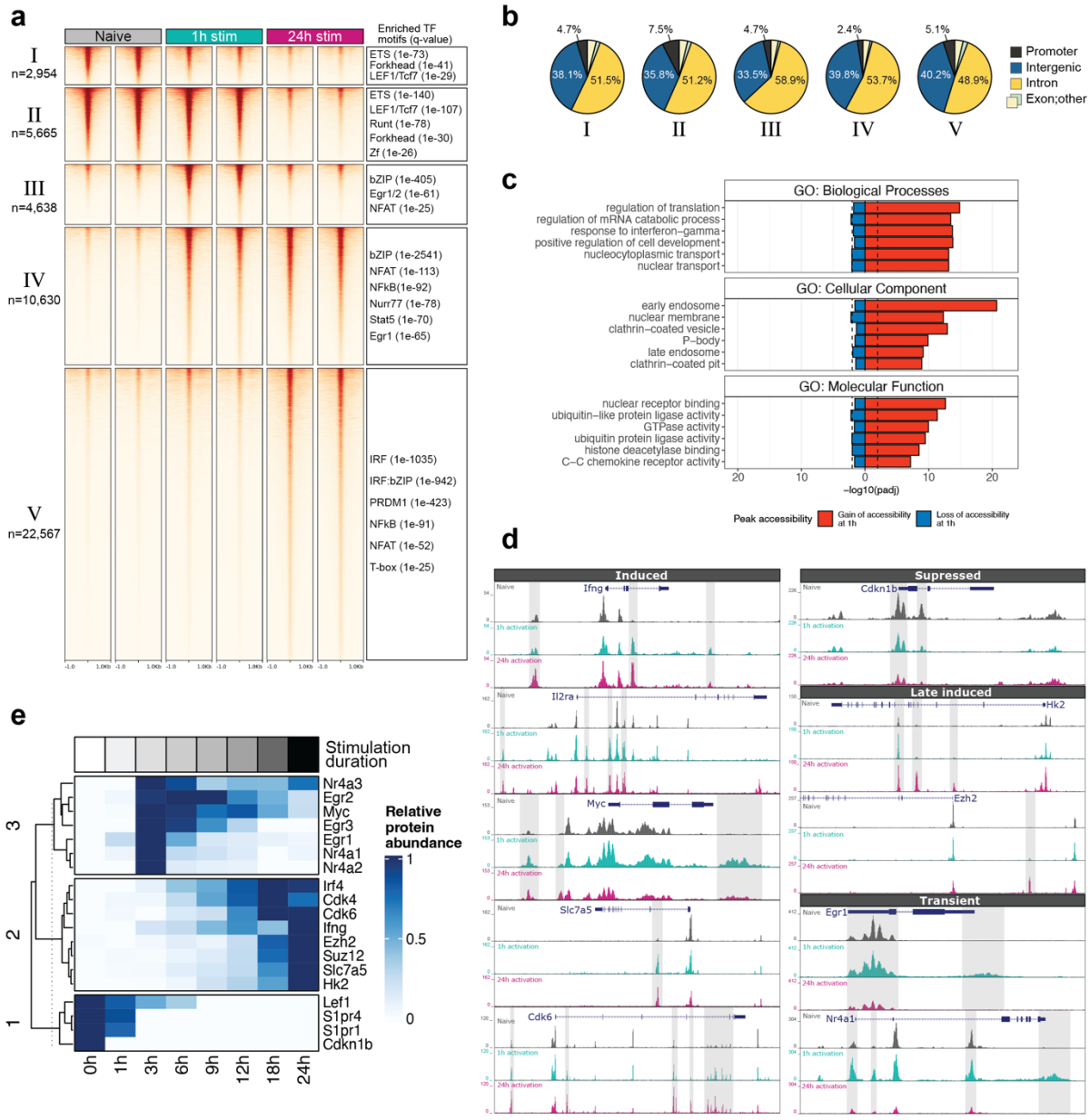

Figure 2.2 **Early activated accessible regions are enriched in cell cycle and effector response-associated genes.** (**a**) ATAC-seq signal tracks and clusters. Highly enriched TF binding motifs and associated enrichment q-values for each cluster are indicated. (**b**) Gene Ontology enrichment analysis of protein-coding genes annotated to differential OCRs between 1 hour-stimulated and naïve cells. (**c**) Gene Ontology (GO) enrichment of OCRs gained or lost in 1 hour stimulated cells. (**d**) ATAC-seq signal tracks at *Ifng*, *Il2ra*, *Myc*, *Slc7a5*, *Cdk6*, *Cdkn1b*, *Hk2*, *Ezh2*, *Egr1*, and *Nr4a1* loci. (**e**) Heatmap of Immpres T cell receptor activation timecourse proteomes[126].

2.4 Discussion

Our study reveals that chromatin remodeling activity is rapidly induced following antigen receptor-dependent activation, but that this remodeling activity continues for at least 24 hours in the presence of continuous antigenic stimulation. Sets of genes underwent remodeling with distinct kinetics. For example, early response genes like, Myc, EGR1/2 and NR4A1/2/3 that are transiently expressed shortly after activation exhibit similar kinetics of transient increases in open chromatin after 1 hour but decreasing or baseline accessibility at 24 hours. Conversely, late response genes, like *Cdk6*, *Ezh2*, and *Hk2*, with peak protein abundance between 18-24 hours post-activation required sustained activation before full remodeling was achieved across each respective locus.

We and others previously demonstrated that *Ezh2* was required to suppress the memory-associated genetic program in order for cells to terminally differentiate[18,68]. Our analysis identified a potential upstream *Ezh2* enhancer that was present at 24 hours, but not 1 hour after activation, pointing to a potential time-dependent *cis*-regulatory mechanism controlling EZH2 expression. Indeed, EZH2, EED, and SUZ12 protein abundance reached peak values after 18 hours of activation, suggesting that a sustained antigenic stimulation was required to induce expression and allow for PRC2 activity, possibly to suppress the naïve T cell epigenetic program via polycomb repression only under conditions of sustained antigen receptor signaling.

Interestingly, positive cell cycle regulator genes (e.g. *Cdk6*) increased accessibility at multiple putative intronic enhancers. Given that T cells undergoing programmed proliferation divide every 6-8 hours[129], we speculate that generational inheritance of an accessible *Cdk6* locus allows for rapid re-engagement of the cell cycle immediately after

mitotic exit in order to sustain this high proliferative rate. On the other hand, while negative regulation of the cyclin-dependent kinase inhibitor $p27^{Kip1}$ (*Cdkn1b*) has largely been ascribed to its proteolytic degradation[130], our analysis points to an potential additional mechanism by which *Cdkn1b* levels may be regulated via the loss of accessible chromatin at its regulatory sequences.

In summary, we have outlined early temporal kinetics of chromatin remodeling in acutely stimulated naïve $CD8^+$ T cells and mapped genome-wide patterns of opening and closing of *cis*-regulatory regions. Chromatin remodeling is extensive in the first hour following stimulation, and while insufficient to enable effector cell fate commitment, this early response likely prepares the cells for eventual proliferative and effector gene programming that can only proceed to completion in the presence of subsequent continuous stimulation. By analogy to the kinetic proofreading model, where 1) short-duration antigen receptor engagement (1 hour) represents non-specific, or perhaps non-pathogenic interactions, and 2) long-duration (>6 hour) stimuli represents specific or pathogenic interactions, and 3) assuming that naive and proliferation-competent effector-primed cells represent distinct quantized functional states; we propose that the rate of chromatin remodeling may be sufficiently slow so as to allow for discrimination between these two lengths of stimulation, and ensure proper proliferative responses by optimally stimulated cells while averting proliferation and host tissue-directed responses by sub-optimally stimulated T cells. In fitting with such a model, certain assumptions will need to be formally demonstrated: namely, that early activation-induced chromatin states revert back to naïve baseline states if antigen signaling is halted before ~6 hours. Though our study focused exclusively on T cell differentiation, this model may serve as a

generalizable framework to understand how differentiation and cell fates are regulated in all types of cells responding to extrinsic signals.

2.5 Methods

2.5.1 Mice

C57BL/6J were purchased from Jackson Laboratories. P14 mice[131] have been previously described. Animals were housed in specific-pathogen-free facilities at the Salk Institute. All experimental studies were approved and performed in accordance with guidelines and regulations implemented by the Salk Institute Animal Care and Use Committee.

2.5.2 Cell Isolation

Spleens and lymph nodes were mechanically dissociated with 1mL syringe plungers over a 70um nylon strainer. Cells were incubated in ammonium chloride potassium (ACK) buffer for 5 minutes to lyse red blood cells. P14 cells were isolated by negative selection with biotinylated antibodies against CD4, CD19, B220, MHCII, CD11b, CD11c, and CD49b in MACS buffer, and MojoSort beads were added at 5% v/v for 5 minutes before placing the cell suspension on a magnet and collecting the supernatant.

2.5.3 *In vitro* Stimulations

24-well plates were coated with anti-Armenian Hamster IgG (Jackson ImmunoResearch #127-005-099) at 30µg/mL in PBS at 4C overnight. Purified P14 CD8+ T cells were stimulated at $1x10^6$ cells in 300µL complete RPMI (RPMI with 10% FBS, Pen/strep, L-glutamine, 50uM β-ME) with 2µg/mL anti-CD3e (BD #567114), anti-CD28 (BD #567110), and 100U/mL recombinant human IL-2 (PeproTech #212-02).

2.5.4 Adoptive Transfer and immunization

P14 cells were labeled with CellTrace Violet in warm PBS for 8 minutes, and then washed with excess cold complete RPMI (RPMI with 10% FBS, Pen/strep, L-glutamine, 50uM β-ME). Recipient mice received 0.8-1.5x10^6 cells in 100µL PBS via retroorbital injection. Immunized mice received an i.p. injection containing 5µg GP33 peptide and 25µg CpG-B (ODN-1826) in 100µL PBS at the time of P14 transfer.

2.5.5 Flow Cytometry

Cell suspensions were first incubated with eBioscience Fixable Viability Dye eFluor 780 for 5 minutes at room temp. Cells were stained with primary surface antibodies in PBS with 2% FBS, 0.1% NaN_3 for 20 minutes on ice.

2.5.6 ATAC-Seq library preparation and sequencing

ATAC-seq was performed as previously described [132]. Briefly, 5,000-50,000 viable cells were washed with cold PBS, collected by centrifugation, then lysed in resuspension buffer (RSB) (10 mM Tris-HCl, pH 7.4, 10 mM NaCl, 3 mM MgCl2) supplemented with 0.1% NP40, 0.1% Tween-20, and 0.01% digitonin. Samples were incubated on ice for 3 min, then washed out with 1 ml RSB containing 0.1% Tween-20. Nuclei were pelleted by centrifugation at 500g for 10 min at 4°C then resuspended in 50 ul transposition mix (25ul 2x TD buffer, 2.5 ul transposase (100 nM final), 16.5 ul PBS, 0.5 ul 1% digitonin, 0.5 ul 10% Tween-20, 5 ul H_2O) and incubated at 37°C for 30 min in a thermomixer with 1000 RPM mixing. DNA was purified using a Qiagen MinElute PCR cleanup kit, then PCR amplified using indexed oligos. The optimal number of amplification cycles for each

sample was determined by qPCR. Libraries were size selected using AmpureXP beads and sequenced using an Illumina NextSeq500 for 75bp paired-end reads.

2.5.7 Data Availability

All sequencing data from this paper are available in GEO under accession series GSE236306.

2.5.8 ATAC-Seq analysis

Paired-end reads were aligned to the *M. musculus* mm10 genome using STAR[133] with default parameters. ATAC-seq peaks were called using HOMER[134] findPeaks.pl using parameters `-style dnase`. Peaks were called when enriched >4.0-fold over local tag counts. Reads mapped to peaks were quantified using featureCounts[135]. Differentially accessible regions were identified using DESeq2[136] with fold change ≥2.0 or ≤−2.0, FDR < 0.05. Peaks sets were annotated with HOMER, and visualizations were created using deepTools v3.5.1[137].

2.5.9 Transcription factor binding motif analysis

Sequences within 100 bp of peak centers were compared to known motifs in the HOMER database using the findMotifsGenome.pl command with default parameters. Random GC content-matched genomic regions were used as background. Enriched motifs are statistically significant motifs in input over background by a P value of less than 0.05 using a cumulative binomial distribution.

2.6 Acknowledgement

Chapter 2 contains material submitted for publication at *Yale Journal of Biology and Medicine* in July 2023. McDonald B, Chick BY, Hargreaves DC, Kaech SM. The dissertation author was the primary investigator and author of this paper.

CHAPTER 3: Canonical BAF complex activity shapes the enhancer landscape that licenses CD8+ T cell effector and memory fates

3.1 Summary and graphical abstract

CD8$^+$ T cells provide host protection against pathogens by differentiating into distinct effector and memory cell subsets, but how chromatin is site-specifically remodeled during their differentiation is unclear. Due to its critical role in regulating chromatin and enhancer accessibility through its nucleosome remodeling activities, we investigated the role of the canonical BAF (cBAF) chromatin remodeling complex in antiviral CD8$^+$ T cells during infection. ARID1A, a subunit of cBAF, was recruited early after activation and established *de novo* open chromatin regions at enhancers. *Arid1a* deficiency impaired the opening of thousands of activation-induced enhancers, leading to loss of TF binding, dysregulated proliferation, gene expression, and failure to undergo terminal effector differentiation. While *Arid1a* was dispensable for circulating memory cell formation, tissue-resident memory formation was strongly impaired. Thus, cBAF governs the enhancer landscape of activated CD8$^+$ T cells that orchestrates TF recruitment and activity and the acquisition of specific effector and memory differentiation states.

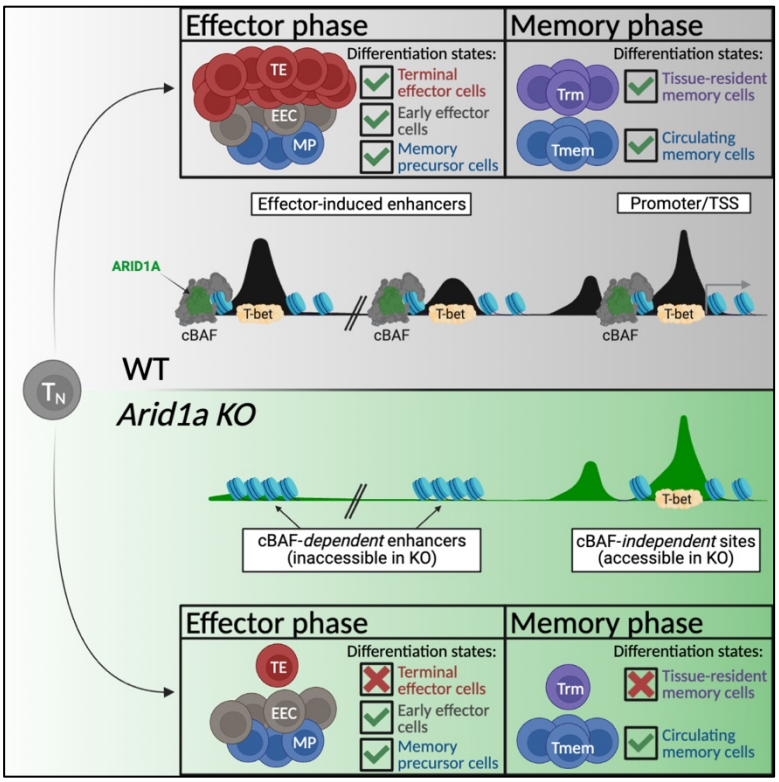

Figure 3.1 **ARID1A-containing canonical BAF complex establishes regions of open chromatin at activation-induced enhancers in activated effector CD8+ T cells during acute viral infection.**

3.2 Introduction

$CD8^+$ T cells play an essential role in host protection against intracellular pathogens and cancer. Naive $CD8^+$ T cells become activated upon recognition of cognate antigen (signal 1) concurrent with engagement of costimulatory receptors (signal 2) and cytokine signaling (signal 3), enabling epigenetic and transcriptional reprogramming to promote cell growth, proliferation, and the acquisition of specialized effector functions[1]. Activated effector cells exhibit transcriptional and epigenetic heterogeneity, display diverse modes of tissue homing patterns and memory-forming potential, and can be distinguished by expression of markers like IL7R (CD127), KLRG1 and CX_3CR_1[6]. Memory

precursor (MP) cells express higher levels of CD127 and preferentially give rise to the long-lived circulating memory cell pool[7]. High inflammatory conditions promote the formation of short-lived terminal effector (TE) cells expressing KLRG1 and CX_3CR_1 that exhibit potent cytotoxic potential but preferentially die following the resolution of infection[8–10]. Early effector cells (EEC) express low levels of CD127, KLRG1, and CX_3CR_1, and can give rise to both TE and MP cells[10–12]. Recent studies have begun to identify distinguishing features of effector cells that preferentially migrate into non-lymphoid tissues to form tissue-resident memory (Trm) cells[62,138]. Importantly, while the identities of transcription factors (TFs) that promote effector (*Id2*, *Tbx21* (T-bet), *Batf*), tissue-residency (*Runx3*, *Zfp683*, *Bhlhe40*), and memory cell fates (*Eomes*, *Tcf7*, *Id3*, *Myb*) are well described[1,62–65], the underlying biological processes that regulate the binding and activity of these TFs are largely undefined. Indeed, individual TFs exert overlapping and distinct roles across many cell states (e.g., *Tbx21* and *Eomes* in memory versus exhausted T cells[66]) highlighting the need to better understand how TF binding site accessibility is regulated to control the behavior of TFs and the differentiation states they specify.

Mammalian SWI/SNF complexes (aka BAF, BRG/BRM-associated factors) are chromatin remodelers that facilitate reorganization of nucleosomes along DNA[77]. There are three variants: canonical BAF (cBAF), Polybromo-associated BAF (PBAF), and non-canonical BAF (ncBAF), each composed of many shared subunits, but distinguishable by inclusion of unique subunits, including ARID1A/ARID1B (cBAF), PBRM1/ARID2/BRD7 (PBAF), and GLTSCR1/GLTSCR1L/BRD9 (ncBAF)[78–80]. Enhancer accessibility is particularly sensitive to the loss of ARID1A, a key subunit of the cBAF complex[81–83].

Normal leukocyte development is accompanied by substantial chromatin remodeling and establishment of novel enhancers; and deletion of either *Arid1a* or *Smarca4* during murine hematopoiesis eliminates the formation of essentially all leukocyte lineages[84–86]. ARID1A mutations lead to dysregulated gene expression and differentiation patterns and are commonly found in human cancers[87,88], including T cell lymphomas[88–90]. However, it is unknown what role ARID1A plays in differentiating mature T lymphocytes and the generation of $CD8^+$ T cell memory. Given the importance of cBAF in regulating cellular differentiation in diverse contexts, we reasoned that cBAF could play a critical role in regulating the differentiation and functional diversification of activated T lymphocytes, a process that involves extensive chromatin remodeling[91,92].

Here we investigated the role of ARID1A-containing cBAF in promoting $CD8^+$ T cell effector differentiation upon acute systemic viral infection. We found that ARID1A was necessary for terminal effector cell differentiation and establishment of long-lived Trm cell populations but was dispensable for circulating memory cell formation. However, *Arid1a*-deficient circulating memory cells were deficient in production of cytokines, chemokines, and cytotoxic proteins, suggesting that ARID1A was critical for optimizing the functional capabilities of memory cells. Mechanistically, ARID1A was required to induce early expression of TFs that specify TE and Trm fates, as well as to open chromatin at sites where those TFs bind. *Arid1a*-deficient effector cells displayed reduced global chromatin accessibility and failed to open chromatin regions containing binding sites for ETS, RUNX, bZIP (AP-1), and T-box family transcription factors. Our results demonstrate that ARID1A-containing cBAF complexes act to remodel chromatin that licenses effector differentiation

during acute infections and provide insight into how TF recruitment and activity is regulated to instruct the formation of different types of effector and memory $CD8^+$ T cells.

3.3 Results

3.3.1 Differentiating antiviral effector $CD8^+$ T cells display highly dynamic accessible chromatin and cBAF occupancy patterns

To better understand the initial waves of $CD8^+$ T cell differentiation during infection, we transferred P14 TCR transgenic cells that recognize the GP_{33-41} epitope of the LCMV glycoprotein[131] into wild-type recipients infected with LCMV-Armstrong, and on days 3 (d3), 5 (d5), and 8 (d8) post-infection (p.i.) we mapped the changes in open chromatin regions (OCRs) and ARID1A binding sites in donor P14 cells using Assay for Transposase-Accessible Chromatin sequencing (ATAC-seq)[139] and CUT&RUN[140], respectively. In parallel, to assess even earlier changes we performed ATAC-seq on 48-hour *in vitro* activated P14 cells. We defined 5 OCR clusters corresponding to regions that are unique or conserved across differentiation timespace: (1) **Conserved-** OCRs conserved at all timepoints (n=21650), (2) **Naive-** OCRs unique to naive T cells (n=3157), (3) **Early Activation-** OCRs more selectively found at day 3 p.i. *in vivo* or 48h post-activation *in vitro* (n=7883), (4) **Activation-** OCRs open in all activated cells (n=8781), or (5) **Late Activation-** OCRs predominantly found at day 5 and day 8 p.i. *in vivo* effector timepoints (n=1250) (**Figures 3.2 A-C**). ARID1A binding was highly enriched at OCRs and correlated with the dynamics of open chromatin across the time course of activation (**Figures 3.2 A**, **D; Figure 3.8 A**). Cluster annotations revealed that nearly half of Conserved sites align to promoters, while OCRs that were either lost or gained during

activation were more frequently found at intergenic and intronic regions (**Figure 3.2 C**). Consistent with the notion that enhancer rather than promoter accessibility patterns are the predominant determinants of cellular states[141], OCRs that opened and closed upon $CD8^+$ T cell activation were predominantly found in enhancers as defined by H3K4me1, H3K27ac[142], while promoter-specific H3K4me3 was more strongly enriched at Conserved OCRs than activation-induced OCRs (**Figure 3.2 E**). In general, regions with increased chromatin accessibility annotated to genes with increased gene expression and vice versa whereas regions with unchanging chromatin accessibility exhibited little changes in gene expression (**Figure 3.8B**).

TF motif analysis on the five OCR clusters revealed a specific enrichment of HMG motifs (TCF, LEF) in Naive OCRs, while AP-1 (bZIP) motifs were enriched in Early and general Activation OCRs, and the nuclear receptor (NR) and T-box motifs were enriched in the Activation and Late Activation OCRs (**Figure 3.2 F; Figure 3.8C**). Next, we overlapped physical TF binding patterns from naive, *in vitro* activated[143,144], and *in vivo* day 7 $CD8^+$ effector cells[145] with our peak clusters (**Figure 3.2 G**). TF binding of ETS1, TCF1 and RUNX1 in naive cells was primarily restricted to Conserved and Naive OCRs with some binding in Late Activation OCRs, while binding of most TFs including BATF, IRF4, and T-bet strongly overlapped with Early Activation (*in vitro* activated cells) and Activation (*in vitro* activated and *in vivo* d7 cells) induced OCRs. Together, these data outline the temporal kinetics of newly formed enhancers in differentiating virus-specific $CD8^+$ T effector cells and demonstrate that these sites are associated with ARID1A-containing cBAF complexes and distinct sets of TFs at different phases of effector cell differentiation. These findings imply that the cBAF complex plays a central role in shaping

the chromatin accessibility landscape and differentiation process in antiviral effector $CD8^+$ T cells.

Figure 3.2 **Differentiating antiviral effector CD8$^+$ T cells exhibit highly dynamic accessible chromatin and cBAF occupancy patterns.** (A) Signal tracks of ATAC-seq, ARID1A C&R, H3K27ac ChIP-Seq and H3K4me1 ChIP-Seq (GSE89036) in naïve, 48h *in vitro* activated, or d3, d5, or d8 P14 CD8$^+$ T cells from LCMV-Armstrong infection. (B) ATAC-seq signal coverage and (C) annotation of OCRs from clusters in A. (D-G) Using the OCRs from clusters in (A) we correlated those with ARID1A binding (D), histone modifications to define enhancers (E), predicted TF motif enrichment (F) and actual TF binding (observed/expected) of the indicated TFs from public datasets (GSE54191, GSE192390, GSE166718) (G).

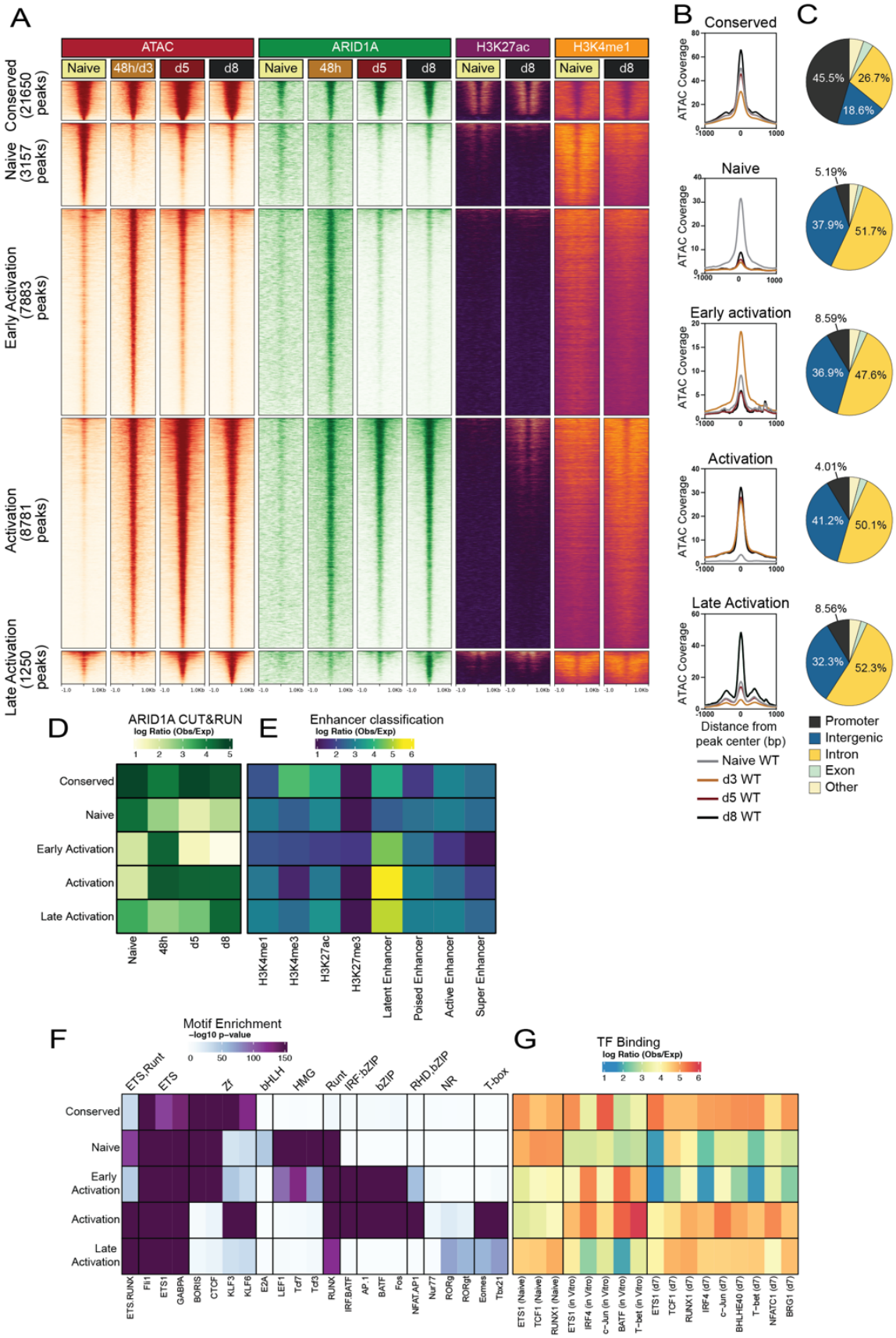
A
ATAC
ARID1A
H3K27ac
H3K4me1
Naive
48h/d3
48h
d5
d8
Conserved (21650 peaks)
Naive (3157 peaks)
Early Activation (7883 peaks)
Activation (8781 peaks)
Late Activation (1250 peaks)
B
Conserved
Naive
Early activation
Activation
Late Activation
ATAC Coverage
Distance from peak center (bp)
Naive WT
d3 WT
d5 WT
d8 WT
C
45.5%
26.7%
18.6%
5.19%
37.9%
51.7%
8.59%
36.9%
47.6%
4.01%
41.2%
50.1%
8.56%
32.3%
52.3%
Promoter
Intergenic
Intron
Exon
Other
D
ARID1A CUT&RUN
log Ratio (Obs/Exp)
Conserved
Naive
Early Activation
Activation
Late Activation
E
Enhancer classification
log Ratio (Obs/Exp)
H3K4me1
H3K4me3
H3K27ac
H3K27me3
Latent Enhancer
Poised Enhancer
Active Enhancer
Super Enhancer
F
Motif Enrichment
−log10 p−value
ETS:Runt
ETS
Zf
bHLH
HMG
Runt
IRF-bZIP
bZIP
RHD,bZIP
NR
T-box
ETS:RUNX
Fli1
ETS1
GABPA
BORIS
CTCF
KLF3
KLF6
E2A
LEF1
Tcf7
Tcf3
RUNX
IRF:BATF
AP-1
BATF
Fos
NFAT:AP1
Nur77
RORg
RORgt
Eomes
Tbx21
G
TF Binding
log Ratio (Obs/Exp)
ETS1 (Naive)
TCF1 (Naive)
RUNX1 (Naive)
ETS1 (in Vitro)
IRF4 (in Vitro)
c−Jun (in Vitro)
BATF (in Vitro)
T−bet (in Vitro)
ETS1 (d7)
TCF1 (d7)
RUNX1 (d7)
IRF4 (d7)
c−Jun (d7)
BHLHE40 (d7)
T−bet (d7)
NFATC1 (d7)
BRG1 (d7)

3.3.2 *Arid1a* promotes clonal expansion and opening of activation-induced enhancers

To elucidate the function of ARID1A-containing cBAF in activated CD8$^+$ cells while avoiding developmental defects seen with early T cell *Arid1a* deletions[84,86], we crossed *Arid1a*$^{fl/fl}$ mice with *Gzmb-Cre*$^+$ mice (in which Cre is conditionally active after T cell activation) with *Arid1a*$^{fl/fl}$ mice to generate *Gzmb-Cre*$^+$ *Arid1a*$^{fl/+}$ (*Arid1a*^{cKO}) and *Gzmb-Cre*$^+$ *Arid1a*$^{fl/+}$ (*Arid1a*^{cHet}) mice[102]. *Gzmb-Cre*$^-$ *Arid1a*$^{fl/fl}$ or *Gzmb-Cre*$^-$ *Arid1a*$^{fl/+}$ mice were used as wild-type (WT) littermate controls. We further crossed these mice with P14 TCR transgenic mice (*Arid1a*^{cKO} P14). We then transferred 25,000 wild-type (WT) or *Arid1a*^{cKO} P14 CD8$^+$ T cells into naive congenic recipient mice and infected those mice with LCMV-Armstrong to induce acute viral infection. We confirmed the loss of ARID1A protein in virus-specific CD8$^+$ T cells within 72h of activation *in vivo* using flow cytometry (**Figure 3.9A**).

Clonal expansion of *Arid1a*^{cKO} cells was slightly impaired (~3-fold) early during the expansion phase (day 5 p.i.) and more strongly impaired (~7-fold) at the peak of the effector response (day 8 p.i.) **(Figure 3.3 A**). P14 CD8$^+$ T cells electroporated with Cas9 *Arid1a* sgRNA ribonucleoproteins (RNP) similarly expanded less robustly relative to control RNP electroporated cells (**Figure 3.9 B**). In line with these findings, *Arid1a*^{cKO} cells proliferated slower relative to WT cells as observed using CellTrace violet staining at day 3 p.i. (**Figure 3.3 B**). Deletion of *Arid1a* in endogenous effector CD8$^+$ T cells coincided with ~10X higher LCMV titers at day 5 p.i. compared to the *Arid1a*^{cHet} and WT mice (**Figure 3.9 C**), but then titers were undetectable in all mice by d8 p.i. (data not shown). However, *Arid1a* deletion had little impact on the numbers of memory CD8$^+$ T cells that

formed in the spleen 30-60 days p.i. (**Figures 3.3 A and 3.9 B**). Thus, there was a strong dependence on ARID1A for the initial effector cell expansion phase, but not for contraction and seeding of the circulating memory pool.

To interrogate how ARID1A-dependent cBAF complexes control chromatin remodeling and enhancer accessibility during $CD8^+$ T cell differentiation we performed ATAC-seq on WT, *Arid1a*^{cHet}, and *Arid1a*^{cKO} P14 cells at d3, d5, and d8 p.i. and assessed chromatin accessibility at the five OCR clusters defined in **Figure 3.2 A**. As early as day 3 p.i. *Arid1a*^{cKO} cells exhibited defects in chromatin accessibility in ~30-40% (n=2020) of the OCRs in the Early and Activation clusters (**Figures 3.3 C-E**). By days 5 and 8 p.i., the KO effector cells showed greater loss in ~40-60% (n=4766 (d5), 2789 (d8)) of the Activation and ~30-40% (n=435 (d5), 350 (d8)) of Late Activation OCRs (**Figures 3.3 C-E**). Several of these OCRs map to activation-induced genes, including effector-associated TFs, *Bhlhe40*, *Tbx21* (T-bet), *Zeb2*, and *Batf* (**Figure 3.9 D**). Sites with reduced accessibility in KO cells were also depleted of H3K27ac deposition indicating that cBAF promotes histone acetyltransferase activity at the enhancers it remodels (**Figure 3.3 F**). In contrast, accessibility in Conserved OCRs was not affected by *Arid1a*-deficiency (**Figures 3.3 C-E**), suggesting that although ARID1A was bound to these promoters and other sites (**Figures 3.2 A, D**), it was not necessary for maintaining their accessibility. These data demonstrate that cBAF is necessary for the initial opening and/or maintenance of thousands of activation-induced enhancers created during effector $CD8^+$ T cell differentiation.

We next assessed transcriptional changes of d3 early effector WT and KO cells and identified 534 genes significantly lower and 595 genes higher in *Arid1a*^{cKO} cells

compared to WT cells (**Figure 3.3 G**). Interestingly, *Arid1a*^{cKO} cells are markedly deficient in the expression of several effector-associated TFs, including *Bhlhe40*, *Tbx21* (T-bet), *Zeb2*, and *Batf*, but expressed higher levels of naive-associated TFs like *Maf*, *Myb*, and *Tcf7* (**Figure 3.3 H**). Gene set enrichment analysis (GSEA)[146] revealed a strong decrease in Hallmark MYC target genes in *Arid1a*^{cKO} cells (**Figure 3.3 I**), including *Myc*, *Srm*, and *Dusp2*, as well as other critical regulators of murine T lymphocyte function and cell growth, *Tfrc* (CD71) and *Slc7a5* (CD98) (**Figure 3.3 H**)[127]. Additionally, several genes encoding cyclin-dependent kinase inhibitors including *Cdkn1b, Cdkn2d*, *Cdkn2a* were more highly expressed in *Arid1a*^{cKO} cells, which together with decreased *Myc* expression may explain the reduced proliferative rate (**Figure 3.3 B**). Overall, these data indicate that ARID1A acts early in CD8^{+} T cell activation to establish OCRs at the enhancers of key T cell differentiation genes, including driver TFs. Failure to open these enhancers and achieve optimal gene expression leads to an overall dampening of early effector CD8^{+} T cell expansion and differentiation and likely many downstream deficiencies in the activation of subsequent OCRs and late-stage effector differentiation programs.

Figure 3.3 **Differentiating antiviral effector CD8$^+$ T cells exhibit highly dynamic accessible chromatin and cBAF occupancy patterns.** (A) Signal tracks of ATAC-seq, ARID1A C&R, H3K27ac ChIP-Seq and H3K4me1 ChIP-Seq (GSE89036) in naïve, 48h *in vitro* activated, or d3, d5, or d8 P14 CD8$^+$ T cells from LCMV-Armstrong infection. (B) ATAC-seq signal coverage and (C) annotation of OCRs from clusters in A. (D-G) Using the OCRs from clusters in (A) we correlated those with ARID1A binding (D), histone modifications to define enhancers (E), predicted TF motif enrichment (F) and actual TF binding (observed/expected) of the indicated TFs from public datasets (GSE54191, GSE192390, GSE166718) (G).

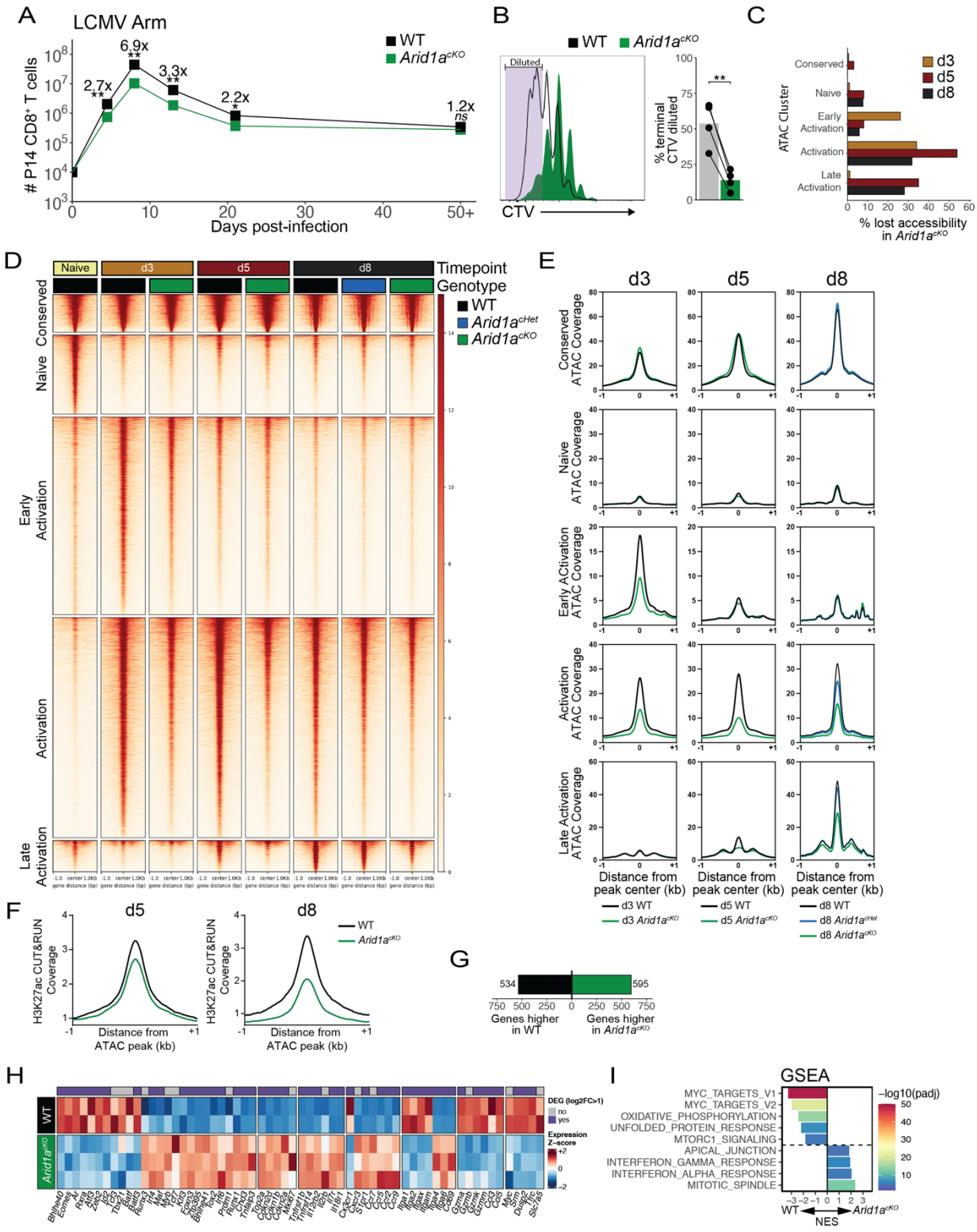
A
LCMV Arm
WT
Arid1a^cKO
P14 CD8+ T cells
Days post-infection
6.9x
3.3x
2.7x
2.2x
1.2x
ns
B
WT
Arid1a^cKO
Diluted
CTV
% terminal CTV diluted
C
ATAC Cluster
Conserved
Naive
Early Activation
Activation
Late Activation
d3
d5
d8
% lost accessibility in Arid1a^cKO
D
Naive
d3
d5
d8
Timepoint
Genotype
WT
Arid1a^cHet
Arid1a^cKO
Conserved
Naive
Early Activation
Activation
Late Activation
E
d3
d5
d8
Conserved ATAC Coverage
Naive ATAC Coverage
Early ACtivation ATAC Coverage
Activation ATAC Coverage
Late Activation ATAC Coverage
Distance from peak center (kb)
d3 WT
d3 Arid1a^cKO
d5 WT
d5 Arid1a^cKO
d8 WT
d8 Arid1a^cHet
d8 Arid1a^cKO
F
d5
d8
H3K27ac CUT&RUN Coverage
Distance from ATAC peak (kb)
WT
Arid1a^cKO
G
534
595
Genes higher in WT
Genes higher in Arid1a^cKO
H
WT
Arid1a^cKO
DEG (log2FC>1)
no
yes
Expression Z-score
I
GSEA
MYC_TARGETS_V1
MYC_TARGETS_V2
OXIDATIVE_PHOSPHORYLATION
UNFOLDED_PROTEIN_RESPONSE
MTORC1_SIGNALING
APICAL_JUNCTION
INTERFERON_GAMMA_RESPONSE
INTERFERON_ALPHA_RESPONSE
MITOTIC_SPINDLE
–log10(padj)
WT
Arid1a^cKO
NES

3.3.3 *Arid1a* acts in a dose-dependent manner to specify effector subsets

To understand how cBAF regulates the formation of different specialized effector subtypes we first compared WT and *Arid1a*^{cKO} effector cells at 8 days p.i. by flow cytometry and found that the *Arid1a*^{cKO} cells contained very few KLRG1^{+} and CX3CR1^{hi} cells and were skewed towards a CD127^{hi} MP-like phenotype[7] (**Figures 3.4 A-B)**, indicating that terminal effector differentiation was impaired but that cells retained similar potential to give rise to a long-lived circulating memory cell pool. Similar results were obtained in P14 cells in which *Arid1a* was deleted via Cas9 RNP as well as comparing WT and *Arid1a*^{cKO} endogenous, polyclonal LCMV-specific effector CD8^{+} T cells (**Figures 3.10 A-C**). Between 5-20% of KLRG1^{+} CD127^{lo} TE cells, but not EEC or MP cells, retained ARID1A expression, suggesting the strict requirement for ARID1A for TE differentiation selects for Cre recombinase escapers (**Figures 3.10 D-E**). *Arid1a*^{cHet} cells displayed an intermediate TE/MP phenotype between that of WT and KO cells (**Figures 3.4 A-B**), indicating that ARID1A acts in a dose-dependent manner to promote effector cell fates. *Arid1a*^{cKO} effector cells mounted similar cytokine responses as WT cells after GP_{33-41} peptide stimulation, but produced significantly less IFNγ after stimulation by IL-12 and IL-18 and expressed lower levels of granzyme A (**Figures 3.10 F-G**). As T-bet is a critical inducer of TE cells[10,147], we measured T-bet expression (**Figures 3.4 C-D; Figure 3.10 H**) and observed ~50% lower T-bet protein in *Arid1a*^{cKO} cells compared to WT cells, consistent with a reduction in *Tbx21* transcripts at d3 (**Figure 3.3 H**). Together, these results indicated that ARID1A-dependent cBAF is needed to permit the differentiation of TE cells, and in the absence of ARID1A, activated T cells fail to upregulate T-bet and preferentially acquired EEC- and MP-like differentiation states.

We next performed bulk RNA-seq on FACS-purified KLRG1^{+} CD127^{lo} (TE), KLRG1^{-} CD127^{lo} (EEC), and KLRG1^{-} CD127^{hi} (MP) subsets from WT, *Arid1a*^{cHet,} and *Arid1a*^{cKO} cells at d8 p.i. Principal component analysis (PCA) revealed that the majority of transcriptional variation was explained by the underlying donor cell genotype, and secondarily by subset, indicating that *Arid1a*^{cHet} and *Arid1a*^{cKO} subsets are transcriptionally distinct from their WT cell counterparts (**Figures 3.4 E-F**). Differential gene expression analysis revealed that 446 TE, 779 EEC, and 986 MP genes were downregulated and 597 TE, 973 EEC, and 679 MP genes were upregulated in *Arid1a*^{cKO} cells relative to WT cells (**Figure 3.4 F**). DEGs in *Arid1a*^{cHet} cells (downregulated: 61 TE, 151 EEC, 99 MP; upregulated: 75 TE, 150 EEC, 65 MP) were almost entirely a subset of those affected in *Arid1a*^{cKO} cells.

Across all effector subsets, *Arid1a*^{cKO} cells expressed lower levels of several TFs (*Tbx21*, *Zeb2*, *Eomes*, *Zfp683*, *Bhlhe40*), trafficking and adhesion molecules (*Cx3cr1*, *S1pr1, Itga1*, *Itga4*) and NK cell-associated genes (*Klrk1* (NKG2D), *Klrc1* (NKG2A)) relative to the WT cells (**Figure 3.4 G**). Conversely, *Arid1a*^{cKO} cells expressed higher levels of TFs (*Irf4, Myb*, *Maf*, *Batf3*), chemokine receptors (*Ccr9, Ccr7, Ccr5*) and the cytokine *Il21*. In general, *Arid1a*^{cHet} cells had an intermediate gene expression phenotype between WT and *Arid1a*^{cKO} cells, except for a small number of genes (*Klrc2, Klra1, Klra4, Lrp6*) that exhibited ectopic expression in *Arid1a*^{cHet} cells, but not in *Arid1a*^{cKO} cells (**Figure 3.4 G**). Additionally, *Cxcr3* gene expression and CXCR3 protein was reduced in *Arid1a*^{cHet} cells but increased in the *Arid1a*^{cKO} cells (**Figures 3.4 A, G**). Analysis of TE- and MP-signature genes within the individual subsets showed that several TE-signature genes such as *Tbx21, S1pr5, Cx3cr1, Zeb2, GzmA,* and *Klrg1* were downregulated and

several MP-signature genes like *Tcf7, Id3, Cxcr3* were upregulated in *Arid1a*^{cKO} KLRG1^{+} CD127^{lo} TE cells relative to WT TE cells (**Figure 3.4 H**). Indeed, GSEA showed that *Arid1a*^{cKO} TE cells were enriched with a more MP-like transcriptional signature relative to WT TE cells (**Figure 3.4 I**). The failure to activate TE-signature genes and repress MP-signature genes was also observed in the *Arid1a*^{cKO} KLRG1^{-} CD127^{lo} EECs (**Figures 3.4 G-H**). Conversely, comparison of WT and *Arid1a*^{cKO} KLRG1^{-} CD127^{hi} cells revealed aberrant expression patterns of both MP- and TE-signature genes in *Arid1a*^{cKO} MP cells (**Figures 3.4 G-H**). Specifically, *Arid1a*^{cKO} MP cells expressed higher levels of MP-signature genes like *Ccr7* and *Slamf6* and TE-signature genes like *Prdm1, Gzmk, GzmB* and *Ccr5*, but lower levels of other MP-signature genes like *Gzmm* and *Aqp9* (**Figures 3.4 G-H**). In general, the *Arid1a*^{cKO} cells shared gene expression patterns similar to those observed in *Tbx21* KO[148] and *Runx3* KO CD8^{+} T cells[149] (**Figure 3.4 I**). These data reveal that loss of *Arid1a* has profound effects on the ability of activated CD8^{+} T cells to properly engage canonical effector and memory gene expression programs and that *Arid1a* is haploinsufficient for the expression of many of these genes.

Figure 3.4 ***Arid1a* acts in a dose-dependent manner to specify effector subset gene expression patterns** (A,B) Surface marker expression of WT (black, n=11), *Arid1a*^{cHet} (blue, n=7), and *Arid1a*^{cKO} (green, n=7) P14 cells at d8-9 p.i. was analyzed by flow cytometry (A) and mean ± SEM frequencies of TE (KLRG1^{+}CD127^{-}), MP (KLRG1^{-}CD127^{+}), KLRG1^{+}CX$_3$CR1^{+}, KLRG1^{+}CXCR3^{-}, and KLRG1^{-}CXCR3^{+} cells are shown in bar graphs (B). (C,D) T-bet expression in WT and *Arid1a*^{cKO} P14 cells at d3 p.i. (D) Paired t-test. (E-I) WT, *Arid1a*^{cKO} and *Arid1a*^{cHet} effector cells were isolated at d8 p.i. and sorted based on expression of TE, EEC and MP markers as defined in (A) and differentially expressed genes (DEGs) were identified by RNA-seq. Principal component analysis plot of all the samples (E), number of DEGs (F), heatmap of select DEGs (G), volcano plots of all DEGs including highlighted TE-signature genes (red) and MP-signature genes (blue) (H), and GSEA (I) were used to assess the DEGs in each subset affected by loss of one or two copies of *Arid1a*. GSEA analysis in (I) directly compared DEGs between WT and *Arid1a*^{cKO} cells and previously published datasets: Activated vs Naive: GSE10739; d2.5TbetKO: PRJNA547650; Batf3OE vs EV: GSE143504; Runx3KO: GSE81888; d8BRD4KO: GSE173515). *ns*, not significant; *p<0.05, **p<0.005, ***p<0.0005.

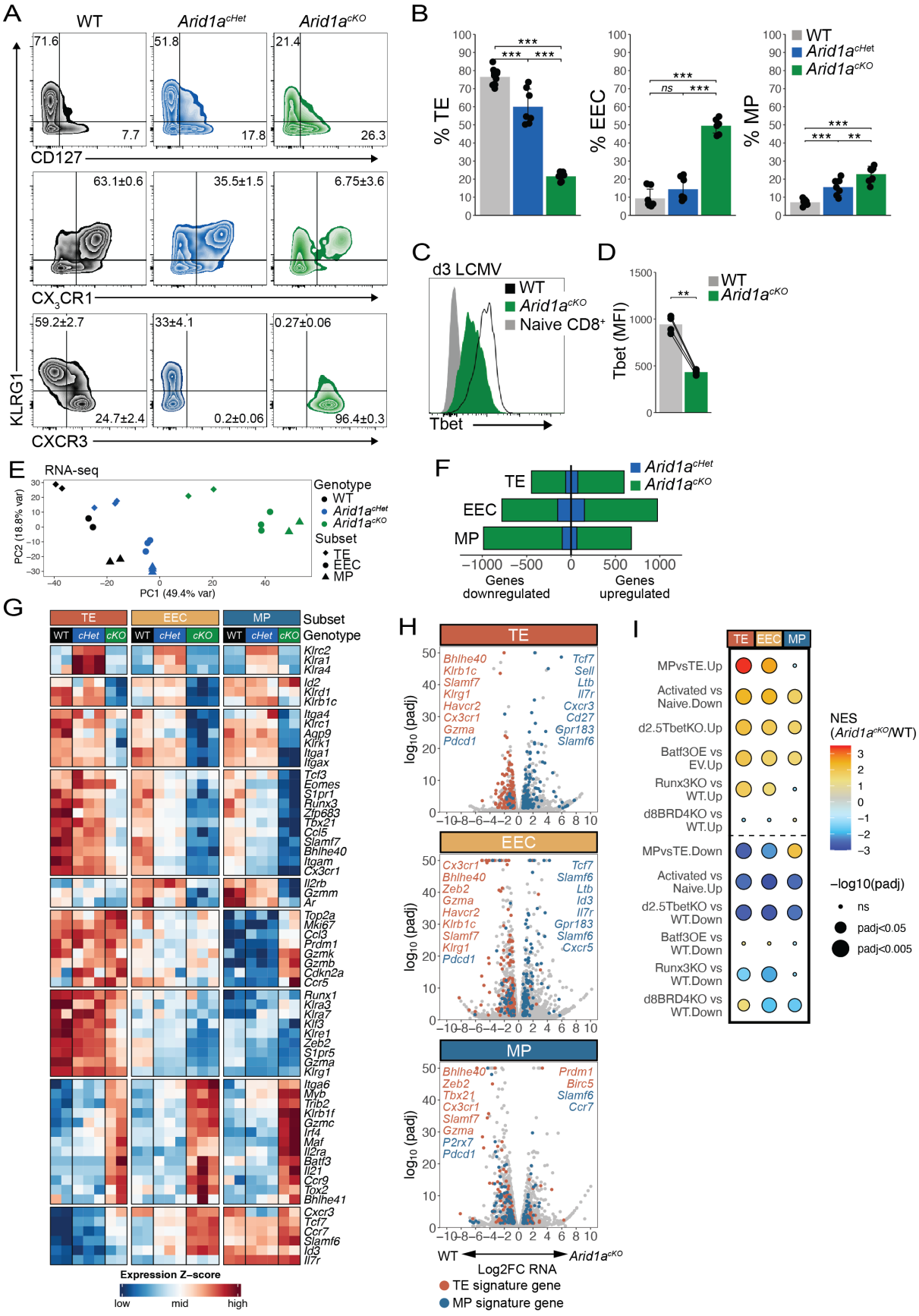
A
WT
Arid1a^cHet
Arid1a^cKO
71.6
7.7
51.8
17.8
21.4
26.3
CD127
63.1±0.6
35.5±1.5
6.75±3.6
CX3CR1
59.2±2.7
24.7±2.4
33±4.1
0.2±0.06
0.27±0.06
96.4±0.3
KLRG1
CXCR3
B
% TE
% EEC
% MP
WT
Arid1a^cHet
Arid1a^cKO
***
ns
**
C
d3 LCMV
WT
Arid1a^cKO
Naive CD8+
Tbet
D
Tbet (MFI)
E
RNA-seq
PC2 (18.8% var)
PC1 (49.4% var)
Genotype
Subset
TE
EEC
MP
F
Genes downregulated
Genes upregulated
G
Subset
Genotype
Expression Z-score
low
mid
high
H
log10 (padj)
Log2FC RNA
TE signature gene
MP signature gene
I
MPvsTE.Up
Activated vs Naive.Down
d2.5TbetKO.Up
Batf3OE vs EV.Up
Runx3KO vs WT.Up
d8BRD4KO vs WT.Up
MPvsTE.Down
Activated vs Naive.Up
d2.5TbetKO vs WT.Down
Batf3OE vs WT.Down
Runx3KO vs WT.Down
d8BRD4KO vs WT.Down
NES (Arid1a^cKO/WT)
−log10(padj)
ns
padj<0.05
padj<0.005

3.3.4 *Arid1a*-dependent OCRs in d8 effector cells are largely shared across subsets

To better understand how *Arid1a* regulates gene expression and cell fate specification of $CD8^+$ T cells, we analyzed OCRs in TE, EEC and MP subsets from WT, $Arid1a^{cHet}$, and $Arid1a^{cKO}$ cells at d8 p.i. PCA revealed that the principal source of variation in global chromatin accessibility was dictated by donor cell genotype rather than subset (**Figure 3.5 A**). Critically, comparison of differential OCRs between WT and $Arid1a^{cKO}$ subsets showed that nearly all differential OCRs lost accessibility in $Arid1a^{cKO}$ cells whereas only a fraction of sites gained accessibility (**Figure 3.5 B**), indicating that the primary function of cBAF in activated $CD8^+$ T cells is to create and/or maintain OCRs through nucleosome remodeling. Analysis of $Arid1a^{cHet}$ cells showed a statistically significant loss (≥2-fold) of chromatin accessibility at ~1000 sites, all of which were also affected in $Arid1a^{cKO}$ cells, and essentially no gains (**Figures 3.5 B-C**). Additionally, nearly every OCR significantly lost in $Arid1a^{cKO}$ cells displayed a substantial reduction in accessibility in the $Arid1a^{cHet}$ cells (**Figure 3.5 C**), indicating that the level of accessibility is sensitive to the dosage of cBAF activity, which has clinical relevance to T cell lymphoma where *Arid1a* haploinsufficiency is commonly observed[89]. Next, we compared the differential OCRs between TE, EEC and MP subsets to see if loss of *Arid1a* affected one subset more than another. *Arid1a*-deficiency impaired the opening of 12,260 OCRs in TE cells, which helps to explain the lack of TE development in the $Arid1a^{cKO}$ cells, but surprisingly, even more OCRs (EEC n=16400, MP n=15110) were affected in the EEC- and MP-like subsets (**Figures 3.5 B, D**). Further, of the OCRs lost in the $Arid1a^{cKO}$ d8 effector subsets, the majority were common to all three subsets (n=7802) whereas a

minority were subset-specific (TE n=2169, EEC n=2843, MP n=2943) (**Figure 3.5 D**). Together, these data demonstrate that although *Arid1a*-deficiency preferentially impaired the formation of KLRG1^{+} TE cells, there was no biased requirement for cBAF activity in any one subset. Rather, all three subsets required cBAF to create thousands of enhancers both common to and uniquely found in each subset, and loss of cBAF activity resulted in aberrant gene expression patterns and differentiation states in all three subsets.

It is well established that accessibility of *cis*-regulatory elements strongly correlates with gene expression. Indeed, we found that many DEGs in EEC, TE and MP cells also lost OCR accessibility in the absence of ARID1A (**Figure 3.5 E**). We focused on the expression of TE- and MP-signature genes within each subset and as predicted there was a strong requirement for *Arid1a* for both the accessibility and expression of TE- and MP-signature genes in all the subsets (although, by definition, the expression of TE-signature genes in MP cells was considerably lower than in TE cells and *vice versa* (see **Figure 3.4 G**)). Most *Arid1a*-dependent OCRs that were annotated to genes downregulated in *Arid1a*^{cKO} vs. WT cells had reduced H3K27ac, as exemplified by *Tbx21*, *Bhlhe40*, *Zfp683*, and *Prdm1* (**Figures 3.5 F; Figure 3.11 A**). Interestingly, we also observed loss of chromatin accessibility at sites annotated to genes that were upregulated in *Arid1a*^{cKO} EEC, TE, and MP cells (**Figure 3.5 E**, lower right quadrants), including many MP-signature genes. At such loci (e.g. *Sell*, *Ccr7*, *Cd9*, and *Tcf7*), H3K27me3 was reduced in *Arid1a*^{cKO} EEC and TE cells suggesting that ARID1A promotes Polycomb-dependent silencing of MP-signature genes in these subsets (**Figures 3.11 B**). Collectively, these data indicate that ARID1A is required in a dose-dependent manner to

generate chromatin accessibility at shared and subset-specific OCRs induced during $CD8^+$ T cell differentiation. Failure to generate these accessible regions in *Arid1a*^{cKO} cells impairs their ability to properly activate 'pro-effector' genes and regulate 'pro-memory' genes, perhaps due to a loss in the binding of TFs and epigenetic modifiers with activating and repressive regulatory properties at ARID1A-dependent accessible sites.

Figure 3.5 **ARID1A-dependent OCRs in d8 MP, EEC, and TE cells are largely shared across subsets**. WT, *Arid1a*^{cKO} and *Arid1a*^{cHet} effector cells were isolated at d8 p.i. and sorted based on expression of TE, EEC and MP markers as defined in Figure 3A and differential OCRs were compared by ATAC-sequencing (2-fold change, adjusted p value<0.05, Benjamini-Hochberg). (A) Principal component analysis plot of ATAC-seq from WT, *Arid1a*^{cHet}, and *Arid1a*^{cKO} subsets at d8 post-infection. (B) Number of OCRs lost and gained in *Arid1a*^{cKO} and *Arid1a*^{cHet} subsets relative to WT cells. (C-D) ATAC-seq signal heatmaps of WT, *Arid1a*^{cHet}, and *Arid1a*^{cKO} d8 subsets. OCRs are clustered by whether they are lost in the *Arid1a*^{cKO} relative to WT cells in individual subsets or lost in all three subsets (C) and UpSet plot shows the number of shared and subset-specific OCRs lost in *Arid1a*^{cKO} subsets relative to WT cells (D). (E) Gene expression and paired chromatin accessibility of annotated OCRs in *Arid1a*^{cKO} and WT d8 subsets. TE- and MP-signature genes are highlighted in blue and red, respectively. (F) H3K27ac CUT&RUN signal coverage centered on ARID1A-dependent ATAC-seq peaks in WT vs. *Arid1a*^{cKO} cells TE, EEC, and MP cells.

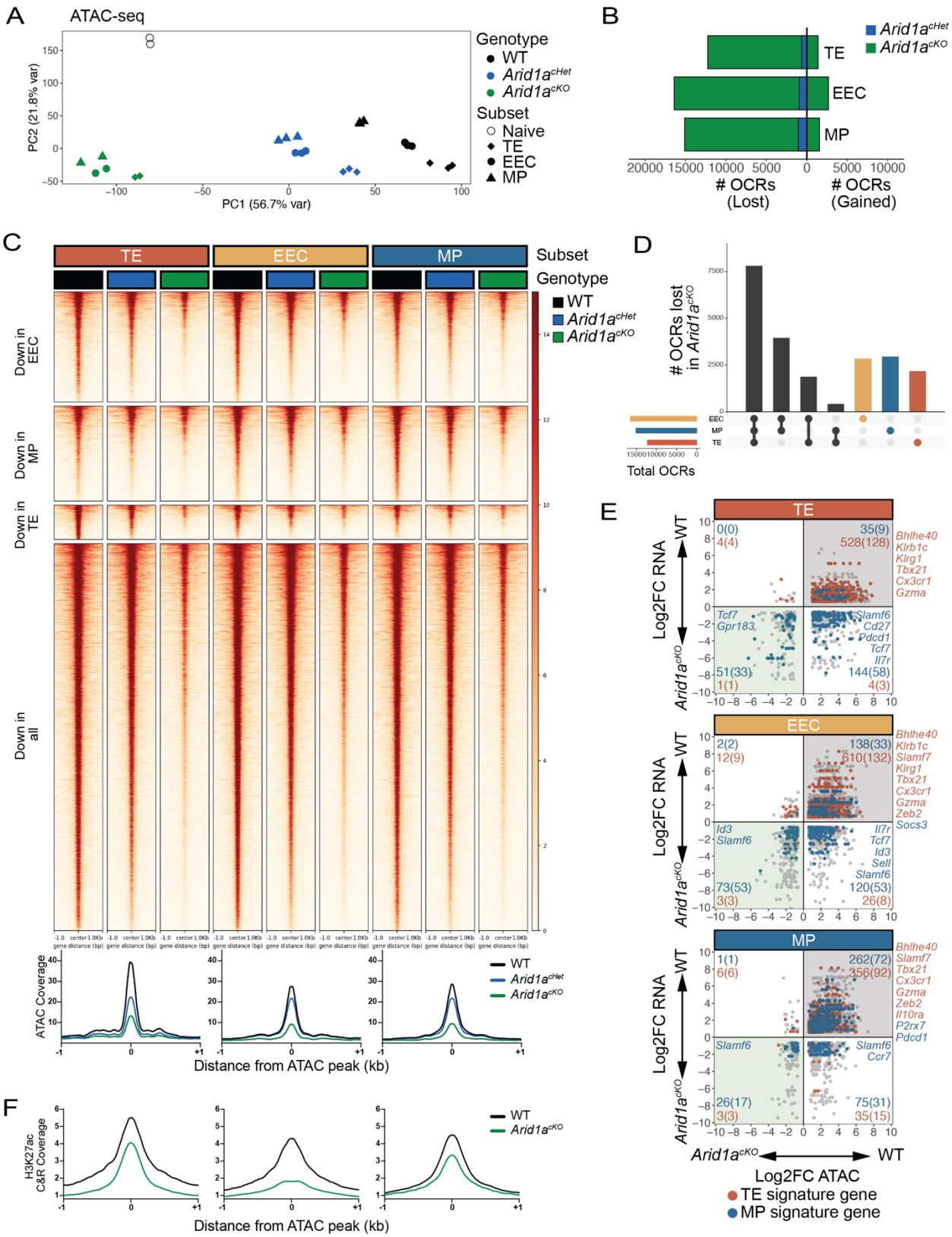
A
ATAC-seq
PC2 (21.8% var)
PC1 (56.7% var)
Genotype
WT
Arid1a^cHet
Arid1a^cKO
Subset
Naive
TE
EEC
MP
B
Arid1a^cHet
Arid1a^cKO
TE
EEC
MP
OCRs (Lost)
OCRs (Gained)
C
TE
EEC
MP
Subset
Genotype
Down in EEC
Down in MP
Down in TE
Down in all
ATAC Coverage
Distance from ATAC peak (kb)
D
OCRs lost in Arid1a^cKO
Total OCRs
E
Log2FC RNA
Log2FC ATAC
TE signature gene
MP signature gene
F
H3K27ac C&R Coverage
Distance from ATAC peak (kb)

3.3.5 cBAF is required for targeting of T-bet to enhancers in effector CD8$^+$ T cells

To determine which TFs were most dependent on ARID1A activity, we performed TF motif enrichment on the ARID1A-dependent OCRs for each d8 effector subset. This revealed an enrichment of ETS, Runt, bZIP, T-box, and other TF family motifs, suggesting that binding sites for these factors may be less accessible in *Arid1a*-deficient effector cells, while CTCF motifs were enriched among gained sites (**Figure 3.6 A**). In support of this, binding of FOSL2, EOMES, BATF, and T-bet[144] was selectively and highly enriched at ARID1A-dependent, but not ARID1A-independent OCRs (**Figure 3.6 B**). To directly examine how certain TFs were affected by ARID1A deficiency we performed CUT&RUN on WT and *Arid1a*^{cKO} d5 effector cells against ETS1, BATF, and T-bet (representing ETS, bZIP, and T-box family members) and mapped their binding at ARID1A-dependent and -independent OCRs (**Figure 3.6 C**). This showed a significant and strong reduction in ETS1, BATF, and T-bet binding at ARID1A-dependent OCRs, while ETS1 and BATF binding was less affected at ARID1A-independent OCRs. T-bet binding was universally affected genome-wide, likely because of both reduced T-box motif availability and reduced T-bet expression. The TF binding sites most affected by ARID1A-deficiency were predominantly found at intergenic and intronic sites (*i.e.*, enhancers), whereas those bound to ARID1A-independent sites were more frequently annotated to promoters (**Figure 3.6 C**). These data demonstrate that cBAF-dependent remodeling is predominantly required in activated CD8$^+$ T cells to create enhancers that allow the binding of many key TFs that in turn, govern the gene regulatory networks controlling effector and memory CD8$^+$ T cell differentiation.

However, a potential caveat in the experiments above is that the defects in TF binding could stem from several alterations in the ARID1A-deficient cells including reduced expression of certain TFs. Therefore, to bypass some of these confounding issues we used a model of acute disruption of cBAF subunits in *in vitro* activated T cells with ACBI1[150], a PROTAC targeting BRG1, BRM, and PBRM1, or BRM014[151], an allosteric ATPase inhibitor of BRG1 and BRM. P14 $CD8^+$ T cells were activated *in vitro* for 48 hours and then treated with either DMSO or ACBI1/BRM014 for 4h prior to 2h treatment with IL-12 to enhance T-bet expression and binding, after which the cells were collected for T-bet ChIP-seq and ATAC-seq. This revealed that BAF complexes were required to maintain chromatin accessibility at ~7500 sites following BAF disruption (**Figures 3.6 D-E**) and T-bet binding was selectively reduced at these sites. In contrast, T-bet binding was preserved or enhanced at BAF-independent OCRs (**Figures 3.6 D-E**). Again, cBAF-dependent T-bet binding sites were almost universally annotated to intronic and intergenic elements, while cBAF-independent sites were more highly enriched for promoters (**Figure 3.6 F**). These data indicate that ATP-dependent cBAF complex remodeling is acutely required to maintain T-bet binding at enhancers in activated $CD8^+$ T cells.

To further assess how T-bet and cBAF may cooperate, we compared the OCRs between WT or *Tbx21* KO P14 $CD8^+$ T cells at d8 p.i. and found that *Tbx21*-deficiency resulted in reduced and gained accessibility at several thousand sites (**Figure 3.12 A**). Notably, the majority of sites that lost accessibility in *Tbx21* KO cells also lost accessibility in *Arid1a*^{cKO} cells (n=2531, 90.4% (TE); n=3285, 76.1% (MP) (**Figure 3.6 G**), and ARID1A binding was strongly reduced in *Tbx21* KO cells at these T-bet/ARID1A co- dependent

OCRs (**Figure 3.6 H**), strongly suggesting that T-bet engages ARID1A to promote accessibility at this subset of activation-induced OCRs. Finally, we tested if the requirement for cBAF to generate TE cells could be overridden by T-bet over-expression. To this end, we over-expressed T-bet in WT or *Arid1a*^{cKO} P14 cells and transferred them into mice infected with LCMV-Armstrong. Intriguingly, T-bet overexpression was unable to restore the ability of *Arid1a*^{cKO} cells to form TE cells (**Figure 3.6 I; Figure 3.12 B**), indicating that higher levels of T-bet are insufficient to compensate for the loss of cBAF activity due to decreased enhancer accessibility. Furthermore, while T-bet overexpression led to a significant enhancement of T-bet binding in WT cells, the stark inability of T-bet to bind chromatin in *Arid1a*^{cKO} cells was essentially unaltered by T-bet overexpression (**Figure 3.6 J**), indicating that T-bet is completely reliant on ARID1A to make its binding sites accessible. Collectively, these data demonstrate that cBAF is critical for establishing and maintaining accessibility of thousands of enhancers and binding of several effector-associated TFs, particularly T-bet, in activated CD8^{+} T cells. Further, while T-bet is necessary and sufficient to induce TE cell differentiation, this activity is entirely reliant on ARID1A.

Figure 3.6 **cBAF is required for targeting of T-bet to enhancers in effector CD8$^+$ T cells**. (A-B) As described in Figure 4, OCRs (2-fold change, adjusted p value<0.05, Benjamini-Hochberg) lost in *Arid1a*^{cKO} d5 effector cells or d8 TE, EEC, and MP subsets relative to WT cells were analyzed for enrichment of predicted TF motifs (A) or TF binding signals (observed/expected) of indicated TFs from public ChIP-seq datasets (GSE192390) in ARID1A-dependent (green) and -independent (gray) OCRs (B). (C) Genomic annotations and CUT&RUN signal heatmaps of ARID1A, BATF, ETS1, and T-bet at ARID1A-dependent or -independent OCRs from WT and *Arid1a*^{cKO} effector P14 CD8$^+$ T cells d5 post-infection. (D-F) CD8$^+$ T cells were activated *in vitro* for 48hrs and then treated with DMSO (black, red), ACBI1 (green) or BRM014 (purple) for 4 hours, and then treated with IL-12 (red, green, purple) for 2 hours, and analyzed for changes in ATAC-seq and T-bet binding by ChIP-seq. Signal coverage heatmaps of ATAC-seq and T-bet ChIP-seq (D) and histograms measuring chromatin accessibility (E) are shown. (F) Genomic annotations of ACBI1-dependent and -independent ATAC-seq OCRs. (G) Overlap of OCRs lost relative to WT (2-fold change, adjusted p value<0.05, Benjamini-Hochberg) in *Arid1a*^{cKO} or *Tbx21* KO TE and MP cells. (H) ARID1A CUT&RUN signal heatmap in WT or *Tbx21* KO effector cells at d5 p.i. Signal is centered on ARID1A- or Tbet-dependent OCR peaks identified in (G). (I) Retroviral overexpression of T-bet fails to rescue TE formation in *Arid1a*^{cKO} cells at d8 p.i. (J) T-bet CUT&RUN signal coverage histograms at Activation and Late Activation OCRs in WT or *Arid1a*^{cKO} cells transduced with either empty vector (EV) or T-bet overexpression (Tbet-OE) retrovirus at d5 p.i.*p<0.05, **p<0.005, ***p<0.0005.

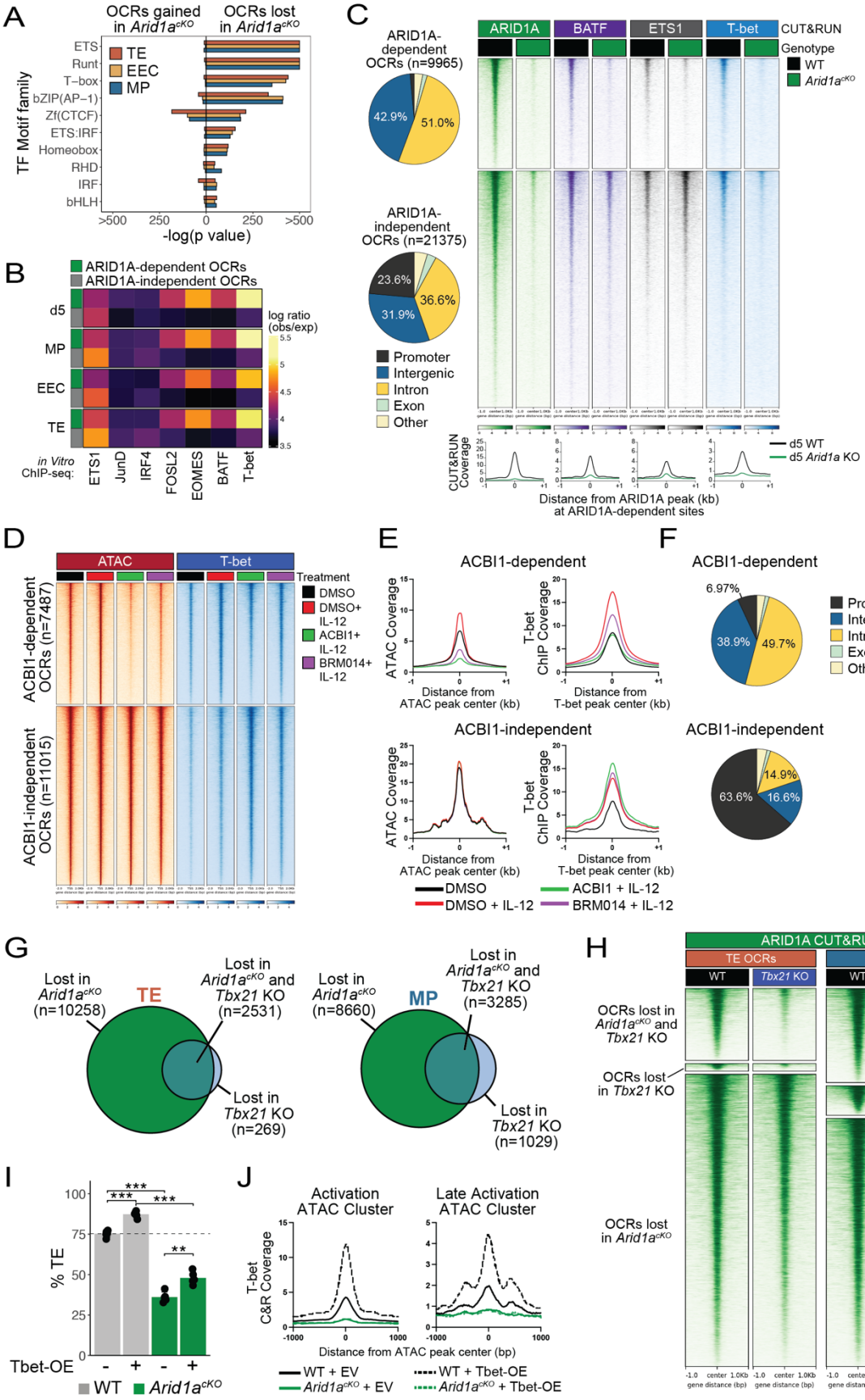
A
OCRs gained in Arid1a^cKO
OCRs lost in Arid1a^cKO
TF Motif family
ETS
Runt
T−box
bZIP(AP−1)
Zf(CTCF)
ETS:IRF
Homeobox
RHD
IRF
bHLH
TE
EEC
MP
>500
250
0
250
>500
-log(p value)
B
ARID1A-dependent OCRs
ARID1A-independent OCRs
d5
MP
EEC
TE
log ratio (obs/exp)
5.5
5
4.5
4
3.5
in Vitro ChIP-seq:
ETS1
JunD
IRF4
FOSL2
EOMES
BATF
T-bet
C
ARID1A-dependent OCRs (n=9965)
42.9%
51.0%
ARID1A-independent OCRs (n=21375)
23.6%
36.6%
31.9%
Promoter
Intergenic
Intron
Exon
Other
ARID1A
BATF
ETS1
T-bet
CUT&RUN
Genotype
WT
Arid1a^cKO
CUT&RUN Coverage
d5 WT
d5 Arid1a KO
Distance from ARID1A peak (kb) at ARID1A-dependent sites
D
ATAC
T-bet
Treatment
DMSO
DMSO+ IL-12
ACBI1+ IL-12
BRM014+ IL-12
ACBI1-dependent OCRs (n=7487)
ACBI1-independent OCRs (n=11015)
E
ACBI1-dependent
ATAC Coverage
Distance from ATAC peak center (kb)
T-bet ChIP Coverage
Distance from T-bet peak center (kb)
ACBI1-independent
DMSO
DMSO + IL-12
ACBI1 + IL-12
BRM014 + IL-12
F
ACBI1-dependent
6.97%
38.9%
49.7%
Promoter
Intergenic
Intron
Exon
Other
ACBI1-independent
14.9%
63.6%
16.6%
G
Lost in Arid1a^cKO (n=10258)
TE
Lost in Arid1a^cKO and Tbx21 KO (n=2531)
Lost in Tbx21 KO (n=269)
Lost in Arid1a^cKO (n=8660)
MP
Lost in Arid1a^cKO and Tbx21 KO (n=3285)
Lost in Tbx21 KO (n=1029)
H
ARID1A CUT&RUN
TE OCRs
MP OCRs
WT
Tbx21 KO
OCRs lost in Arid1a^cKO and Tbx21 KO
OCRs lost in Tbx21 KO
OCRs lost in Arid1a^cKO
I
% TE
Tbet-OE
WT
Arid1a^cKO
J
Activation ATAC Cluster
Late Activation ATAC Cluster
T-bet C&R Coverage
Distance from ATAC peak center (bp)
WT + EV
Arid1a^cKO + EV
WT + Tbet-OE
Arid1a^cKO + Tbet-OE

3.3.6 *Arid1a* is critical for CD8$^+$ T_{RM} formation

Our results demonstrated that similar numbers of WT and *Arid1a*^{cKO} memory CD8$^+$ T cells formed in the spleen following LCMV-Armstrong infection, yet the genetic and epigenetic analysis of MP-like cells revealed several alterations in the *Arid1a*^{cKO} cells. Therefore, to more broadly understand how *Arid1a* affected memory T cell development we computationally predicted the TFs most functionally impacted in MP cells by *Arid1a*-deficiency using the Taiji PageRank algorithm that assesses the global influence of TFs in a given cell state[152]. This analysis identified ZFP683, BHLHE40, RUNX3, RXRA and SMAD3 in addition to T-bet and EOMES as top-ranked TFs whose activity is predicted to be impaired in *Arid1a*^{cKO} MP cells (**Figure 3.7 A; Figure 3.13 A**). This was noteworthy because ZFP683, BHLHE40, and RUNX3 are critical to the formation of tissue-resident memory (Trm) cells[62,64,65] and indeed, MP cells required ARID1A for promoting expression of both *Zfp683* and *Bhlhe40*, as well as increasing accessibility and H3K27ac deposition at *cis*-regulatory elements for both genes (**Figure 3.4 G; Figure 3.11 A**). Furthermore, GSEA showed significant similarity between the DEGs in *Arid1a*^{cKO} and *Runx3* KO cells (**Figure 3.4 I**). These data prompted us to compare the numbers and types of WT and *Arid1a*^{cKO} memory CD8$^+$ T cells that form in lymphoid vs. non-lymphoid organs. In the spleen, we observed similar numbers of circulating WT and *Arid1a*^{cKO} TCM and TEM cells (**Figure 3.7 B**); however, fewer CD127^{lo} terminal TEM (t-TEM) cells were present in the *Arid1a*^{cKO} cells as expected given that this population descends from TE cells[10,153]. Circulating *Arid1a*^{cKO} memory cells were also less proficient in cytokine production after restimulation *ex vivo* (**Figure 3.7 C; Figure 3.13 B**) and failed to undergo terminal effector differentiation following secondary heterologous infection (**Figure 3.7 D**),

indicating that despite being dispensable for circulating memory cell formation, ARID1A was required for preserving critical memory cell antiviral functions. *Arid1a*^{cKO} memory cells also expressed higher levels of TCF1 (**Figure 3.7 E**). In contrast to the spleen, in the peripheral tissues such as the liver, small intestine intraepithelial layer (SI-IEL) and salivary gland (SG), there was a profound reduction in the number of Trm cells in the *Arid1a*^{cKO} memory cells relative to the WT controls (**Figure 3.7 F; Figure 3.13 C**). Further, the memory cells found in the SI-IEL and SG lacking *Arid1a* failed to upregulate several canonical features of T_{RM}, including CD103, CD49a (**Figure 3.7 G; Figure 3.13 D**), and Granzyme B (**Figure 3.7 H**), while expression of CD69 and Granzyme A were comparable with WT T_{RM} expression levels (**Figure 3.7 G; Figure 3.13E**). *Arid1a*^{cKO} cells infiltrated into the small intestine at slightly lower rates early during infection (**Figure 3.13 F**), suggesting that the initial seeding of tissues also contributes to, but does not fully account for the diminished T_{RM} pool. Interestingly, as seen in the circulating memory T cells in the spleen (**Figure 3.7 E**), *Arid1a*^{cKO} T_{RM} maintained high expression of TCF1 (**Figure 3.7 I**), a known suppressor of T_{RM} formation[154]. This is in spite of the fact that TCF1 was similarly repressed in WT and *Arid1a*^{cKO} early effector cells in both lymphoid tissues and in the SI-IEL (**Figure 3.13 G**). However, cBAF activity was seemingly required to sustain repression of TCF1 as effector cells underwent further effector cell diversification (**Figure 3.13 H**). Taken together, these results demonstrate that despite observing normal numbers of circulating memory CD8$^+$ T cells, *Arid1a* is required in progenitor cells to open key loci that permit the cells to enter tissues and respond to local cues that induce T_{RM} properties. In summary, we have mapped how cBAF remodels chromatin in virus-specific CD8$^+$ T cells during the first week of infection by creating thousands of enhancers that

recruit TFs to cooperatively drive gene expression programs that govern the multitude of effector and memory differentiation states.

Figure 3.7 **ARID1A is critical for T_{RM} formation**. (A) PageRank and mRNA expression analysis of *Arid1a*^{cKO} and WT MP cells from d8 p.i. (B) Absolute numbers of WT (n=8) and *Arid1a*^{cKO} (n=8) P14 splenic memory cells at d30-d60 p.i. (C) Representative cytokine production in WT (n=4) and *Arid1a*^{cKO} (n=4) memory P14 cells in the spleen at d60 p.i. Mean frequency of IFNg^{+}TNF^{+} (top) and IFNg^{+}CCL3^{+} (bottom) populations are shown. (D) Frequency of KLRG1+CD127 or KLRG1+CX3CR1+ secondary effector cells day 8 p.i. following LM-GP33 infection in mice that previously received CD127+ WT and Arid1acKO LCMV memory P14 cells. (E) TCF1 staining in WT and Arid1acKO CD127hi spleen memory cells at day 50 p.i. (F) Absolute numbers of WT and Arid1acKO P14 cells in the liver (n = 7) and SI-IEL (n = 7) at days 50–60 p.i. (G) Representative flow cytometry plots of WT and Arid1acKO P14 SI-IELs at day 60 p.i. Mean frequency of CD69+CD103+ (top) and CD49a+CD103+ (bottom) populations are shown. (H and I) Granzyme B (H) and TCF1 (I) staining in WT and Arid1acKO P14 SI-IELs at day 60 p.i. Paired t test; *p < 0.05, **p < 0.005, ***p < 0.0005.

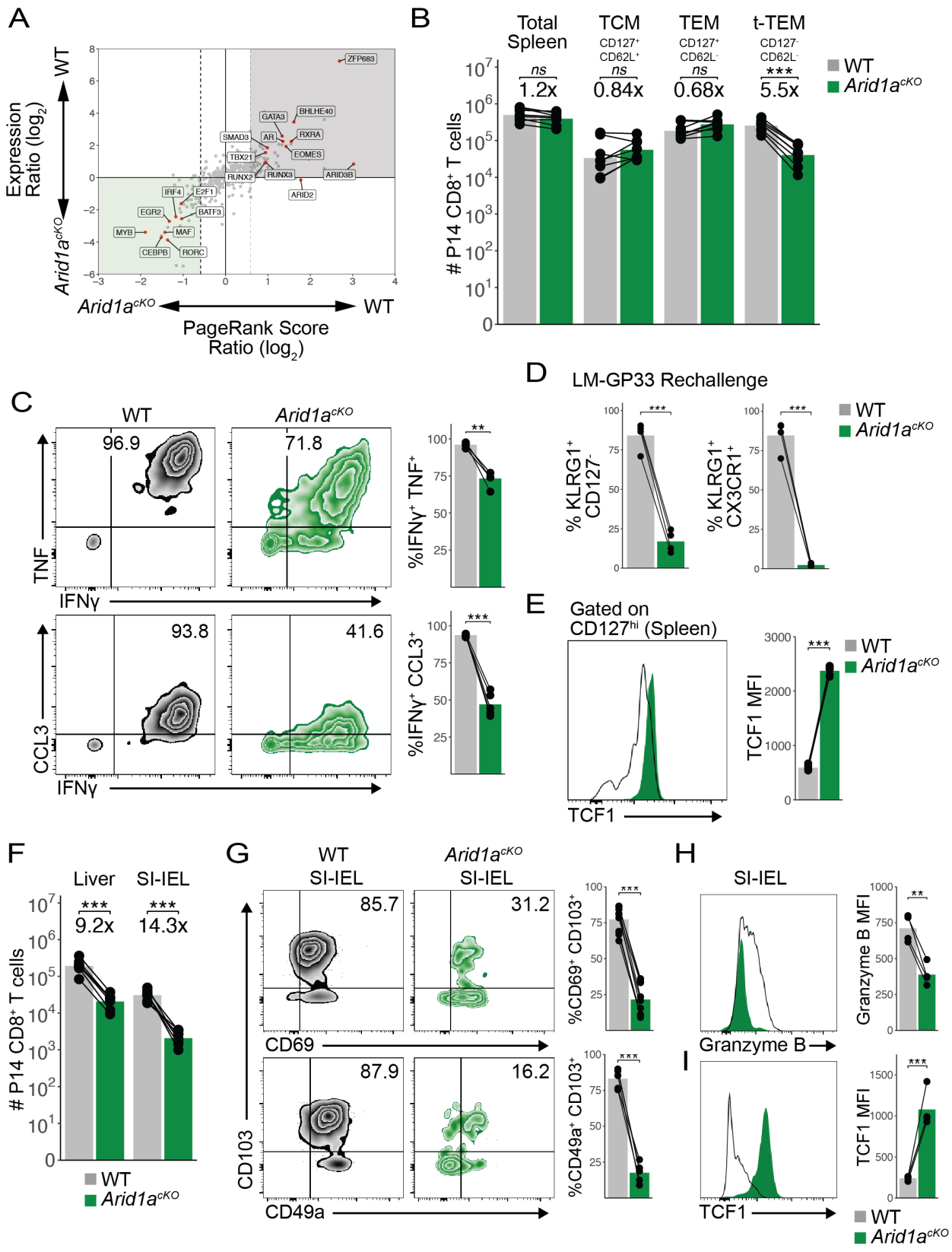
A
Expression Ratio (log2)
WT
Arid1acKO
ZFP683
BHLHE40
GATA3
SMAD3
AR
RXRA
EOMES
TBX21
RUNX2
RUNX3
ARID3B
ARID2
IRF4
E2F1
EGR2
BATF3
MYB
MAF
CEBPB
RORC
Arid1acKO
WT
PageRank Score Ratio (log2)
B
Total Spleen
TCM CD127+ CD62L+
TEM CD127+ CD62L-
t-TEM CD127- CD62L-
ns
1.2x
ns
0.84x
ns
0.68x
***
5.5x
P14 CD8+ T cells
WT
Arid1acKO
C
WT
Arid1acKO
96.9
71.8
TNF
IFNγ
93.8
41.6
CCL3
IFNγ
**
%IFNγ+ TNF+
***
%IFNγ+ CCL3+
D
LM-GP33 Rechallenge
***
% KLRG1+ CD127-
***
% KLRG1+ CX3CR1+
WT
Arid1acKO
E
Gated on CD127hi (Spleen)
TCF1
***
TCF1 MFI
WT
Arid1acKO
F
Liver
SI-IEL
***
9.2x
***
14.3x
P14 CD8+ T cells
WT
Arid1acKO
G
WT SI-IEL
Arid1acKO SI-IEL
85.7
31.2
CD69
87.9
16.2
CD103
CD49a
***
%CD69+ CD103+
***
%CD49a+ CD103+
H
SI-IEL
Granzyme B
**
Granzyme B MFI
I
TCF1
***
TCF1 MFI
WT
Arid1acKO

3.4 Discussion

Effector CD8$^+$ T cell differentiation is a progressive process that occurs over several days to weeks[155], with the earliest known cell fate imprinting events occurring as early as the first cell division[31]. This process is critical to host defense as it generates several types of effector and memory cells that work cooperatively to protect the host from the current infection as well as from future infections. Over the past 15 years the field has discovered many TFs that control the formation of effector and memory CD8$^+$ T cells, but what we don't understand very well is '*how these TFs find their binding sites to regulate target gene expression and T cell differentiation?*' The purpose of this study was to characterize how TF binding sites become accessible within activated CD8$^+$ T cells during an immune response by nucleosome remodeling machinery, like the cBAF complex, to govern the spectrum of effector and memory differentiation states produced.

To address this question, we profiled open chromatin profiles over the first week of infection and found that activated CD8$^+$ T cells simultaneously lose accessibility of naive-associated sites while gaining thousands of activation-induced sites in a time-dependent fashion. Loss of cBAF activity strongly prevented the gain of accessibility at activation-induced sites as early as 48-72 hours post activation *in vivo*, in agreement with a recent report[32]. However, the loss of naive-associated sites upon T cell activation was not affected by cBAF-deficiency. Most ARID1A-dependent OCRs were annotated as enhancers, and indeed many of these sites required ARID1A to become decorated with H3K27ac and enhance transcriptional activation, indicating that cBAF predominantly shapes the enhancer landscape in activated CD8$^+$ T cells. In contrast, several pro-memory genes like *Tcf7*, *Cd9*, *Sell*, and *Ccr7* that become epigenetically silenced via

PRC2 (H3K27me3) in late-stage TE cells[18,68] had reduced H3K27me3 and were derepressed in the absence of ARID1A. Notably, cBAF directly antagonizes PRC1, resulting in the redistribution of PRC2 upon deletion/disruption of cBAF subunits, impacting H3K27me3 levels and gene expression both positively and negatively[156–161]. While PRC2 activity is targeted selectively to many pro-memory genes as the effector cells terminally differentiate and lose memory cell potential[18,68,142,162], the mechanism of targeting is unclear. Further dissection of the OCRs and TFs that regulate PRC2 targeting in activated $CD8^+$ T cells will illuminate whether cBAF-dependent remodeling is required for the binding of TFs and associated repressors at these sites, particularly for enhancers bound by TE-inducing TFs, such as T-bet, ZEB2, and Blimp-1[147,163–165], that help to silence such pro-memory loci to enforce terminal differentiation in TE cells.

Our study revealed how cBAF regulates the binding potential of TF families (e.g. ETS, Runt, bZIP, T-box) at enhancers, but not promoters, in activated $CD8^+$ T cells during the first week of infection. Reduced TF binding in *Arid1a*^{cKO} cells can be attributed to a combination of both reduced binding site availability and reduced TF expression. For example, overexpression of T-bet, a factor necessary and sufficient for TE formation, was unable to restore TE differentiation in *Arid1a*-deficient cells that lacked accessible binding sites. Furthermore, pharmacological cBAF disruption in effector cells reduced both chromatin accessibility and T-bet binding within hours, suggesting that cBAF is also required to maintain late-stage TF activity, consistent with recent reports that loss of chromatin accessibility is observed within minutes of acute BAF degradation[166,167]. Given the importance of sustained activity by TFs such as FOXO1 for the active maintenance of long-lived memory cells[109], future work is thus needed to understand the role of

continuous cBAF activity in maintaining the longevity and functional competency of effector and memory T cells.

In the absence of ARID1A, activated $CD8^+$ T cells were defective in developing into TE cells, but not circulating TEM or TCM cells. A recent publication from Guo *et al.*[32] similarly found *Arid1a* was important for TE cell formation, but in contrast to our findings, they suggested that disruption of cBAF *enhanced* the formation of memory T cells while we observed no significant difference in memory cells numbers. These differences may be attributed to differences in the timing of *Arid1a* deletion, or incomplete deletion or generation of *Arid1a* heterozygous cells in the CRISPR KO setting. Given that they propose a potential translational application of treating activated $CD8^+$ T cells with BAF inhibitors (BD98) to generate more tenacious anti-tumor T cells for adoptive cell therapy, it is worth emphasizing that our study illuminated that ARID1A-deficient memory precursor cells were epigenetically and transcriptionally aberrant and lacked thousands of enhancers. Moreover, our data indicate that ARID1A-deficient effector and memory cells were less proficient at cytokine production and expressed lower levels of Granzyme A, suggesting potential deficiencies in functionality and cytotoxicity. Therefore, ARID1A is evidently dispensable for some aspects of memory cell differentiation (e.g. clonal expansion of IL-$7R^+$ MP-like cells) during LCMV infection, but it is necessary for other key functions and most importantly, for the establishment of tissue residency as elaborated below.

A major finding from our study, which was not explored in Guo *et al.*, is that ARID1A was needed for T_{RM} cell development in non-lymphoid tissues after LCMV infection. Fewer $Arid1a^{cKO}$ cells initially infiltrated into the intestines and expressed lower levels of

tissue retention molecules, indicating that ARID1A promotes both trafficking into and survival within peripheral tissues. Further, intestinal *Arid1a*^{cKO} cells displayed decreased expression of T_{RM} -signature proteins CD103 and Granzyme B, indicating that these cells were developmentally less mature and likely less protective. Failure of *Arid1a*^{cKO} cells to efficiently form Trm several weeks after infection is likely a consequence of reduced expression of relevant TFs (e.g., *Zfp683*, *Bhlhe40*, *Runx3*) in addition to reduced binding motif accessibility. Runx3 promotes T_{RM} formation in non-lymphoid organs[65], but was downregulated in *Arid1a*^{cKO} MP cells, and the Runt (Runx1/2/3) motif is among those most profoundly lost in KO cells. Likewise, *Bhlhe40* was identified as a core Trm signature gene[65], and was strongly induced in WT effector cells but not in *Arid1a*^{cKO} cells. As was the case with T-bet, overexpression of any individual Trm-associated TF in *Arid1a*^{cKO} cells is unlikely to rescue the T_{RM} formation due to a lack of available binding sites, and because several non-redundant T_{RM}-associated TFs are simultaneously downregulated in these cells. Conversely, *Arid1a*^{cKO} T_{RM} expressed higher levels of TCF1, a factor known to suppress lung T_{RM} formation[154]. In line with these observations, we observed decreased H3K27me3 deposition at the *Tcf7* locus in effector *Arid1a*^{cKO} cells. TGFβ signaling suppresses *Tcf7* expression[154] and drives T_{RM} formation in many tissues[168], and therefore another possible explanation for reduced T_{RM} is that *Arid1a*^{cKO} cells fail to transmit TGFβ signals via SMAD2/3 binding to repress *Tcf7*, a hypothesis supported by the reduction in SMAD3 activity in MP cells as predicted by PageRank analysis. $CD8^+$ T_{RM} cells provide protection against mucosal infections[169] and have promising beneficial prognostic value in human tumors[170,171], therefore it will be critical to more carefully examine how BAF inhibitors modulate the differentiation states of TILs in more preclinical

models and human T cells as our data demonstrate cBAF is critical for acquisition of T_{RM} differentiation states.

Lastly, this work has high relevance to the understanding of lymphoma etiology because our analysis of *Arid1a*^{cHet} T cells revealed that cBAF operated in a dose-dependent manner to regulate both accessibility and effector cell differentiation states. Most *ARID1A* mutations in human cancers are heterozygous, and in particular, *ARID1A* hemizygosity is common to cutaneous T cell lymphoma[89]. Our data indicate that ARID1A heterozygosity affects accessibility at all sites sensitive to ARID1A loss, resulting in intermediate gene expression changes and cellular phenotypes relative to those of ARID1A-deficient cells. Future work is needed to determine what gene attributes confer sensitivity to ARID1A haploinsufficiency.

In summary, this study characterizes the dynamic regulation of the chromatin landscape in antiviral T cells *in vivo* through the lens of a chromatin remodeler and ascertains how DNA accessibility is created to orchestrate the transcriptional and epigenetic machinery that governs effector and memory CD8$^+$ T cell differentiation. We anticipate that ARID1A and cBAF carry out similar biological functions in effector CD4$^+$ T cells and other lymphocytes. Indeed, deletion of *Arid1a* or *Smarca4* at various stages of hematopoiesis revealed the critical nature of cBAF in driving development of essentially all hematopoietic lineages[84–86] as well as terminal differentiation of CD8$^+$ T cells[32,94,96] and regulatory T cells[172,173] in tumors. Further, most human pathogenic SNPs map to non-coding regions (i.e. enhancers)[174], implying individual enhancers may have a role in modulating gene expression and influencing cell states. This work thus provides data that may clarify the mechanistic basis for certain human immune-related diseases and

establishing new opportunities to fine-tune immune cell function via manipulation of cBAF activity in adoptive cell therapies.

3.5 Limitation of the study

Our study primarily relied on the use of Granzyme-B Cre to delete *Arid1a* after T cell activation, and thus we cannot infer what role cBAF may play in early activation (0-48h) events. Secondly, we focused our analysis on memory cells in the spleen and non-lymphoid organs, but it is possible that studying additional lymphoid organs (lymph nodes and bone marrow) may yield further insight into how cBAF more broadly shapes the circulating memory cell pool after infection. Lastly, while we know that cBAF promotes $CD8^+$ T cell expansion, differentiation, and expression of certain cytotoxic molecules (granzyme A) *in vivo*, we have not experimentally assessed whether cBAF is required for cytotoxic capacity.

3.6 Acknowledgement

Chapter 3, in full, is a reprint of the material as it appears in *Immunity* 2023. McDonald B, Chick BY, Ahmed NS, Burns M, Ma S, Casillas E, Chen D, Mann TH, O'Connor C, Hah N, Hargreaves DC, Kaech SM. The dissertation author was the primary investigator and author of this paper. We thank the Kaech lab for helpful discussion; N. Claffey, M. Liem at the Salk Flow Cytometry core. This work was supported by NIH grants F31HL158235 and F99CA274688 (B.M.), 5T32GM133351 (B.Y.C), 2T32CA009370 (N.S.A.), R37 AI066232 (to S.M.K.) and AI151123 (to D.C.H.), the Pew-Stewart Scholars for Cancer Research (D.C.H.), and the American Cancer Society Research Scholar Award (D.C.H.) as well as fellowships from the Cancer Research Institute (S.M.), Damon Runyon Cancer Research Foundation (T.M.), and the NOMIS Center (D.C.). Additional

support came from the Flow Cytometry Core Facility of the Salk Institute with funding from NIH-NCI CCSG: P30 014195 and Shared Instrumentation Grant S10-OD023689 (Aria Fusion cell sorter) and by the NGS Core Facility of the Salk Institute with funding from NIH-NCI CCSG: P30 014195, the Chapman Foundation and the Helmsley Charitable Trust.

3.7 Methods

3.7.1 Mice

C57BL/6J were purchased from Jackson Laboratories. P14 mice (Pircher et al., 1987) and Arid1a$^{fl/fl}$mice (Chandler et al., 2015) have been previously described. Arid1a$^{fl/fl}$ GzmB-Cre mice were generated by crossing P14 mice with Arid1a$^{fl/fl}$ and Gzmb-Cre mice. Both female and male mice were used for all studies. Animals were housed in specific-pathogen-free facilities at the Salk Institute. All experimental studies were approved and performed in accordance with guidelines and regulations implemented by the Salk Institute Animal Care and Use Committee.

3.6.2 Infections

Mice were infected with 2x10^5 PFU LCMV-Armstrong by intraperitoneal injection. For recombinant GP33-expressing *Listeria monocytogenes* (LM-GP33) infections, mice were injected with 5x10^4 CFU by retro-orbital injection under anesthesia. LCMV-Armstrong and LM-GP33 stocks were prepared as previously described (Kaech and Ahmed, 2001; Welsh and Seedhom, 2008).

3.6.3 Cell Isolation

Spleens, lymph nodes, and livers were mechanically dissociated with 1mL syringe plungers over a 70um nylon strainer. Livers were resuspended in 8mL 40% isotonic

percoll and centrifuged at 800g for 12 minutes at 20C. Spleens and livers were incubated in ammonium chloride potassium (ACK) buffer for 5 minutes. For isolation of small intestinal IEL, Peyer's patches were first removed by dissection. Intestines were longitudinally cut and then cut into 1cm pieces and washed in PBS. Pieces were incubated in 30mL HBSS with 10% FBS, 10mM HEPES, and 1mM dithioerythritol with vigorous shaking at 37C for 30 minutes. Supernatants were collected, washed, and further isolated using a 40/67% discontinuous percoll density centrifugation for 20 minutes at room temp with no brakes. Salivary glands were minced with scissors and incubated in RPMI with 5% FBS and 0.5mg/mL Collagenase IV, 0.1mg/mL DNAse1, and 2mM CaCl2 for 30 minutes at 37C with gentle shaking, and then strained over 70um nylon strainers.

3.6.4 Flow Cytometry and cell sorting

Cell suspensions were first incubated with eBioscience Fixable Viability Dye eFluor 780 for 5 minutes at room temp. Cells were stained with primary surface antibodies in PBS with 2% FBS, 0.1% NaN3 for 20 minutes on ice. For sorting, staining was performed in PBS with 2% FBS, 2mM EDTA, and 10mM HEPES. DAPI was added to stained cell suspensions at 0.1ug/mL prior to sorting. For experiments involving retroviral transduction, cells were fixed with Biolegend Fixation buffer for 20 minutes at room temp. For intracellular staining, cells were first fixed with eBioscience Foxp3/Transcription Factor Staining buffer fixation/permeabilization buffer for 30 minutes at room temp, and staining was performed in 1X permeabilization buffer for 30 minutes at room temp. Flow cytometry analysis samples were acquired on a BD Symphony A3. Cell sorting was performed on a BD FACSAria Fusion.

3.6.5 *In vitro* Stimulations and intracellular cytokine staining

Spleen cell suspensions were stimulated in complete RPMI (RPMI with 10% FBS, Pen/strep, L-glutamine, 50uM β-ME) in the presence of 0.1ng/mL GP_{33-41} peptide or DMSO and brefeldin A for 5 hours at 37C. For cytokine stimulations, cells were cultured for 5 hours with 10ng/mL recombinant mouse IL-12 and IL-18 without brefeldin A, at which point brefeldin A was added for 1 hour prior to staining. Cells were stained for viability and surface markers as described above, and then fixed/permeabilized with cytofix/cytoperm buffer (BD) for 25 minutes at room temp. Intracellular cytokine staining was performed in 1X permeabilization buffer (BD) for 30 minutes at room temp.

3.6.6 Adoptive T cell transfer

Naive WT, $Arid1a^{fl/+}$, or $Arid1a^{fl/fl}$ CD8+ P14 cells were isolated by negative selection with biotinylated antibodies against CD4, CD19, B220, MHCII, CD11b, CD11c, CD49b, and Ter119 in MACS buffer, and MojoSort beads were added at 5% v/v for 5 minutes before placing the cell suspension on a magnet and collecting the supernatant. $2.5x10^4$ P14 cells were injected into recipient mice 18-24 hours before infection. For 72h sorting experiments, $5x10^5$ P14 cells were transferred. For proliferation experiments, P14 cells were labeled with 5uM CTV (CellTrace Violet) in warm PBS for 8 minutes at 37C, and $1x10^6$ cells were transferred. For secondary infection experiments, splenocytes and peripheral LNs from 30d LCMV immune P14 chimeric mice were enriched for $CD127^+$ $CD8^+$ cells. Briefly, negative magnetic selection was performed with biotinylated antibodies against CD4, MHCII, Thy1.2, and KLRG1 in MACS buffer, and MojoSort beads were added at 5% v/v for 5 minutes before placing the cell suspension on a magnet and collecting the supernatant. WT and $Arid1a^{cKO}$ memory-enriched populations were mixed

to form a 1:1 ratio of WT and *Arid1a*^{cKO} P14 memory cells, and then 6x10^4 memory cells were transferred into naïve recipient mice prior to infection with 1x10^5 CFU of LM-GP33.

3.6.7 Retrovirus production and transduction

Tbet-MIGR1 was previously described (Joshi et al., 2007). Retrovirus was prepared by transfection of 293T cells with pCL-Eco and T-bet-MIGR1 or EV-MIGRs plasmids using XtremeGene9 transfection reagent. For transductions, P14 cells were stimulated for 18 hours with plate-bound 2ug/mL anti-CD3, 1ug/mL anti-CD28, and 20ng/mL human recombinant IL-2. Supernatant was removed from activated cells, and retroviral supernatants supplemented with polybrene (10ug/mL) were carefully overlayed onto cells, and then cells were centrifuged for 90 minutes at 1500g at 30C. Cells were incubated for 4h at 37C, washed, and adoptively transferred into recipient mice.

3.6.8 Cas9 RNP Electroporation

Cas9/sgRNA mixtures were prepared (0.6uL 62nM recombinant Cas9, 0.3nmol sgRNA, 3.5uL RNAse-free H2O) and incubated for 10 minutes at room temperature. 2-5x10^6 MACS-purified naive P14 cells were washed in PBS and suspended in 20uL supplemented P3 buffer (Lonza; 16.4uL P3 buffer and 3.6uL Supplement 1). Resuspended cells were immediately mixed with 5uL Cas9/sgRNA mixture and transferred to a Lonza nucleofector strip. Cells were electroporated using the program DN100. 130uL pre-warmed complete RPMI was added to cells prior to incubation for 10 minutes at 37C. Cells were washed extensively with complete RPMI prior to transfer into recipient mice. The sequences of sgRNA used to target *Arid1a*: UACCCAAAUAUGAAUCAAGG.

3.6.9 ATAC-Seq library preparation and sequencing

ATAC-seq was performed as previously described (Corces et al., 2017). Briefly, 5,000-50,000 viable cells were washed with cold PBS, collected by centrifugation, then lysed in resuspension buffer (RSB) (10 mM Tris-HCl, pH 7.4, 10 mM NaCl, 3 mM MgCl2) supplemented with 0.1% NP40, 0.1% Tween-20, and 0.01% digitonin. Samples were incubated on ice for 3 min, then washed out with 1 ml RSB containing 0.1% Tween-20. Nuclei were pelleted by centrifugation at 500g for 10 min at 4°C then resuspended in 50 ul transposition mix (25ul 2x TD buffer, 2.5 ul transposase (100 nM final), 16.5 ul PBS, 0.5 ul 1% digitonin, 0.5 ul 10% Tween-20, 5 ul H_2O) and incubated at 37°C for 30 min in a thermomixer with 1000 RPM mixing. DNA was purified using a Qiagen MinElute PCR cleanup kit, then PCR amplified using indexed oligos. The optimal number of amplification cycles for each sample was determined by qPCR. Libraries were size selected using AmpureXP beads and sequenced using an Illumina NextSeq500 for 75bp paired-end reads.

3.6.10 RNA-Seq library preparation and sequencing

Cells were FACS sorted directly into buffer RLT (Qiagen) supplemented with 2-mercaptoethanol and frozen at -80°C. Total RNA was isolated using a Qiagen RNeasy Plus Micro kit according to the manufacturer's instructions and quantified using an Agilent 4200 TapeStation. Purified RNA was library prepped using a SMART-Seq v4 Ultra Low Input RNA kit. Libraries were quantified and size distribution was determined before 51bp single-end sequencing was performed.

3.6.11 ChIP-seq library preparation and sequencing

Purified polyclonal $CD8^+$ T cells were activated with plate-bound 2ug/mL anti-CD3, 1ug/mL anti-CD28, and 20ng/mL human recombinant IL-2 for 48 hours. Cells were

collected and approximately $5x10^6$ cells each were treated with either 1μM ACBI1, 300nM BRM04, or 0.01% DMSO for 4 hours. Recombinant mouse IL-12p70 was added after 4 hours culture for an additional 2 hours. Cells were cross linked in 3 mM disuccinimidyl glutarate for 30 min then in 1% formaldehyde for 10 min at room temperature. After quenching with 125 mM glycine, the cells were washed in 1× PBS, pelleted, flash frozen in liquid nitrogen, and stored at 80 °C. Cell pellets were thawed on ice and incubated in lysis solution (50 mM Hepes KOH pH 8, 140 mM NaCl, 1 mM EDTA, 10% glycerol, 0.5% NP-40, and 0.25% Triton X-100) for 10 min. The isolated nuclei were washed (10 mM TrisHCl pH 8, 1 mM EDTA, 0.5 mM EGTA, and 200 mM NaCl) and sheared in (0.1% SDS, 1 mM EDTA, and 10 mM TrisHCl pH 8) with the Covaris E229 sonicator for 10 min. After centrifugation, chromatin was immunoprecipitated overnight at 4 °C with 1:50 T-bet/TBX21 (Cell Signaling Technology, mAb #97135S). The next day, the antibody-bound DNA was incubated with Protein A+G Dynabeads (Invitrogen) in ChIP buffer (50 mM Hepes KOH pH 7.5, 300 mM NaCl, 1 mM EDTA, 1% Triton X-100, 0.1% sodium deoxycholate, and 0.1% SDS), washed, and treated with Proteinase K and RNase A and reverse cross linked. Purified ChIP DNA was used for library generation (NEBNext Ultra II DNA Library Prep Kit for Illumina) according to manufacturer's instructions.

3.6.12 CUT&RUN library preparation and sequencing

CUT&RUN for murine T cells was performed as previously described (Meers et al., 2019) with modifications (van der Veeken et al., 2020). Briefly, 75-150k cells per sample were washed with PBS, counted, and collected in a V-bottom 96 well plate by centrifugation. Cells were washed once in antibody buffer (buffer 1 (1x permeabilization buffer from eBioscience Foxp3/Transcription Factor Staining Buffer Set diluted in

nuclease free water, 1X EDTA-free protease inhibitors, 0.5mM spermidine) containing 2mM EDTA), then incubated with antibodies for 1h on ice. After 2 washes in buffer 1, cells were incubated with pA/G-MNase at 1:4000 dilution in buffer 1 for 1h at 4 degrees. Cells were washed twice in buffer 2 (0.05% (w/v) saponin, 1X EDTA-free protease inhibitors, 0.5mM spermidine in PBS) and resuspended in calcium buffer (buffer 2 containing 2mM CaCl2) to activate the MNase fusion protein. Following a 30 minute incubation on wet ice, 2x stop solution (20mM EDTA, 4mM EGTA in buffer 2) was added and cells were incubated for 12 minutes in a 37 degree incubator to release cleaved chromatin fragments. Supernatants were collected by centrifugation and DNA was extracted using a Qiagen MinElute kit.

CUT&RUN libraries were prepared using a NEBNext Ultra II kit. Histone modification sample libraries were prepared according to the manufacturer's protocol, and protein factor samples were prepared according to a factor-specific protocol (Liu, 2021). Briefly, protein factor dA-tailing temperature was decreased to 50°C, and the reaction time was increased to 1 hour. After adaptor ligation, 2.1x volume of AMPure XP beads was added to the reaction to ensure high recovery efficiency of short fragments. After 10-12 cycles of PCR amplification, the reaction was cleaned up with 0.8x AMPureXP beads selection to remove PCR products >350bp, followed by a second round of 1.2X AMPureXP bead size-selection to remove PCR products shorter than 150bp. Barcoded libraries were quantified on an Agilent TapeStation and PCR dimers were removed with 1.2X AmpureXP bead size selection. Samples were mixed at equal molar ratios and pooled libraries were loaded to a NextSeq 300 High Output Kit v2 (150 cycles), and

sequenced in the NextSeq 300 platform. To enable determination of fragment length, paired-end sequencing was performed (2x42 bp, 6 bp index).

3.6.13 RNA-seq analysis

Single-end 51-bp reads were aligned to the *M. musculus* mm10 genome using STAR v2.5.3a (Dobin et al., 2013) with default parameters. RNA expression was quantified as raw integer counts using analyzeRepeats.pl in HOMER using the following parameters: -strand both -count exons -condenseGenes -noadj. Differentially expressed genes (DEGs) were identified with getDiffExpression.pl in HOMER using DESeq2 (Love et al., 2014) (cut-offs were set at log2 FC = 0.585 and false discovery rate (FDR) at 0.05 [Benjamini–Hochberg]). GSEA was performed on DEGs against HALLMARK gene sets. For GSEA enrichment plots, fgsea was used with 10,000 permutations = 10,000.

3.6.14 ATAC-Seq analysis

Paired-end 42-bp, or paired-end 75-bp reads were aligned to the *M. musculus* mm10 genome using STAR (Dobin et al., 2013) with default parameters. ATAC-seq peaks were called using the HOMER findPeaks program using parameters for DNAse-seq (-style dnase). Peaks were called when enriched >4.0-fold over local tag counts. Differentially accessible regions were identified using DESeq2 (Love et al., 2014) by calling getDifferentialPeaksReplicates.pl in HOMER with fold change ≥2.0 or ≤−2.0, FDR < 0.05. Peaks sets were annotated with HOMER, and visualizations were created using deepTools. *k*-means clustering of ATAC-seq data was performed using DESeq2. Signal heatmaps were generated using deepTools v3.5.1 (Ramírez et al., 2016).

3.6.15 ChIP-Seq analysis

Paired-end 75-bp reads were aligned to the *M. musculus* mm10 genome using STAR (Dobin et al., 2013) with default parameters. ChIP-seq peaks were called using findPeaks within HOMER using -style factor and an -i input control. Differential ChIP peaks were called using getDiffExpression.pl with fold change ≥ 1.5 or ≤ 1.5, Poisson P value < 0.0001. ChIP-seq peaks were annotated by mapping to the nearest transcription start site (TSS) using the annotatePeaks.pl program. Metaplots were generated using annotatePeaks.pl with parameters -size 2000 and -hist 10. Heatmaps showing overlap of binding sites were generated using mergePeaks in HOMER with flag -matrix, which outputs hypergeometric P values of overlap and the observed/expected ratio of overlap. Peaks sets were annotated with HOMER, and visualizations were created using deepTools.

3.6.16 CUT&RUN analysis

Similar to ChIP-seq analysis, paired-end 75-bp reads were aligned to the *M. musculus* mm10 genome using STAR (Dobin et al., 2013) with default parameters. Peaks were called with Sparse Enrichment Analysis for CUT&RUN (SEACR) with options -stringent and -norm against an IgG control sample (Meers et al., 2019). Metaplots were generated using annotatePeaks.pl with parameters -size 2000 and -hist 10. Heatmaps showing overlap of binding sites were generated using mergePeaks in HOMER with flag -matrix, which outputs hypergeometric P values of overlap and the observed/expected ratio of overlap. Peaks sets were annotated with HOMER, and visualizations were created using deepTools.

3.6.17 Transcription factor binding motif analysis

Sequences within 100 bp of peak centers were compared to known motifs in the HOMER database using the findMotifsGenome.pl (Heinz et al., 2010) command with default parameters. Random GC content-matched genomic regions were used as background. Enriched motifs are statistically significant motifs in input over background by a P value of less than 0.05 using a cumulative binomial distribution.

3.6.18 Quantification and statistical analysis

Statistical analyses were performed using the two-tailed, unpaired, Student's t-test unless otherwise specified. Each point represented a biological replicate and all data were presented as the mean ± SEM. The P values were represented as follows: *ns*, not significant, *p<0.05, **p<0.005, ***p<0.0005.

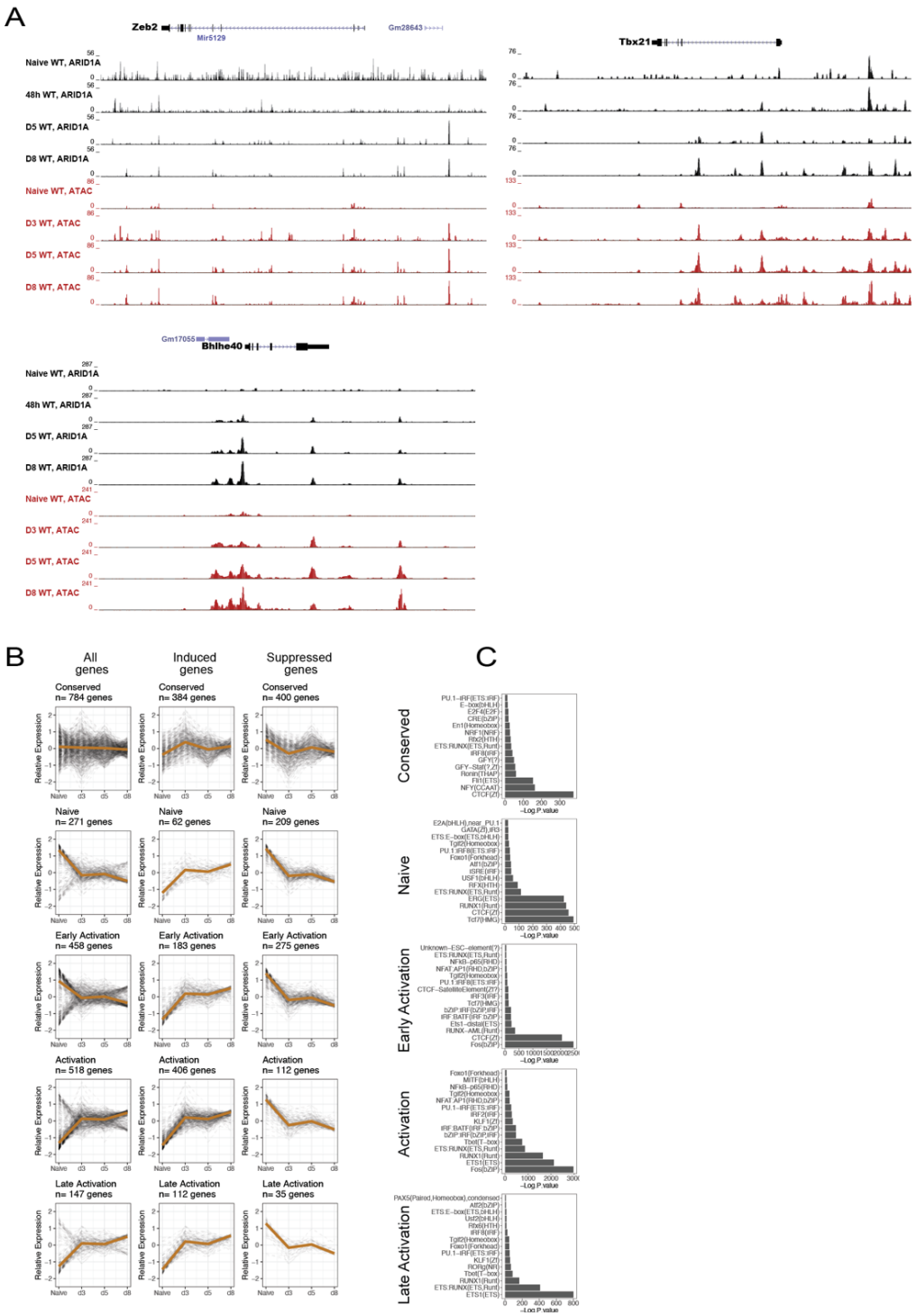

Figure 3.8 **Chromatin accessibility and ARID1A binding in antiviral CD8⁺ T cells.** (A) ARID1A CUT&RUN and ATAC-seq signal tracks at *Zeb2*, *Tbx21*, and *Bhlhe40*. (B) Relative gene expression of genes annotated to OCR clusters in Fig 1A. Naïve samples are from GSE152841[79]. (C) Top 15 motifs enriched in OCR clusters.

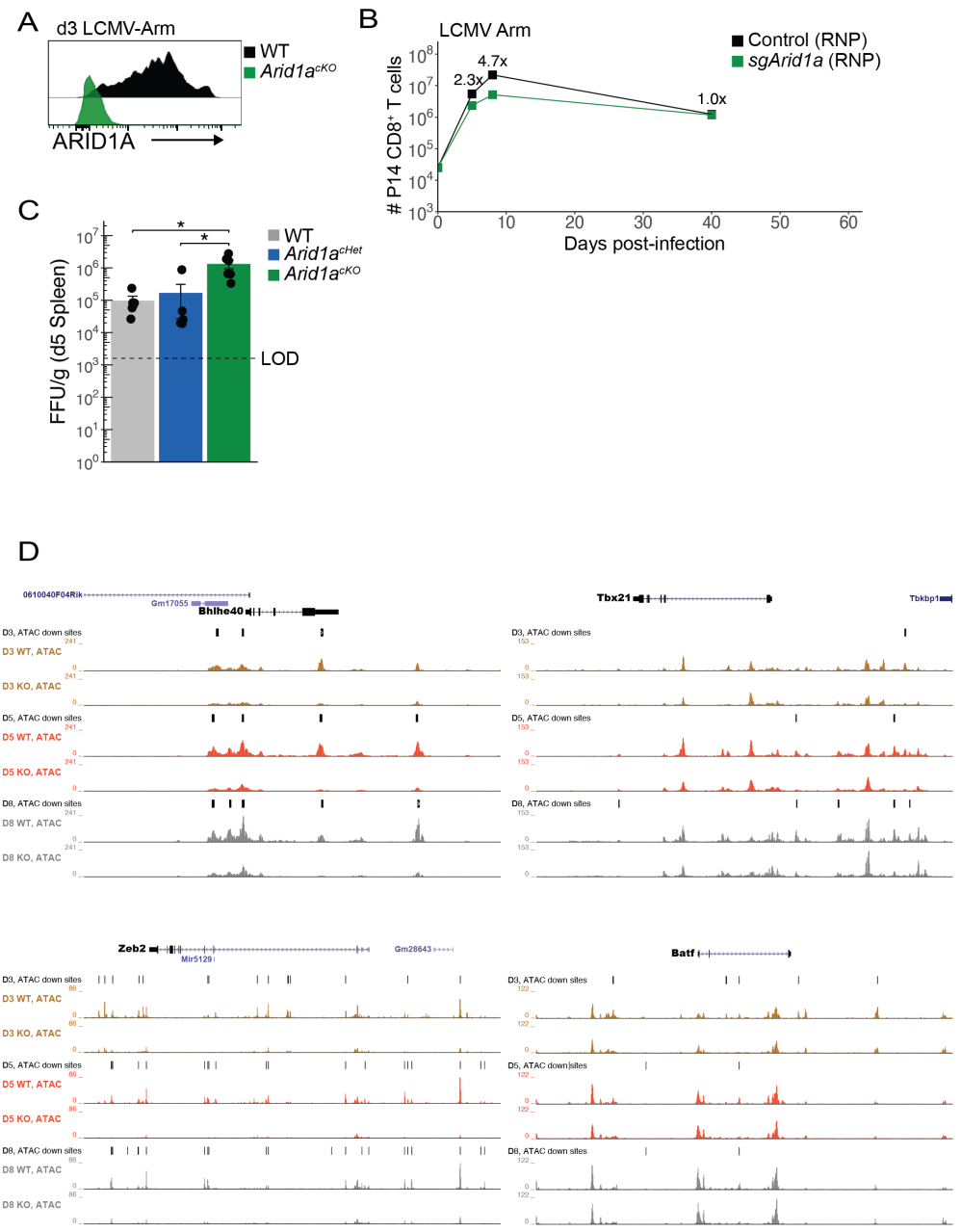

Figure 3.9 **ARID1A regulates accessibility of effector-associated TFs.** (A) Confirmation of efficient ARID1A deletion at 72h post-infection in *Arid1a* KO P14 spleen cells. (B) Numbers of control RNP or sg*Arid1a* RNP (*Arid1a* KO) P14 cells following LCMV-Armstrong infection. (C) LCMV titers in the spleen of WT (n=5), Arid1a Het (n=6), and Arid1a KO (n=6) mice d5 p.i. (D) ATAC-seq signal tracks at *Bhlhe40*, *Tbx21*, *Zeb2*, and *Batf*.. LOD; limit of detection. *p<0.05.

Figure 3.10 ***Arid1a* KO antiviral CD8$^+$ T cells are developmentally and functionally impaired.** (A) TE and MP cells in control or sg*Arid1a* RNP (*Arid1a* KO) P14 cells at 7d post-infection. Mean ± SEM of TE (KLRG1$^+$CD127$^-$) and MP (KLRG1$^-$CD127$^+$) cells are shown. (B) GP_{33}- and (C) NP_{396}-tetramer$^+$ endogenous CD8$^+$ T cells at d8 post-infection. (D,E) ARID1A deletion efficiency in d8-d10 *Arid1a* KO effector subsets (n=11). Mean ± SEM of ARID1A-deleted cells are shown for each subset. (F) Cytokine production from WT or *Arid1a* KO P14 cells 7-8 days post-infection stimulated with either GP33 peptide or IL-12 and IL-18. Representative flow plots show the frequency of IFNg$^+$TNF$^+$ (top) cells after peptide stimulation and frequency of IFNg$^+$ (bottom) cells after IL-12 and IL-18 stimulation. Paired t-test. (G) Granzyme A staining in WT and *Arid1a* P14 cells at d8 p.i. (H) T-bet staining in WT, *Arid1a* Het, and *Arid1a* KO effector cells at d4.5 or d9 post-infection. *ns*, not significant; *p<0.05, **p<0.005

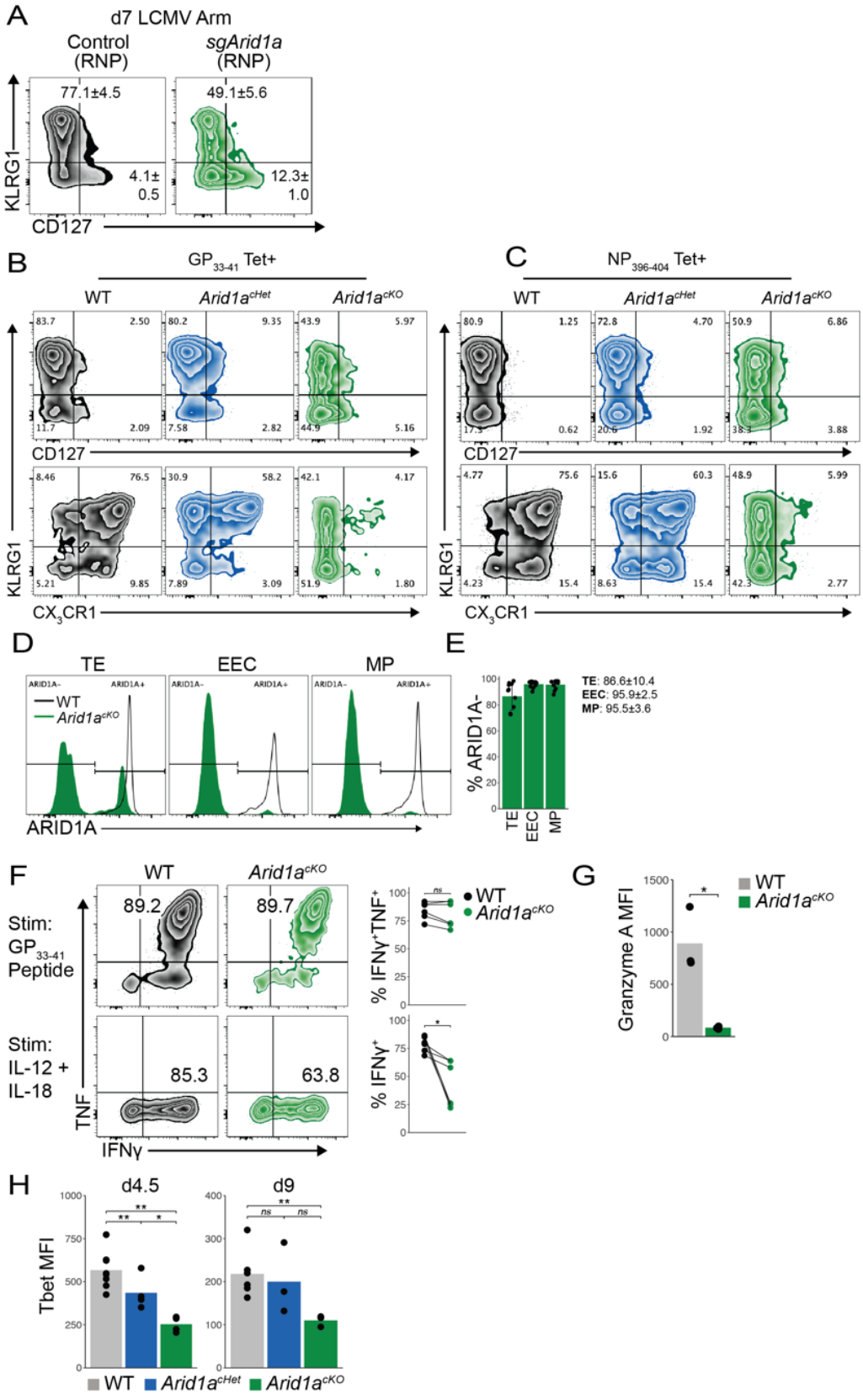
A
d7 LCMV Arm
Control (RNP)
sgArid1a (RNP)
77.1±4.5
49.1±5.6
4.1± 0.5
12.3± 1.0
KLRG1
CD127
B
GP33-41 Tet+
WT
Arid1acHet
Arid1acKO
CD127
KLRG1
CX3CR1
C
NP396-404 Tet+
WT
Arid1acHet
Arid1acKO
CD127
KLRG1
CX3CR1
D
TE
EEC
MP
WT
Arid1acKO
ARID1A
E
% ARID1A-
TE
EEC
MP
TE: 86.6±10.4
EEC: 95.9±2.5
MP: 95.5±3.6
F
WT
Arid1acKO
Stim: GP33-41 Peptide
Stim: IL-12 + IL-18
89.2
89.7
85.3
63.8
TNF
IFNγ
% IFNγ+TNF+
% IFNγ+
WT
Arid1acKO
G
Granzyme A MFI
WT
Arid1acKO
H
d4.5
d9
Tbet MFI
WT
Arid1acHet
Arid1acKO

Figure 3.11 **Figure 3.3.S4. ARID1A regulates accessibility and deposition of histone modifications**. (A) ATAC-seq and H3K27ac CUT&RUN signal tracks at (A) *Bhlhe40*, *Tbx21*, *Prdm1,* and *Zfp683*. (B) ATAC-seq and H3K27me3 CUT&RUN signal tracks at *Tcf7*, *Cd9*, *Ccr7*, and *Sell*.

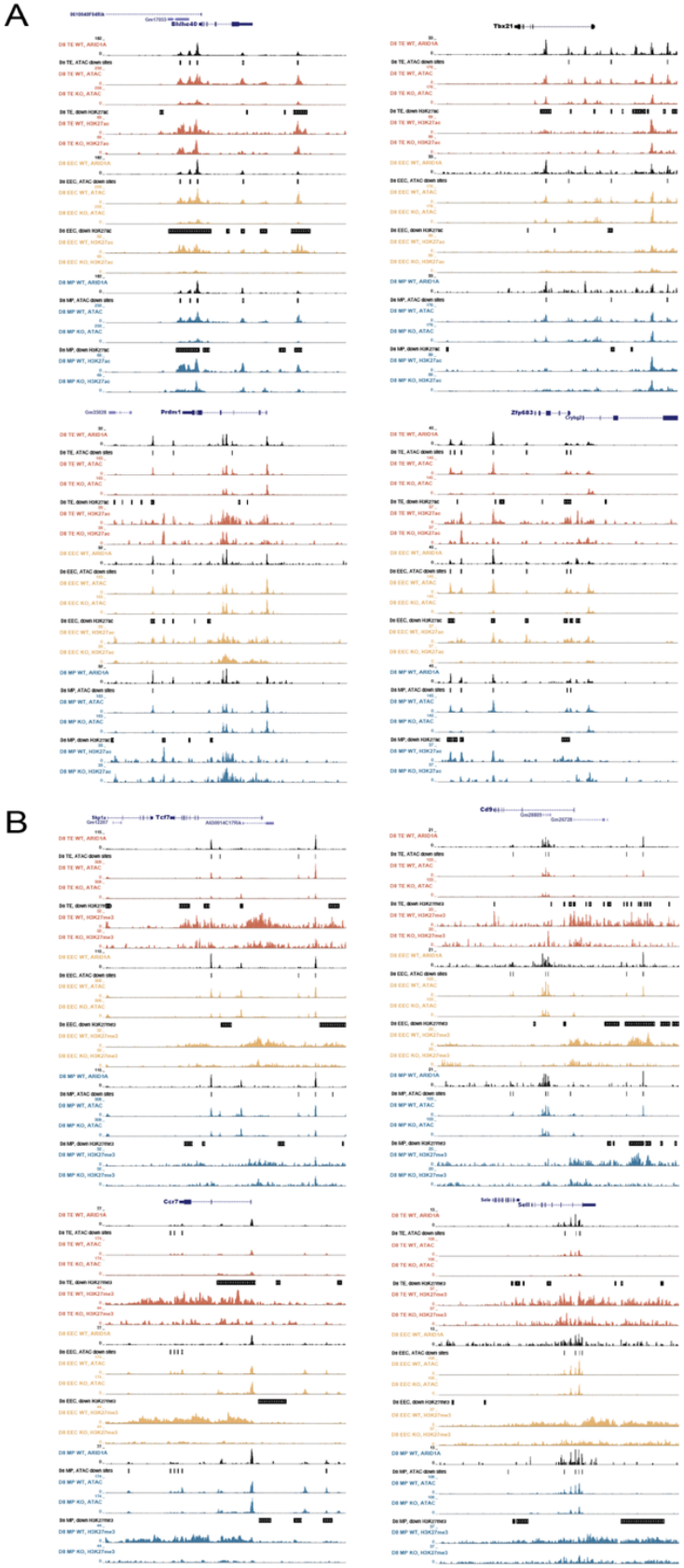
A
B

A

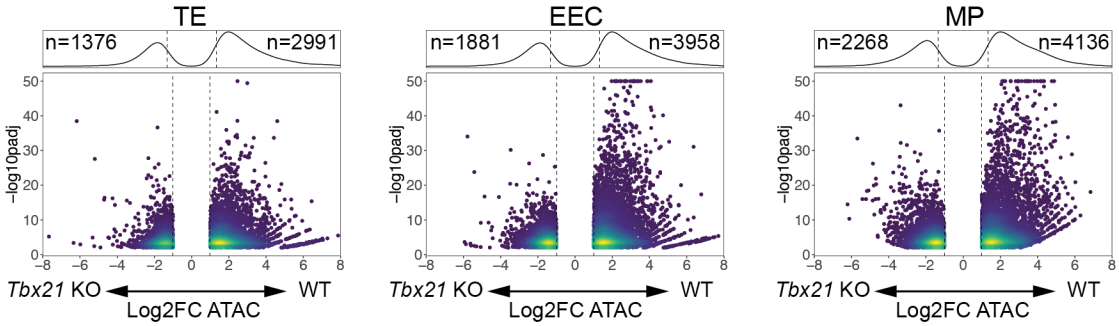

B

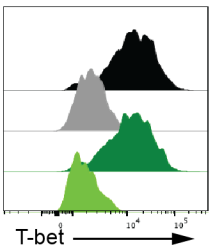

Genotype	Tbet-OE	Tbet MFI
WT	+	11885
WT	-	2424
Arid1a^{cKO}	+	10570
Arid1a^{cKO}	-	1828

Figure 3.12 **T-bet regulates chromatin accessibility profiles in effector CD8^{+} T cells.** (A) Differential accessibility analysis of WT and *Tbx21* KO TE, EEC, and MP P14 cells at d8 p.i. Numbers of differentially accessible peaks are shown (Fold change ≥ 2, adjusted p value < 0.01, Benjamini-Hochberg). (B) T-bet expression in WT and *Arid1a* KO cells transduced with control or T-bet overexpression retrovirus and cultured *in vitro* for 72h.

Figure 3.13 **ARID1A promotes T_{RM} formation.** (A) Taiji PageRank TF score ratios in WT versus *Arid1a* KO MP cells. The top 30 TFs with a threshold ratio of fold change > 1.5 in each direction are shown. (B) IFNγ production by WT and *Arid1a* KO memory P14 cells stimulated with IL-12 and IL-18 *in vitro* at d60 post-infection. (C) Absolute numbers and (D) CD69/CD103 expression profiles of IV- WT and *Arid1a* KO salivary gland T_{RM} cells at d50 post-infection. (E) Granzyme A staining in WT and *Arid1a* KO SI-IEL T_{RM}. (F) Absolute numbers of WT and *Arid1a* KO SI-IEL and SI-LPL cells at d4.5 p.i. (G) TCF1 expression in naïve WT $CD8^+$ T cells and WT or *Arid1a* KO effector cells 5d p.i in spleen, mesenteric lymph node (mesLN), and SI-IEL. (H) TCF1 expression in WT and *Arid1a* KO MP, EEC, and TE cells 13d p.i. Paired t-test was used in cases where line connects observations. *ns*, not significant; *p<0.05, **p<0.005, ***p<0.0005.

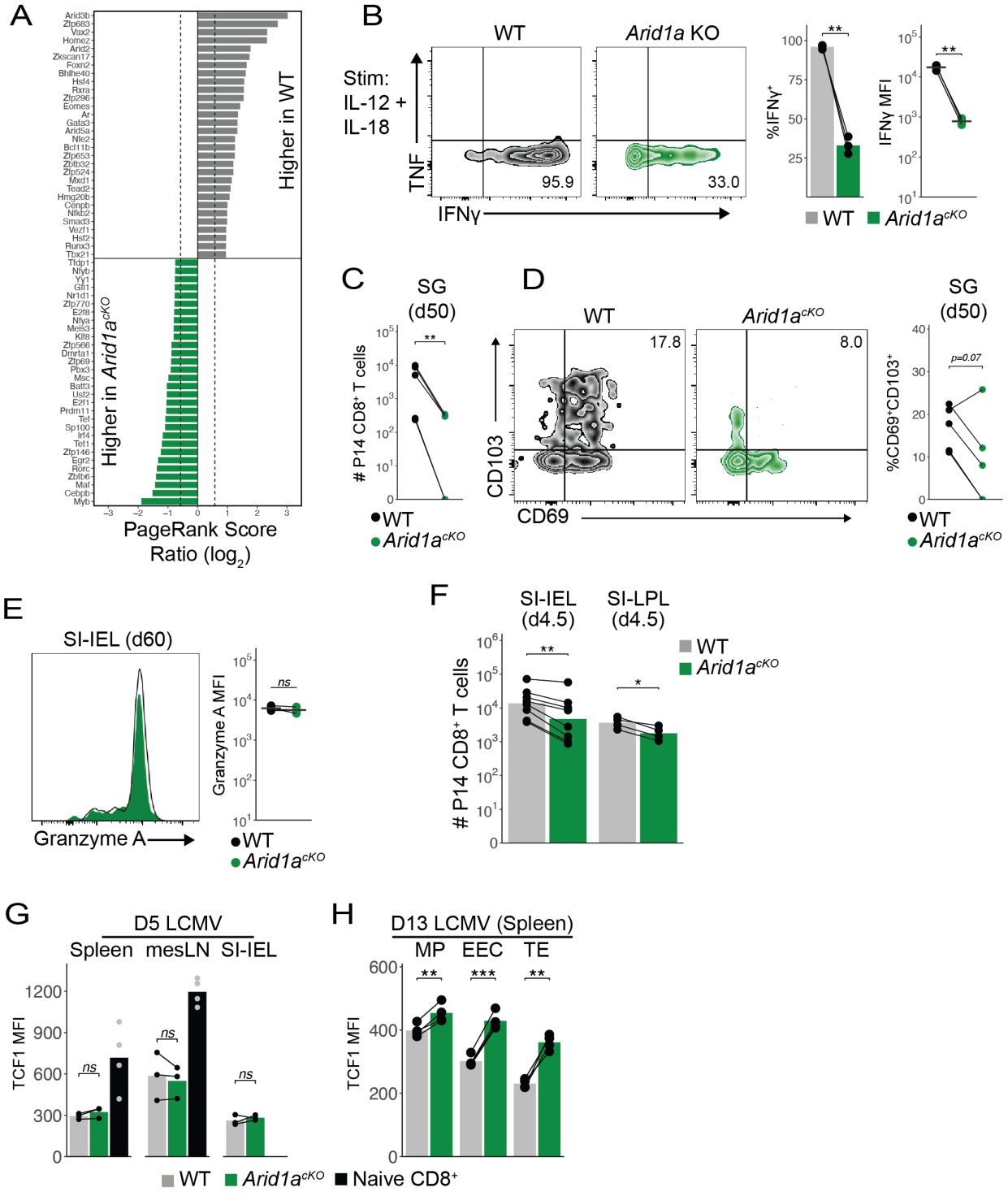
A
Higher in WT
Higher in Arid1a cKO
PageRank Score
Ratio (log2)
B
WT
Arid1a KO
Stim:
IL-12 +
IL-18
TNF
IFNγ
95.9
33.0
%IFNγ+
IFNγ MFI
WT
Arid1acKO
C
SG
(d50)
P14 CD8+ T cells
WT
Arid1acKO
D
WT
Arid1acKO
17.8
8.0
CD103
CD69
SG
(d50)
%CD69+CD103+
p=0.07
E
SI-IEL (d60)
Granzyme A
Granzyme A MFI
ns
F
SI-IEL
(d4.5)
SI-LPL
(d4.5)
P14 CD8+ T cells
G
D5 LCMV
Spleen
mesLN
SI-IEL
TCF1 MFI
Naive CD8+
H
D13 LCMV (Spleen)
MP
EEC
TE
TCF1 MFI

CHAPTER 4 Investigation of the role of ARID1B-cBAF, PBAF, and ncBAF in CD8+ T cell differentiation

4.1 Introduction

BAF complexes (cBAF, PBAF, and ncBAF) are composed of sets of both shared (e.g. *Smarca4*) and complex-specific subunits (e.g. ARID1A for cBAF, PBRM1 and ARID2 for PBAF, and BRD9 for ncBAF)[78–80]. Our prior work demonstrated a critical role for the ARID1A-containing canonical BAF complex in directing $CD8^+$ T cell fates *in vivo*[93]. However, it is unclear what role alternative forms of BAF complex may play in this context.

ARID1B is structurally similar to ARID1A and incorporate into cBAF complexes in a mutually exclusive manner[175,176]. In general, ARID1A is more highly expressed than ARID1B[175], including in $CD8^+$ T cells[177]. Prior work in human cancer cell lines demonstrated that knockdown of *ARID1B* had minimal effects on chromatin accessibility in ARID1A-sufficient cells, but that *ARID1B* knockdown in the context of *ARID1A* mutant cells synergistically resulted in altered chromatin accessibility[82], demonstrating that ARID1B plays a relatively minor role in this context. However, germline *ARID1B* mutations are strongly linked to intellectual disabilities[178], potentially through its role in neural progenitor development and/or function[179,180], indicating that ARID1B may play cell-type specific and/or differentiation state-specific roles. In this study, we demonstrate that *Arid1b* deletion has minimal if any effect on $CD8^+$ effector cell differentiation or effector functions during acute viral infection.

PBAF and ncBAF were recently demonstrated to play critical roles in regulatory $CD4^+$ T cell biology; ncBAF promoted *Foxp3* expression while PBAF suppressed *Foxp3*[173]. However, genetic deletion of PBAF-specific subunit *Pbrm1* or the ncBAF-specific subunits *Brd9* and *Bicra* yielded minimal effects on cellular phenotypes in

antigen-specific $CD8^+$ T cells during *Listeria monocytogenes* infection[32]. In this study, we investigated the role of *Pbrm1* and *Brd9* in LCMV-specific $CD8^+$ T cells. In contrast to *Arid1a* deletion which resulted in substantial reduction clonal expansion and terminal effector differentiation, and in support of recent findings from Guo et al.[32], *Pbrm1* and *Brd9* deletion had minimal effects on expansion or differentiation.

Lastly, in support of our initial findings of ARID1A in effector cell development, we investigated the temporal requirement of *Arid1a* by generating a tamoxifen-inducible *Arid1a* deletion model. Interestingly, late deletion (after day 3) of *Arid1a* nearly completely recapitulated early (day 0) *Arid1a* deletion effects on effector cell phenotypes, indicating that cBAF is critical for both establishing and maintaining activation-induced open chromatin for at least several days after T cell activation to promote appropriate effector cell fates.

4.2 Results

4.2.1 *Arid1b* deletion does not alter differentiation states in LCMV Armstrong infection.

To elucidate the function of *Arid1b* in CD8 T cells, naïve P14 $CD8^+$ T cells were electroporated with sg*Arid1b* Cas9 RNP (*Arid1b* KO) or control RNP (WT) and then transferred into naïve congenic recipient C57BL/6 mice that were infected with LCMV Armstrong. Eight days p.i., WT and *Arid1b* KO P14 cells formed slightly lower frequencies of $KLRG1^+CD127^-$ and $KLRG1^+CX3CR1^+$ cells and expressed similar levels of T-bet protein (**Figure 4.1 A, B**). *Ex vivo* restimulation with either GP33 peptide or IL-12 and IL-18 revealed that WT and *Arid1b* KO effector cells also produced effector cytokines in similar frequencies (**Figure 4.1 C, D**). Together, these data indicate that ARID1B plays a relatively minor role in $CD8^+$ effector cell differentiation *in vivo*.

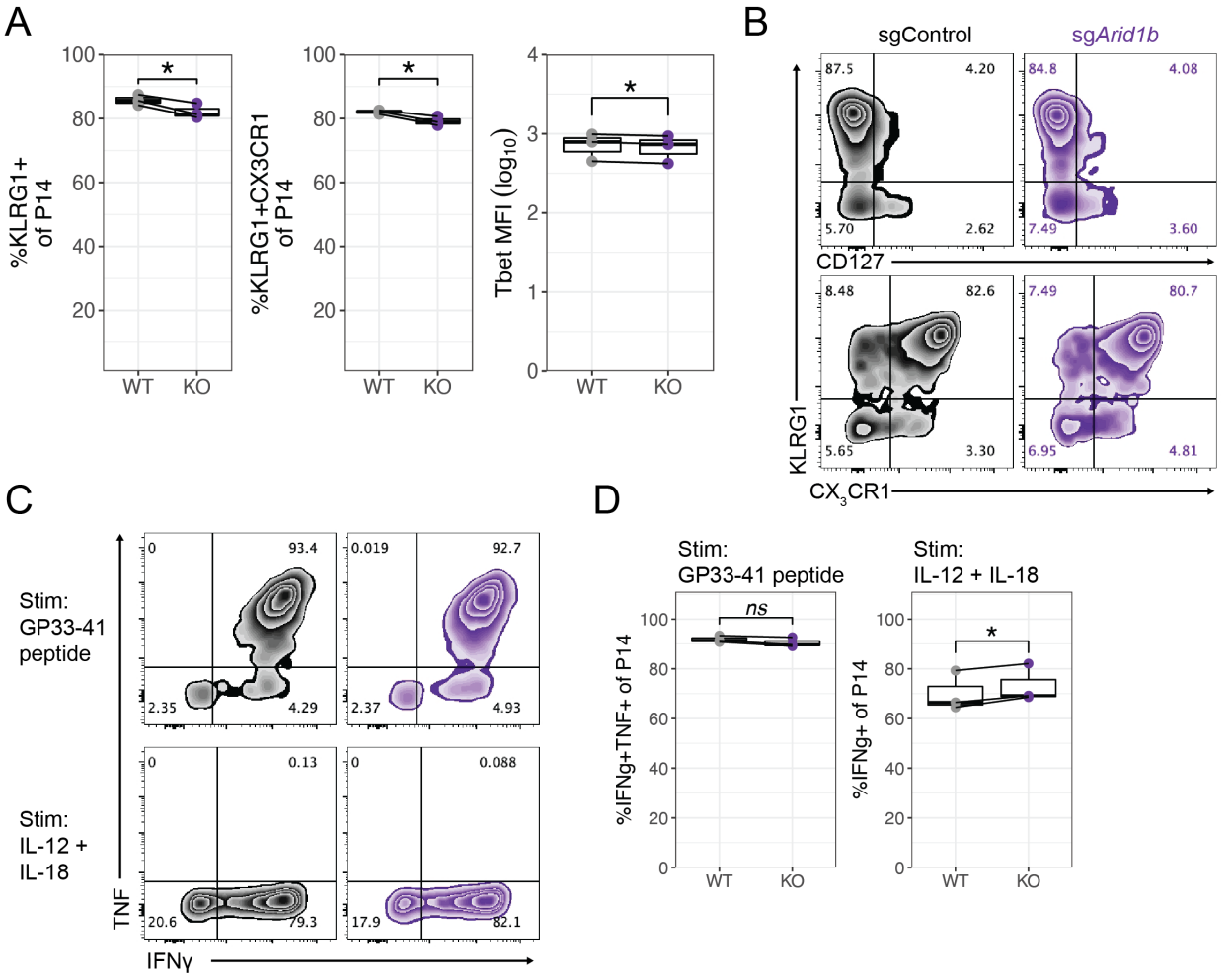

Figure 4.1 ***Arid1b* deletion minimally alter differentiation states in LCMV Armstrong infection.** (A) Frequency of KLRG1+, KLRG1+CX3CR1+, and Tbet MFI in control or sg*Arid1b* RNP P14 cells at d8 p.i. (B) Representative flow plots of cellular phenotypes. (C) Representative flow plots of cytokine production. (D) Summarized frequencies of cytokine-production after restimulation.

4.2.2 *Pbrm1* and *Brd9* minimally affect differentiation states in LCMV Armstrong infection.

To elucidate the function of *Arid1b* in CD8 T cells, naïve P14 $CD8^+$ T cells were electroporated with sg*Arid1a, sgBrd9* or sg*Pbrm1* Cas9 RNP or control RNP (WT) and then transferred into naïve congenic recipient C57BL/6 mice that were infected with LCMV Armstrong. As expected, *sgArid1a* cells were ~4x less abundant relative to WT cells in the blood at d7 p.i. *sgBrd9* cells were ~2x less abundant relative to WT cells at d7, while sg*Pbrm1* cells were present in similar numbers as WT cells (**Figure 4.2 A, B**). Thirty days post-infection, sg*Brd9* P14 cells were slightly less abundant in the SI-IEL, while sg*Pbrm1* P14 cells were present in similar numbers as WT cells in all analyzed tissues. (**Figure 4.2 B**). Together, these data suggest that *Brd9* (ncBAF) may play a role in the initial effector cell differentiation and for establishing T_{RM}, while *Pbrm1* is seemingly dispensable for effector and memory cell formation.

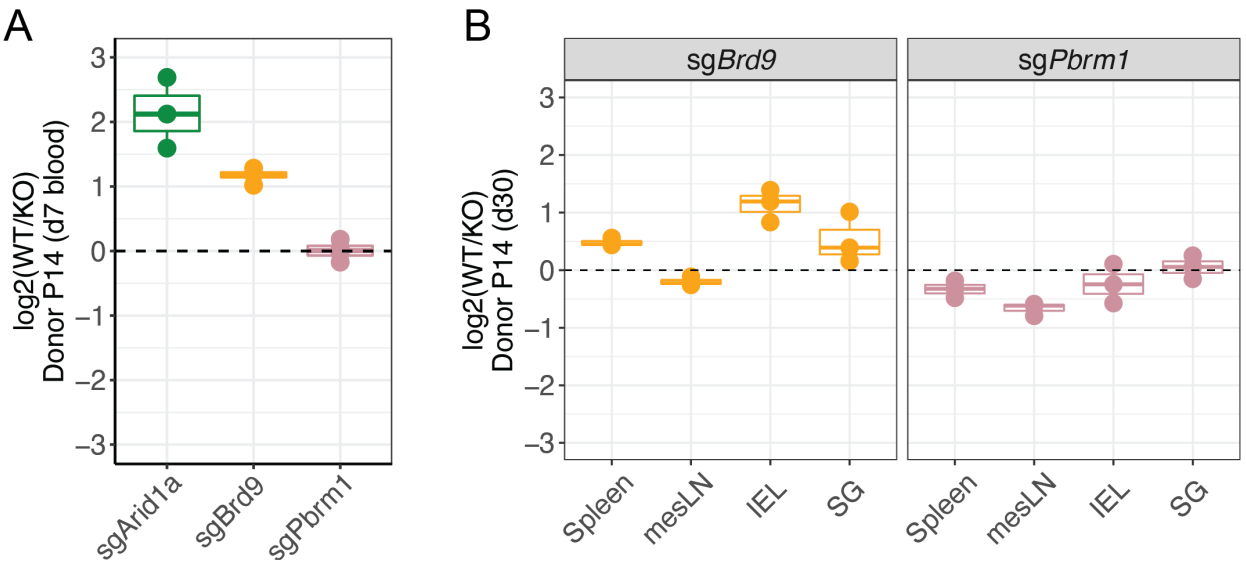

Figure 4.2 **Pbrm1 and Brd9 minimally affect differentiation states in LCMV Armstrong infection.** (A) Donor P14 ratios in the blood at d7 p.i. for WT control RNP versus sg*Brd9* or sg*Pbrm1* RNP electroporated cells. (B) Representative flow plot of effector phenotypes in the blood at d7 p.i. (C) Donor P14 ratios in indicated tissues at d30 p.i. for WT control RNP versus sg*Brd9* or sg*Pbrm1* RNP electroporated cells.

4.2.3 Late inducible *Arid1a* deletion phenocopies early *Arid1a* deletion terminal effector differentiation phenotypes

To disentangle the role of cBAF in establishing versus maintaining open chromatin, we generated an inducible *Arid1a* deletion model by crossing P14 *Arid1a*$^{fl/fl}$ with *ROSA26-LSL-CreERT2* mice (*Arid1a* iKO). Equal numbers of *Arid1a* iKO or WT (CreERT2^{-}) P14 cells were transferred into congenic recipient C57BL/6 mice that were subsequently infected with LCMV Armstrong. Recipient mice treated with tamoxifen (i.p. 50mg/kg) for 5 consecutive days or vehicle control from d0-d4 p.i. (early deletion) or from d3-d7 p.i. (late deletion) and sacrificed on d8 p.i. (**Figure 4.3 A**). Efficient deletion of *Arid1a* (96-99%) was evident in both treatment groups by d8, while iKO cells in vehicle treated mice maintained high WT-like levels of ARID1A (**Figure 4.3 B**). Early *Arid1a* deletion resulted in a marked reduction in KLRG1^{+}CD127^{-} TE cells and concomitant increase in KLRG1^{-} CD127^{+} MP cells, as well as an inability to form KLRG1^{+}CX3CR1^{+} cells (**Figure 4.3 C, D**), similar to that observed with the *Arid1a*$^{fl/fl}$ *Gzmb-cre* model (**Figure 3.3)**. Interestingly, late deletion similarly resulted in a strong reduction in TE and KLRG1^{+}CX3CR1^{+} populations, but only a slight increase in MP cell frequencies (**Figure 4.3 C, D**).

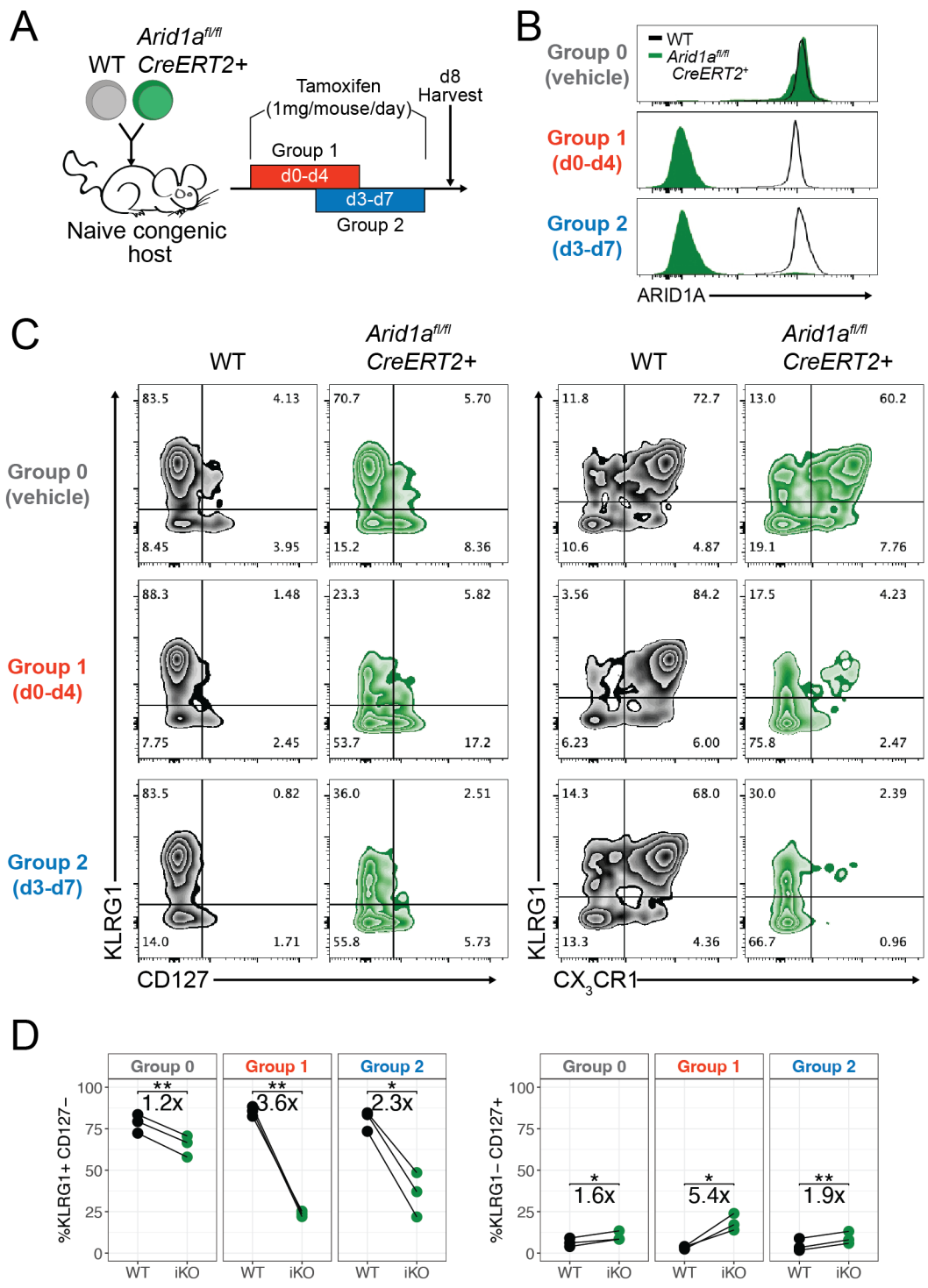

Figure 4.3 **Late inducible Arid1a deletion phenocopies early Arid1a deletion terminal effector differentiation phenotypes** (**A**) Experimental schematic. (**B**) ARID1A staining at d8 p.i. (**C**) Representative flow plots of WT and iKO P14 cells at d8 p.i. (**D**) TE and MP cell frequencies for WT and iKO cells.

4.3 Discussion

In our previous study, we demonstrated that ARID1A-cBAF played a critical role in both establishing and maintaining open chromatin in activated antiviral effector CD8+ T cells. However, activation-induced open chromatin was not completely dependent on ARID1A, indicating that an ARID1A-independent mechanism was responsible for either opening or maintaining an open chromatin state at that subset of regions. One possibility is that ARID1A-cBAF was necessary for initiating the opening of those regions, but was not required for maintaining open chromatin. Alternatively, perhaps ARID1B-cBAF is sufficient to either open or maintain those open sites. The present study cannot distinguish between these two possibilities, and further experimentation is needed to test these hypotheses. However, recent work revealed that in the context of myelopoiesis, open chromatin regions regulated by ARID1A and ARID1B had minimal overlap and ARID1B-dependent OCRs were strongly enriched in promoter regions[181], suggesting that ARID1A-cBAF and ARID1B-cBAF largely regulate distinct regions of the genome and suggest that ARID1B-cBAF is not sufficient to open or maintain ARID1A-dependent OCRs in the absence of ARID1A.

The findings that PBAF and ncBAF play critical and opposing roles in FOXP3+ regulatory T cells[173] led us to speculate that a similar biological paradigm may hold true in $CD8^+$ T cells. Indeed, PBAF disruption enhanced the accumulation or persistence of exhausted CD8+ T cells during chronic LCMV infection[95]. However, consistent with recent findings[32], our study found that deletion of neither *Brd9* nor *Pbrm1* significantly altered any measurable effector or memory cell phenotypes during acute infection. It is possible that more thorough examination of the transcriptome or epigenetic landscape of these

cells may yield greater insight into potential roles for these complexes. It is speculated that PBAF complexes can form in the absence of *Pbrm1*[95,182], and therefore deletion of the essential subunit *Arid2* will be essential to formally assess the role of PBAF in this context.

To more finely dissect the temporal requirement of ARID1A-cBAF for promoting effector cell differentiation, we generated *Arid1a* iKO (CreERT2+) mice. Deletion of *Arid1a* on d3-d7 led to a loss of terminal effector cells at day 8 similar to that observed with early (*Gzmb-Cre* or d0-d4 tamoxifen treatment) deletion. We previously demonstrated that most of the activation-induced remodeling events occur shortly after activation (within 24 hours; **Figure 2.2**). Together, these data indicate that transient (<3 days) activation-induced cBAF-dependent chromatin remodeling is insufficient to promote terminal differentiation, and that continuous cBAF activity is needed to maintain those open chromatin sites and give rise to this subset of cells. These data imply that cells that undergo early cell fate deterministic events, such as asymmetric division during the first mitotic event, require ongoing cBAF even after many rounds of mitosis in order to commit to adopting terminal fates.

Early, but not late *Arid1a* deletion led to a robust increase in MP cell frequency. It is possible that early *Arid1a* deletion results in incomplete early effector programming leading to an early bias towards $CD62L^{hi}$ $TCF1^{hi}$ precursors[99] that preferentially gave rise to $CD127^{+}$ MP-like cells; in contrast, late deletion allowed iKO to undergo WT-like chromatin remodeling and effector differentiation, ultimately precluding the formation of this precursor population. Future studies will be needed to formally demonstrate this and other possible mechanisms. In this study, iKO P14 cells in vehicle control-treated recipient

mice formed fewer TE cells than WT cells in the same host, and this is possibly due to slight confounding genetic background differences between the two donor cells which were not littermate controls. Alternatively, those iKO cells may have received incidental exposure to tamoxifen via excretion of bioactive hydroxytamoxifen in the feces of tamoxifen-treated mice in the same cage[183] leading to spurious *Arid1a* deletion in some cells.

4.4 Methods

4.4.1 Mice and infections

C57BL/6J were purchased from Jackson Laboratories. *Arid1a*$^{fl/fl}$ *CreERT2*$^{+}$ mice were generated by crossing P14 mice with *Arid1a*$^{fl/fl}$ and *R26-LSL-CreERT2*$^{+}$. Tamoxifen was administered daily for 5 consecutive days at 1mg in 100uL sunflower seed oil i.p.. Both female and male mice were used for all studies. Animals were housed in specific-pathogen-free facilities at the Salk Institute. All experimental studies were approved and performed in accordance with guidelines and regulations implemented by the Salk Institute Animal Care and Use Committee. Mice were infected with $2x10^5$ PFU LCMV-Armstrong by intraperitoneal injection. LCMV-Armstrong were prepared as previously described[111].

4.4.2 Cell Isolation

Spleens, lymph nodes, and livers were mechanically dissociated with 1mL syringe plungers over a 70um nylon strainer. For isolation of small intestinal IEL, Peyer's patches were first removed by dissection. Intestines were longitudinally cut and then cut into 1cm pieces and washed in PBS. Pieces were incubated in 30mL HBSS with 10% FBS, 10mM

HEPES, and 1mM dithioerythritol with vigorous shaking at 37C for 30 minutes. Supernatants were collected, washed, and further isolated using a 40/67% discontinuous percoll density centrifugation for 20 minutes at room temp with no brakes.

4.4.3 Flow Cytometry and cell sorting

Cell suspensions were first incubated with eBioscience Fixable Viability Dye eFluor 780 for 5 minutes at room temp. Cells were stained with primary surface antibodies in PBS with 2% FBS, 0.1% NaN3 for 20 minutes on ice. For experiments involving retroviral transduction, cells were fixed with Biolegend Fixation buffer for 20 minutes at room temp. For intracellular staining, cells were first fixed with eBioscience Foxp3/Transcription Factor Staining buffer fixation/permeabilization buffer for 30 minutes at room temp, and staining was performed in 1X permeabilization buffer for 30 minutes at room temp. Flow cytometry analysis samples were acquired on a BD Symphony A3.

4.4.4 *In vitro* Stimulations and intracellular cytokine staining

Spleen cell suspensions were stimulated in complete RPMI (RPMI with 10% FBS, Pen/strep, L-glutamine, 50uM β-ME) in the presence of 0.1ng/mL GP_{33-41} peptide or DMSO and brefeldin A for 5 hours at 37C. For cytokine stimulations, cells were cultured for 5 hours with 10ng/mL recombinant mouse IL-12 and IL-18 without brefeldin A, at which point brefeldin A was added for 1 hour prior to staining. Cells were stained for viability and surface markers as described above, and then fixed/permeabilized with cytofix/cytoperm buffer (BD) for 25 minutes at room temp. Intracellular cytokine staining was performed in 1X permeabilization buffer (BD) for 30 minutes at room temp.

4.4.5 Cas9 RNP Electroporation

Cas9/sgRNA mixtures were prepared (0.6uL 62nM recombinant Cas9, 0.15nmol sgRNA, 3.5uL RNAse-free H2O) and incubated for 10 minutes at room temperature. 2-5x10^6 MACS-purified naive P14 cells were washed in PBS and suspended in 20uL supplemented P3 buffer (Lonza; 16.4uL P3 buffer and 3.6uL Supplement 1). Resuspended cells were immediately mixed with 5uL Cas9/sgRNA mixture and transferred to a Lonza nucleofector strip. Cells were electroporated using the program DN100. 130uL pre-warmed complete RPMI was added to cells prior to incubation for 10 minutes at 37C. Cells were washed extensively with complete RPMI prior to transfer into recipient mice. The sequences of sgRNA used to target *Arid1b*: AUCUGAGGUGGGAUUCCGUG and CAGAACCCCAACAUAUAGCG.

4.5 Acknowledgement

Chapter 4 contains unpublished material. McDonald B, Kaech SM. The dissertation author was the primary investigator and author of this material.

REFERENCES

1. Kaech, S.M., and Cui, W. (2012). Transcriptional control of effector and memory CD8+ T cell differentiation. Nat. Rev. Immunol. *12*, 749–761. 10.1038/nri3307.

2. Heeg, M., and Goldrath, A.W. (2023). Insights into phenotypic and functional CD8+ TRM heterogeneity. Immunol. Rev. *316*, 8–22. 10.1111/imr.13218.

3. Blattman, J.N., Wherry, E.J., Ha, S.-J., van der Most, R.G., and Ahmed, R. (2009). Impact of epitope escape on PD-1 expression and CD8 T-cell exhaustion during chronic infection. J. Virol. *83*, 4386–4394. 10.1128/JVI.02524-08.

4. Odorizzi, P.M., Pauken, K.E., Paley, M.A., Sharpe, A., and Wherry, E.J. (2015). Genetic absence of PD-1 promotes accumulation of terminally differentiated exhausted CD8+ T cells. J. Exp. Med. *212*, 1125–1137. 10.1084/jem.20142237.

5. Frebel, H., Nindl, V., Schuepbach, R.A., Braunschweiler, T., Richter, K., Vogel, J., Wagner, C.A., Loffing-Cueni, D., Kurrer, M., Ludewig, B., et al. (2012). Programmed death 1 protects from fatal circulatory failure during systemic virus infection of mice. J. Exp. Med. *209*, 2485–2499. 10.1084/jem.20121015.

6. Gerlach, C., Moseman, E.A., Loughhead, S.M., Alvarez, D., Zwijnenburg, A.J., Waanders, L., Garg, R., de la Torre, J.C., and von Andrian, U.H. (2016). The Chemokine Receptor CX3CR1 Defines Three Antigen-Experienced CD8 T Cell Subsets with Distinct Roles in Immune Surveillance and Homeostasis. Immunity *45*, 1270–1284. 10.1016/j.immuni.2016.10.018.

7. Kaech, S.M., Tan, J.T., Wherry, E.J., Konieczny, B.T., Surh, C.D., and Ahmed, R. (2003). Selective expression of the interleukin 7 receptor identifies effector CD8 T cells that give rise to long-lived memory cells. Nat. Immunol. *4*, 1191–1198. 10.1038/ni1009.

8. Cui, W., Joshi, N.S., Jiang, A., and Kaech, S.M. (2009). Effects of Signal 3 during CD8 T cell priming: Bystander production of IL-12 enhances effector T cell expansion but promotes terminal differentiation. Vaccine *27*, 2177–2187. 10.1016/j.vaccine.2009.01.088.

9. Herndler-Brandstetter, D., Ishigame, H., Shinnakasu, R., Plajer, V., Stecher, C., Zhao, J., Lietzenmayer, M., Kroehling, L., Takumi, A., Kometani, K., et al. (2018). KLRG1+ Effector CD8+ T Cells Lose KLRG1, Differentiate into All Memory T Cell Lineages, and Convey Enhanced Protective Immunity. Immunity *48*, 716-729.e8. 10.1016/j.immuni.2018.03.015.

10. Joshi, N.S., Cui, W., Chandele, A., Lee, H.K., Urso, D.R., Hagman, J., Gapin, L., and Kaech, S.M. (2007). Inflammation directs memory precursor and short-lived effector CD8(+) T cell fates via the graded expression of T-bet transcription factor. Immunity *27*, 281–295. 10.1016/j.immuni.2007.07.010.

11. Obar, J.J., Jellison, E.R., Sheridan, B.S., Blair, D.A., Pham, Q.-M., Zickovich, J.M., and Lefrançois, L. (2011). Pathogen-Induced Inflammatory Environment Controls Effector and Memory CD8+ T Cell Differentiation. J. Immunol. *187*, 4967–4978. 10.4049/jimmunol.1102335.

12. Plumlee, C.R., Obar, J.J., Colpitts, S.L., Jellison, E.R., Haining, W.N., Lefrancois, L., and Khanna, K.M. (2015). Early Effector CD8 T Cells Display Plasticity in Populating the Short-Lived Effector and Memory-Precursor Pools Following Bacterial or Viral Infection. Sci. Rep. *5*, 12264. 10.1038/srep12264.

13. Mueller, S.N., and Mackay, L.K. (2016). Tissue-resident memory T cells: local specialists in immune defence. Nat. Rev. Immunol. *16*, 79–89. 10.1038/nri.2015.3.

14. Doedens, A.L., Phan, A.T., Stradner, M.H., Fujimoto, J.K., Nguyen, J.V., Yang, E., Johnson, R.S., and Goldrath, A.W. (2013). Hypoxia-inducible factors enhance the effector responses of CD8+ T cells to persistent antigen. Nat. Immunol. *14*, 1173–1182. 10.1038/ni.2714.

15. Buchholz, V.R., Schumacher, T.N.M., and Busch, D.H. (2016). T Cell Fate at the Single-Cell Level. Annu. Rev. Immunol. *34*, 65–92. 10.1146/annurev-immunol-032414-112014.

16. Joshi, N.S., Cui, W., Chandele, A., Lee, H.K., Urso, D.R., Hagman, J., Gapin, L., and Kaech, S.M. (2007). Inflammation Directs Memory Precursor and Short-Lived Effector CD8+ T Cell Fates via the Graded Expression of T-bet Transcription Factor. Immunity *27*, 281–295. 10.1016/j.immuni.2007.07.010.

17. Arsenio, J., Kakaradov, B., Metz, P.J., Kim, S.H., Yeo, G.W., and Chang, J.T. (2014). Early specification of CD8+ T lymphocyte fates during adaptive immunity revealed by single-cell gene-expression analyses. Nat. Immunol. *15*, 365–372. 10.1038/ni.2842.

18. Kakaradov, B., Arsenio, J., Widjaja, C.E., He, Z., Aigner, S., Metz, P.J., Yu, B., Wehrens, E.J., Lopez, J., Kim, S.H., et al. (2017). Early transcriptional and epigenetic regulation of CD8+ T cell differentiation revealed by single-cell RNA-seq. Nat. Immunol. *18*, 422–432. 10.1038/ni.3688.

19. Kalia, V., Sarkar, S., Subramaniam, S., Haining, W.N., Smith, K.A., and Ahmed, R. (2010). Prolonged Interleukin-2Rα Expression on Virus-Specific CD8+ T Cells Favors Terminal-Effector Differentiation In Vivo. Immunity *32*, 91–103. 10.1016/j.immuni.2009.11.010.

20. Pipkin, M.E., Sacks, J.A., Cruz-Guilloty, F., Lichtenheld, M.G., Bevan, M.J., and Rao, A. (2010). Interleukin-2 and Inflammation Induce Distinct Transcriptional Programs that Promote the Differentiation of Effector Cytolytic T Cells. Immunity *32*, 79–90. 10.1016/j.immuni.2009.11.012.

21. Keppler, S.J., Rosenits, K., Koegl, T., Vucikuja, S., and Aichele, P. (2012). Signal 3 Cytokines as Modulators of Primary Immune Responses during Infections: The Interplay of Type I IFN and IL-12 in CD8 T Cell Responses. PLOS ONE *7*, e40865. 10.1371/journal.pone.0040865.

22. Starbeck-Miller, G.R., Xue, H.-H., and Harty, J.T. (2014). IL-12 and type I interferon prolong the division of activated CD8 T cells by maintaining high-affinity IL-2 signaling in vivo. J. Exp. Med. *211*, 105–120. 10.1084/jem.20130901.

23. Farsakoglu, Y., McDonald, B., and Kaech, S.M. (2021). Motility Matters: How CD8+ T-Cell Trafficking Influences Effector and Memory Cell Differentiation. Cold Spring Harb. Perspect. Biol., a038075. 10.1101/cshperspect.a038075.

24. Groom, J.R., and Luster, A.D. (2011). CXCR3 in T cell function. Exp. Cell Res. *317*, 620–631. 10.1016/j.yexcr.2010.12.017.

25. Duckworth, B.C., Lafouresse, F., Wimmer, V.C., Broomfield, B.J., Dalit, L., Alexandre, Y.O., Sheikh, A.A., Qin, R.Z., Alvarado, C., Mielke, L.A., et al. (2021). Effector and stem-like memory cell fates are imprinted in distinct lymph node niches directed by CXCR3 ligands. Nat. Immunol. *22*, 434–448. 10.1038/s41590-021-00878-5.

26. Hu, J.K., Kagari, T., Clingan, J.M., and Matloubian, M. (2011). Expression of chemokine receptor CXCR3 on T cells affects the balance between effector and memory CD8 T-cell generation. Proc. Natl. Acad. Sci. *108*, E118–E127. 10.1073/pnas.1101881108.

27. Jung, Y.W., Rutishauser, R.L., Joshi, N.S., Haberman, A.M., and Kaech, S.M. (2010). Differential Localization of Effector and Memory CD8 T Cell Subsets in Lymphoid Organs during Acute Viral Infection. J. Immunol. *185*, 5315–5325. 10.4049/jimmunol.1001948.

28. Unsoeld, H., Voehringer, D., Krautwald, S., and Pircher, H. (2004). Constitutive Expression of CCR7 Directs Effector CD8 T Cells into the Splenic White Pulp and Impairs Functional Activity1. J. Immunol. *173*, 3013–3019. 10.4049/jimmunol.173.5.3013.

29. Kurachi, M., Kurachi, J., Suenaga, F., Tsukui, T., Abe, J., Ueha, S., Tomura, M., Sugihara, K., Takamura, S., Kakimi, K., et al. (2011). Chemokine receptor CXCR3 facilitates CD8+ T cell differentiation into short-lived effector cells leading to memory degeneration. J. Exp. Med. *208*, 1605–1620. 10.1084/jem.20102101.

30. Chang, J.T., Palanivel, V.R., Kinjyo, I., Schambach, F., Intlekofer, A.M., Banerjee, A., Longworth, S.A., Vinup, K.E., Mrass, P., Oliaro, J., et al. (2007). Asymmetric T Lymphocyte Division in the Initiation of Adaptive Immune Responses. Science *315*, 1687–1691. 10.1126/science.1139393.

31. Chang, J.T., Ciocca, M.L., Kinjyo, I., Palanivel, V.R., McClurkin, C.E., DeJong, C.S., Mooney, E.C., Kim, J.S., Steinel, N.C., Oliaro, J., et al. (2011). Asymmetric Proteasome Segregation as a Mechanism for Unequal Partitioning of the Transcription Factor T-bet during T Lymphocyte Division. Immunity *34*, 492–504. 10.1016/j.immuni.2011.03.017.

32. Guo, A., Huang, H., Zhu, Z., Chen, M.J., Shi, H., Yuan, S., Sharma, P., Connelly, J.P., Liedmann, S., Dhungana, Y., et al. (2022). cBAF complex components and MYC cooperate early in CD8+ T cell fate. Nature. 10.1038/s41586-022-04849-0.

33. Verbist, K.C., Guy, C.S., Milasta, S., Liedmann, S., Kamiński, M.M., Wang, R., and Green, D.R. (2016). Metabolic maintenance of cell asymmetry following division in activated T lymphocytes. Nature *532*, 389–393. 10.1038/nature17442.

34. Pollizzi, K.N., Sun, I.-H., Patel, C.H., Lo, Y.-C., Oh, M.-H., Waickman, A.T., Tam, A.J., Blosser, R.L., Wen, J., Delgoffe, G.M., et al. (2016). Asymmetric inheritance of mTORC1 kinase activity during division dictates CD8+ T cell differentiation. Nat. Immunol. *17*, 704–711. 10.1038/ni.3438.

35. Gräbnitz, F., Stark, D., Shlesinger, D., Petkidis, A., Borsa, M., Yermanos, A., Carr, A., Barandun, N., Wehling, A., Balaz, M., et al. (2023). Asymmetric cell division safeguards memory CD8 T cell development. Cell Rep. *42*, 112468. 10.1016/j.celrep.2023.112468.

36. Gill, A.L., Wang, P.H., Lee, J., Hudson, W.H., Ando, S., Araki, K., Hu, Y., Wieland, A., Im, S., Gavora, A., et al. (2023). PD-1 blockade increases the self-renewal of stem-like CD8 T cells to compensate for their accelerated differentiation into effectors. Sci. Immunol. *8*, eadg0539. 10.1126/sciimmunol.adg0539.

37. Borsa, M., Barandun, N., Gräbnitz, F., Barnstorf, I., Baumann, N.S., Pallmer, K., Baumann, S., Stark, D., Balaz, M., Oetiker, N., et al. (2021). Asymmetric cell division shapes naive and virtual memory T-cell immunity during ageing. Nat. Commun. *12*, 2715. 10.1038/s41467-021-22954-y.

38. Kaech, S.M., and Ahmed, R. (2001). Memory CD8+ T cell differentiation: initial antigen encounter triggers a developmental program in naïve cells. Nat. Immunol. *2*, 415–422. 10.1038/87720.

39. Wong, P., and Pamer, E.G. (2001). Cutting Edge: Antigen-Independent CD8 T Cell Proliferation. J. Immunol. *166*, 5864–5868. 10.4049/jimmunol.166.10.5864.

40. Guan, T., Dominguez, C.X., Amezquita, R.A., Laidlaw, B.J., Cheng, J., Henao-Mejia, J., Williams, A., Flavell, R.A., Lu, J., and Kaech, S.M. (2018). ZEB1, ZEB2, and the miR-200 family form a counterregulatory network to regulate CD8+ T cell fates. J. Exp. Med. *215*, 1153–1168. 10.1084/jem.20171352.

41. Rutishauser, R.L., Martins, G.A., Kalachikov, S., Chandele, A., Parish, I.A., Meffre, E., Jacob, J., Calame, K., and Kaech, S.M. (2009). Transcriptional Repressor

Blimp-1 Promotes CD8+ T Cell Terminal Differentiation and Represses the Acquisition of Central Memory T Cell Properties. Immunity *31*, 296–308. 10.1016/j.immuni.2009.05.014.

42. Hu, Y., Lee, Y.-T., Kaech, S.M., Garvy, B., and Cauley, L.S. (2015). Smad4 Promotes Differentiation of Effector and Circulating Memory CD8 T Cells but Is Dispensable for Tissue-Resident Memory CD8 T Cells. J. Immunol. *194*, 2407–2414. 10.4049/jimmunol.1402369.

43. Gray, S.M., Amezquita, R.A., Guan, T., Kleinstein, S.H., and Kaech, S.M. (2017). Polycomb Repressive Complex 2-Mediated Chromatin Repression Guides Effector CD8+ T Cell Terminal Differentiation and Loss of Multipotency. Immunity *46*, 596–608. 10.1016/j.immuni.2017.03.012.

44. Dominguez, C.X., Amezquita, R.A., Guan, T., Marshall, H.D., Joshi, N.S., Kleinstein, S.H., and Kaech, S.M. (2015). The transcription factors ZEB2 and T-bet cooperate to program cytotoxic T cell terminal differentiation in response to LCMV viral infection. J. Exp. Med. *212*, 2041–2056. 10.1084/jem.20150186.

45. Intlekofer, A.M., Takemoto, N., Wherry, E.J., Longworth, S.A., Northrup, J.T., Palanivel, V.R., Mullen, A.C., Gasink, C.R., Kaech, S.M., Miller, J.D., et al. (2005). Effector and memory CD8 + T cell fate coupled by T-bet and eomesodermin. Nat. Immunol. *6*, 1236–1244. 10.1038/ni1268.

46. Cui, W., Liu, Y., Weinstein, J.S., Craft, J., and Kaech, S.M. (2011). An Interleukin-21- Interleukin-10-STAT3 Pathway Is Critical for Functional Maturation of Memory CD8+ T Cells. Immunity *35*, 792–805. 10.1016/j.immuni.2011.09.017.

47. Omilusik, K.D., Best, J.A., Yu, B., Goossens, S., Weidemann, A., Nguyen, J.V., Seuntjens, E., Stryjewska, A., Zweier, C., Roychoudhuri, R., et al. (2015). Transcriptional repressor ZEB2 promotes terminal differentiation of CD8+ effector and memory T cell populations during infection. J. Exp. Med. *212*, 2027–2039. 10.1084/jem.20150194.

48. Omilusik, K.D., Nadjsombati, M.S., Shaw, L.A., Yu, B., Milner, J.J., and Goldrath, A.W. (2018). Sustained Id2 regulation of E proteins is required for terminal differentiation of effector CD8+ T cells. J. Exp. Med. *215*, 773–783. 10.1084/jem.20171584.

49. Yu, B., Zhang, K., Milner, J.J., Toma, C., Chen, R., Scott-Browne, J.P., Pereira, R.M., Crotty, S., Chang, J.T., Pipkin, M.E., et al. (2017). Epigenetic landscapes reveal transcription factors that regulate CD8 + T cell differentiation. Nat. Immunol. *18*, 573–582. 10.1038/ni.3706.

50. Milner, J.J., Toma, C., Yu, B., Zhang, K., Omilusik, K., Phan, A.T., Wang, D., Getzler, A.J., Nguyen, T., Crotty, S., et al. (2017). Runx3 programs CD8 + T cell residency in non-lymphoid tissues and tumours. Nature *552*, 253–257. 10.1038/nature24993.

51. Milner, J.J., Toma, C., Quon, S., Omilusik, K., Scharping, N.E., Dey, A., Reina-Campos, M., Nguyen, H., Getzler, A.J., Diao, H., et al. (2021). Bromodomain protein BRD4 directs and sustains CD8 T cell differentiation during infection. J. Exp. Med. *218*, e20202512. 10.1084/jem.20202512.

52. Nayar, R., Schutten, E., Bautista, B., Daniels, K., Prince, A.L., Enos, M., Brehm, M.A., Swain, S.L., Welsh, R.M., and Berg, L.J. (2014). Graded Levels of IRF4 Regulate CD8+ T Cell Differentiation and Expansion, but Not Attrition, in Response to Acute Virus Infection. J. Immunol. *192*, 5881–5893. 10.4049/jimmunol.1303187.

53. Pace, L., Goudot, C., Zueva, E., Gueguen, P., Burgdorf, N., Waterfall, J.J., Quivy, J.-P., Almouzni, G., and Amigorena, S. (2018). The epigenetic control of stemness in CD8+ T cell fate commitment. Science *359*, 177–186. 10.1126/science.aah6499.

54. Crompton, J.G., Narayanan, M., Cuddapah, S., Roychoudhuri, R., Ji, Y., Yang, W., Patel, S.J., Sukumar, M., Palmer, D.C., Peng, W., et al. (2016). Lineage relationship of CD8 + T cell subsets is revealed by progressive changes in the epigenetic landscape. Cell. Mol. Immunol. *13*, 502–513. 10.1038/cmi.2015.32.

55. Shin, H., Blackburn, S.D., Intlekofer, A.M., Kao, C., Angelosanto, J.M., Reiner, S.L., and Wherry, E.J. (2009). A Role for the Transcriptional Repressor Blimp-1 in CD8+ T Cell Exhaustion during Chronic Viral Infection. Immunity *31*, 309–320. 10.1016/j.immuni.2009.06.019.

56. Khan, O., Giles, J.R., McDonald, S., Manne, S., Ngiow, S.F., Patel, K.P., Werner, M.T., Huang, A.C., Alexander, K.A., Wu, J.E., et al. (2019). TOX transcriptionally and epigenetically programs CD8+ T cell exhaustion. Nature, 1–29.

57. Seo, H., Chen, J., González-Avalos, E., Samaniego-Castruita, D., Das, A., Wang, Y.H., López-Moyado, I.F., Georges, R.O., Zhang, W., Onodera, A., et al. (2019). TOX and TOX2 transcription factors cooperate with NR4A transcription factors to impose CD8 +T cell exhaustion. Proc. Natl. Acad. Sci. *37*, 201905675–201905676.

58. Chen, J., pez-Moyado, I.F.L. x000F3, Seo, H., Lio, C.-W.J., Hempleman, L.J., Sekiya, T., Yoshimura, A., Scott-Browne, J.P., and Rao, A. (2019). NR4A transcription factors limit CAR T cell function in solid tumours. Nature *567*, 1–29.

59. Paley, M.A., Kroy, D.C., Odorizzi, P.M., Johnnidis, J.B., Dolfi, D.V., Barnett, B.E., Bikoff, E.K., Robertson, E.J., Lauer, G.M., Reiner, S.L., et al. (2012). Progenitor and Terminal Subsets of CD8+ T Cells Cooperate to Contain Chronic Viral Infection. Science *338*, 1220–1225.

60. Doering, T.A., Crawford, A., Angelosanto, J.M., Paley, M.A., Ziegler, C.G., and Wherry, E.J. (2012). Network Analysis Reveals Centrally Connected Genes and Pathways Involved in CD8+ T Cell Exhaustion versus Memory. Immunity *37*, 1130–1144.

61. Quon, S., Yu, B., Russ, B.E., Tsyganov, K., Nguyen, H., Toma, C., Heeg, M., Hocker, J.D., Milner, J.J., Crotty, S., et al. (2023). DNA architectural protein CTCF facilitates subset-specific chromatin interactions to limit the formation of memory CD8+ T cells. Immunity *56*, 959-978.e10. 10.1016/j.immuni.2023.03.017.

62. Mackay, L.K., Minnich, M., Kragten, N.A.M., Liao, Y., Nota, B., Seillet, C., Zaid, A., Man, K., Preston, S., Freestone, D., et al. (2016). Hobit and Blimp1 instruct a universal transcriptional program of tissue residency in lymphocytes. Science *352*, 459–463. 10.1126/science.aad2035.

63. Gautam, S., Fioravanti, J., Zhu, W., Le Gall, J.B., Brohawn, P., Lacey, N.E., Hu, J., Hocker, J.D., Hawk, N.V., Kapoor, V., et al. (2019). The transcription factor c-Myb regulates CD8+ T cell stemness and antitumor immunity. Nat. Immunol. *20*, 337–349. 10.1038/s41590-018-0311-z.

64. Li, C., Zhu, B., Son, Y.M., Wang, Z., Jiang, L., Xiang, M., Ye, Z., Beckermann, K.E., Wu, Y., Jenkins, J.W., et al. (2019). The Transcription Factor Bhlhe40 Programs Mitochondrial Regulation of Resident CD8+ T Cell Fitness and Functionality. Immunity *51*, 491-507.e7. 10.1016/j.immuni.2019.08.013.

65. Milner, J.J., Toma, C., Yu, B., Zhang, K., Omilusik, K., Phan, A.T., Wang, D., Getzler, A.J., Nguyen, T., Crotty, S., et al. (2017). Runx3 programs CD8+ T cell residency in non-lymphoid tissues and tumours. Nature *552*, 253–257. 10.1038/nature24993.

66. Doering, T.A., Crawford, A., Angelosanto, J.M., Paley, M.A., Ziegler, C.G., and Wherry, E.J. (2012). Network analysis reveals centrally connected genes and pathways involved in CD8+ T cell exhaustion versus memory. Immunity *37*, 1130–1144. 10.1016/j.immuni.2012.08.021.

67. Grewal, S.I.S., and Moazed, D. (2003). Heterochromatin and Epigenetic Control of Gene Expression. Science *301*, 798–802. 10.1126/science.1086887.

68. Gray, S.M., Amezquita, R.A., Guan, T., Kleinstein, S.H., and Kaech, S.M. (2017). Polycomb Repressive Complex 2-Mediated Chromatin Repression Guides Effector CD8+ T Cell Terminal Differentiation and Loss of Multipotency. Immunity *46*, 596–608. 10.1016/j.immuni.2017.03.012.

69. Pace, L., Goudot, C., Zueva, E., Gueguen, P., Burgdorf, N., Waterfall, J.J., Quivy, J.-P., Almouzni, G., and Amigorena, S. (2018). The epigenetic control of stemness in CD8+ T cell fate commitment. Science *359*, 177–186. 10.1126/science.aah6499.

70. Carty, S.A., Gohil, M., Banks, L.B., Cotton, R.M., Johnson, M.E., Stelekati, E., Wells, A.D., Wherry, E.J., Koretzky, G.A., and Jordan, M.S. (2018). The Loss of TET2 Promotes CD8+ T Cell Memory Differentiation. J. Immunol. *200*, 82–91. 10.4049/jimmunol.1700559.

71. Wittkopp, P.J., and Kalay, G. (2012). Cis-regulatory elements: molecular mechanisms and evolutionary processes underlying divergence. Nat. Rev. Genet. *13*, 59–69. 10.1038/nrg3095.

72. Boija, A., Klein, I.A., Sabari, B.R., Dall'Agnese, A., Coffey, E.L., Zamudio, A.V., Li, C.H., Shrinivas, K., Manteiga, J.C., Hannett, N.M., et al. (2018). Transcription Factors Activate Genes through the Phase-Separation Capacity of Their Activation Domains. Cell *175*, 1842-1855.e16. 10.1016/j.cell.2018.10.042.

73. Kim, S., and Wysocka, J. (2023). Deciphering the multi-scale, quantitative cis-regulatory code. Mol. Cell *83*, 373–392. 10.1016/j.molcel.2022.12.032.

74. Fukaya, T., Lim, B., and Levine, M. (2016). Enhancer Control of Transcriptional Bursting. Cell *166*, 358–368. 10.1016/j.cell.2016.05.025.

75. Bartman, C.R., Hsu, S.C., Hsiung, C.C.-S., Raj, A., and Blobel, G.A. (2016). Enhancer Regulation of Transcriptional Bursting Parameters Revealed by Forced Chromatin Looping. Mol. Cell *62*, 237–247. 10.1016/j.molcel.2016.03.007.

76. Kadoch, C., and Crabtree, G.R. Mammalian SWI/SNF chromatin remodeling complexes and cancer: Mechanistic insights gained from human genomics. Sci. Adv. *1*, e1500447. 10.1126/sciadv.1500447.

77. Hargreaves, D.C., and Crabtree, G.R. (2011). ATP-dependent chromatin remodeling: genetics, genomics and mechanisms. Cell Res. *21*, 396–420. 10.1038/cr.2011.32.

78. Alpsoy, A., and Dykhuizen, E.C. (2018). Glioma tumor suppressor candidate region gene 1 (GLTSCR1) and its paralog GLTSCR1-like form SWI/SNF chromatin remodeling subcomplexes. J. Biol. Chem. *293*, 3892–3903. 10.1074/jbc.RA117.001065.

79. Gatchalian, J., Malik, S., Ho, J., Lee, D.-S., Kelso, T.W.R., Shokhirev, M.N., Dixon, J.R., and Hargreaves, D.C. (2018). A non-canonical BRD9-containing BAF chromatin remodeling complex regulates naive pluripotency in mouse embryonic stem cells. Nat. Commun. *9*, 5139. 10.1038/s41467-018-07528-9.

80. Mashtalir, N., D'Avino, A.R., Michel, B.C., Luo, J., Pan, J., Otto, J.E., Zullow, H.J., McKenzie, Z.M., Kubiak, R.L., St Pierre, R., et al. (2018). Modular Organization and Assembly of SWI/SNF Family Chromatin Remodeling Complexes. Cell *175*, 1272-1288.e20. 10.1016/j.cell.2018.09.032.

81. Blümli, S., Wiechens, N., Wu, M.-Y., Singh, V., Gierlinski, M., Schweikert, G., Gilbert, N., Naughton, C., Sundaramoorthy, R., Varghese, J., et al. (2021). Acute depletion of the ARID1A subunit of SWI/SNF complexes reveals distinct pathways for activation and repression of transcription. Cell Rep. *37*, 109943. 10.1016/j.celrep.2021.109943.

82. Kelso, T.W.R., Porter, D.K., Amaral, M.L., Shokhirev, M.N., Benner, C., and Hargreaves, D.C. (2017). Chromatin accessibility underlies synthetic lethality of SWI/SNF subunits in ARID1A-mutant cancers. eLife *6*, e30506. 10.7554/eLife.30506.

83. Mathur, R., Alver, B.H., San Roman, A.K., Wilson, B.G., Wang, X., Agoston, A.T., Park, P.J., Shivdasani, R.A., and Roberts, C.W.M. (2017). ARID1A loss impairs enhancer-mediated gene regulation and drives colon cancer in mice. Nat. Genet. *49*, 296–302. 10.1038/ng.3744.

84. Astori, A., Tingvall-Gustafsson, J., Kuruvilla, J., Coyaud, E., Laurent, E.M.N., Sunnerhagen, M., Åhsberg, J., Ungerbäck, J., Strid, T., Sigvardsson, M., et al. (2020). ARID1a Associates with Lymphoid-Restricted Transcription Factors and Has an Essential Role in T Cell Development. J. Immunol. Baltim. Md 1950 *205*, 1419–1432. 10.4049/jimmunol.1900959.

85. Chi, T.H., Wan, M., Lee, P.P., Akashi, K., Metzger, D., Chambon, P., Wilson, C.B., and Crabtree, G.R. (2003). Sequential roles of Brg, the ATPase subunit of BAF chromatin remodeling complexes, in thymocyte development. Immunity *19*, 169–182. 10.1016/s1074-7613(03)00199-7.

86. Han, L., Madan, V., Mayakonda, A., Dakle, P., Woon, T.W., Shyamsunder, P., Nordin, H.B.M., Cao, Z., Sundaresan, J., Lei, I., et al. (2019). Chromatin remodeling mediated by ARID1A is indispensable for normal hematopoiesis in mice. Leukemia *33*, 2291–2305. 10.1038/s41375-019-0438-4.

87. Kadoch, C., and Crabtree, G.R. (2015). Mammalian SWI/SNF chromatin remodeling complexes and cancer: Mechanistic insights gained from human genomics. Sci. Adv. *1*, e1500447. 10.1126/sciadv.1500447.

88. Kadoch, C., Hargreaves, D.C., Hodges, C., Elias, L., Ho, L., Ranish, J., and Crabtree, G.R. (2013). Proteomic and bioinformatic analysis of mammalian SWI/SNF complexes identifies extensive roles in human malignancy. Nat. Genet. *45*, 592–601. 10.1038/ng.2628.

89. Choi, J., Goh, G., Walradt, T., Hong, B.S., Bunick, C.G., Chen, K., Bjornson, R.D., Maman, Y., Wang, T., Tordoff, J., et al. (2015). Genomic landscape of cutaneous T cell lymphoma. Nat. Genet. *47*, 1011–1019. 10.1038/ng.3356.

90. Wang, L., Ni, X., Covington, K.R., Yang, B.Y., Shiu, J., Zhang, X., Xi, L., Meng, Q., Langridge, T., Drummond, J., et al. (2015). Genomic profiling of Sézary Syndrome identifies alterations of key T-cell signaling and differentiation genes. Nat. Genet. *47*, 1426–1434. 10.1038/ng.3444.

91. Scharer, C.D., Bally, A.P.R., Gandham, B., and Boss, J.M. (2017). Cutting Edge: Chromatin Accessibility Programs CD8 T Cell Memory. J. Immunol. *198*, 2238–2243. 10.4049/jimmunol.1602086.

92. Scott-Browne, J.P., López-Moyado, I.F., Trifari, S., Wong, V., Chavez, L., Rao, A., and Pereira, R.M. (2016). Dynamic Changes in Chromatin Accessibility Occur in CD8+ T Cells Responding to Viral Infection. Immunity *45*, 1327–1340. 10.1016/j.immuni.2016.10.028.

93. McDonald, B., Chick, B.Y., Ahmed, N.S., Burns, M., Ma, S., Casillas, E., Chen, D., Mann, T.H., O'Connor, C., Hah, N., et al. (2023). Canonical BAF complex activity shapes the enhancer landscape that licenses CD8+ T cell effector and memory fates. Immunity *56*, 1303-1319.e5. 10.1016/j.immuni.2023.05.005.

94. Belk, J.A., Yao, W., Ly, N., Freitas, K.A., Chen, Y.-T., Shi, Q., Valencia, A.M., Shifrut, E., Kale, N., Yost, K.E., et al. (2022). Genome-wide CRISPR screens of T cell exhaustion identify chromatin remodeling factors that limit T cell persistence. Cancer Cell, S1535610822002318. 10.1016/j.ccell.2022.06.001.

95. Baxter, A.E., Huang, H., Giles, J.R., Chen, Z., Wu, J.E., Drury, S., Dalton, K., Park, S.L., Torres, L., Simone, B.W., et al. (2023). The SWI/SNF chromatin remodeling complexes BAF and PBAF differentially regulate epigenetic transitions in exhausted CD8+ T cells. Immunity *56*, 1320-1340.e10. 10.1016/j.immuni.2023.05.008.

96. Battistello, E., Hixon, K.A., Comstock, D.E., Collings, C.K., Chen, X., Rodriguez Hernaez, J., Lee, S., Cervantes, K.S., Hinkley, M.M., Ntatsoulis, K., et al. (2023). Stepwise activities of mSWI/SNF family chromatin remodeling complexes direct T cell activation and exhaustion. Mol. Cell. 10.1016/j.molcel.2023.02.026.

97. Guan, T., Dominguez, C.X., Amezquita, R.A., Laidlaw, B.J., Cheng, J., Henao-Mejia, J., Williams, A., Flavell, R.A., Lu, J., and Kaech, S.M. (2018). ZEB1, ZEB2, and the miR-200 family form a counterregulatory network to regulate CD8+ T cell fates. J. Exp. Med. *215*, 1153–1168. 10.1084/jem.20171352.

98. Kretschmer, L., Flossdorf, M., Mir, J., Cho, Y.-L., Plambeck, M., Treise, I., Toska, A., Heinzel, S., Schiemann, M., Busch, D.H., et al. (2020). Differential expansion of T central memory precursor and effector subsets is regulated by division speed. Nat. Commun. *11*, 113. 10.1038/s41467-019-13788-w.

99. Johnnidis, J.B., Muroyama, Y., Ngiow, S.F., Chen, Z., Manne, S., Cai, Z., Song, S., Platt, J.M., Schenkel, J.M., Abdel-Hakeem, M., et al. (2021). Inhibitory signaling sustains a distinct early memory CD8+ T cell precursor that is resistant to DNA damage. Sci. Immunol. *6*, eabe3702. 10.1126/sciimmunol.abe3702.

100. Zhang, P., Sun, Y., and Ma, L. (2015). ZEB1: at the crossroads of epithelial-mesenchymal transition, metastasis and therapy resistance. Cell Cycle Georget. Tex *14*, 481–487. 10.1080/15384101.2015.1006048.

101. Hudson, W.H., Prokhnevska, N., Gensheimer, J., Akondy, R., McGuire, D.J., Ahmed, R., and Kissick, H.T. (2019). Expression of novel long noncoding RNAs

defines virus-specific effector and memory CD8 + T cells. Nat. Commun. *10*, 196. 10.1038/s41467-018-07956-7.

102. Jacob, J., and Baltimore, D. (1999). Modelling T-cell memory by genetic marking of memory T cells in vivo. Nature *399*, 593–597. 10.1038/21208.

103. Krebs, A.M., Mitschke, J., Lasierra Losada, M., Schmalhofer, O., Boerries, M., Busch, H., Boettcher, M., Mougiakakos, D., Reichardt, W., Bronsert, P., et al. (2017). The EMT-activator Zeb1 is a key factor for cell plasticity and promotes metastasis in pancreatic cancer. Nat. Cell Biol. *19*, 518–529. 10.1038/ncb3513.

104. Trzpis, M., McLaughlin, P.M.J., de Leij, L.M.F.H., and Harmsen, M.C. (2007). Epithelial Cell Adhesion Molecule. Am. J. Pathol. *171*, 386–395. 10.2353/ajpath.2007.070152.

105. Zhou, X., Yu, S., Zhao, D.-M., Harty, J.T., Badovinac, V.P., and Xue, H.-H. (2010). Differentiation and persistence of memory CD8(+) T cells depend on T cell factor 1. Immunity *33*, 229–240. 10.1016/j.immuni.2010.08.002.

106. Jeannet, G., Boudousquié, C., Gardiol, N., Kang, J., Huelsken, J., and Held, W. (2010). Essential role of the Wnt pathway effector Tcf-1 for the establishment of functional CD8 T cell memory. Proc. Natl. Acad. Sci. *107*, 9777–9782. 10.1073/pnas.0914127107.

107. Delpoux, A., Lai, C.-Y., Hedrick, S.M., and Doedens, A.L. (2017). FOXO1 opposition of CD8+ T cell effector programming confers early memory properties and phenotypic diversity. Proc. Natl. Acad. Sci. *114*, E8865–E8874. 10.1073/pnas.1618916114.

108. Roychoudhuri, R., Clever, D., Li, P., Wakabayashi, Y., Quinn, K.M., Klebanoff, C.A., Ji, Y., Sukumar, M., Eil, R.L., Yu, Z., et al. (2016). BACH2 regulates CD8+ T cell differentiation by controlling access of AP-1 factors to enhancers. Nat. Immunol. *17*, 851–860. 10.1038/ni.3441.

109. Delpoux, A., Michelini, R.H., Verma, S., Lai, C.-Y., Omilusik, K.D., Utzschneider, D.T., Redwood, A.J., Goldrath, A.W., Benedict, C.A., and Hedrick, S.M. (2018). Continuous activity of Foxo1 is required to prevent anergy and maintain the memory state of CD8+ T cells. J. Exp. Med. *215*, 575–594. 10.1084/jem.20170697.

110. Hofmann, M., and Pircher, H. (2011). E-cadherin promotes accumulation of a unique memory CD8 T-cell population in murine salivary glands. Proc. Natl. Acad. Sci. U. S. A. *108*, 16741–16746. 10.1073/pnas.1107200108.

111. Welsh, R.M., and Seedhom, M.O. (2008). LCMV: Propagation, quantitation, and storage. Curr. Protoc. Microbiol. *CHAPTER*, Unit-15A.1. 10.1002/9780471729259.mc15a01s8.

112. Lin, J., and Weiss, A. (2001). T cell receptor signalling. J. Cell Sci. *114*, 243–244. 10.1242/jcs.114.2.243.

113. Huang, W., Lin, W., Chen, B., Zhang, J., Gao, P., Fan, Y., Lin, Y., and Wei, P. (2023). NFAT and NF-κB dynamically co-regulate TCR and CAR signaling responses in human T cells. Cell Rep. *42*, 112663. 10.1016/j.celrep.2023.112663.

114. Crabtree, G.R., and Clipstone, N.A. (1994). Signal Transmission Between the Plasma Membrane and Nucleus of T Lymphocytes. Annu. Rev. Biochem. *63*, 1045–1083. 10.1146/annurev.bi.63.070194.005145.

115. Chen, Y., Zander, R., Khatun, A., Schauder, D.M., and Cui, W. (2018). Transcriptional and Epigenetic Regulation of Effector and Memory CD8 T Cell Differentiation. Front. Immunol. *9*.

116. Huse, M., Klein, L.O., Girvin, A.T., Faraj, J.M., Li, Q.-J., Kuhns, M.S., and Davis, M.M. (2007). Spatial and Temporal Dynamics of T Cell Receptor Signaling with a Photoactivatable Agonist. Immunity *27*, 76–88. 10.1016/j.immuni.2007.05.017.

117. Voisinne, G., Locard-Paulet, M., Froment, C., Maturin, E., Menoita, M.G., Girard, L., Mellado, V., Burlet-Schiltz, O., Malissen, B., Gonzalez de Peredo, A., et al. (2022). Kinetic proofreading through the multi-step activation of the ZAP70 kinase underlies early T cell ligand discrimination. Nat. Immunol. *23*, 1355–1364. 10.1038/s41590-022-01288-x.

118. Britain, D.M., Town, J.P., and Weiner, O.D. (2022). Progressive enhancement of kinetic proofreading in T cell antigen discrimination from receptor activation to DAG generation. eLife *11*, e75263. 10.7554/eLife.75263.

119. McKeithan, T.W. (1995). Kinetic proofreading in T-cell receptor signal transduction. Proc. Natl. Acad. Sci. U. S. A. *92*, 5042–5046.

120. van Stipdonk, M.J.B., Lemmens, E.E., and Schoenberger, S.P. (2001). Naïve CTLs require a single brief period of antigenic stimulation for clonal expansion and differentiation. Nat. Immunol. *2*, 423–429. 10.1038/87730.

121. Zhao, K., Wang, W., Rando, O.J., Xue, Y., Swiderek, K., Kuo, A., and Crabtree, G.R. (1998). Rapid and Phosphoinositol-Dependent Binding of the SWI/SNF-like BAF Complex to Chromatin after T Lymphocyte Receptor Signaling. Cell *95*, 625–636. 10.1016/S0092-8674(00)81633-5.

122. Henrickson, S.E., Mempel, T.R., Mazo, I.B., Liu, B., Artyomov, M.N., Zheng, H., Peixoto, A., Flynn, M.P., Senman, B., Junt, T., et al. (2008). T cell sensing of antigen dose governs interactive behavior with dendritic cells and sets a threshold for T cell activation. Nat. Immunol. *9*, 282–291. 10.1038/ni1559.

123. Ozga, A.J., Moalli, F., Abe, J., Swoger, J., Sharpe, J., Zehn, D., Kreutzfeldt, M., Merkler, D., Ripoll, J., and Stein, J.V. (2016). pMHC affinity controls duration of

CD8+ T cell–DC interactions and imprints timing of effector differentiation versus expansion. J. Exp. Med. *213*, 2811–2829. 10.1084/jem.20160206.

124. Mashtalir, N., Dao, H.T., Sankar, A., Liu, H., Corin, A.J., Bagert, J.D., Ge, E.J., D'Avino, A.R., Filipovski, M., Michel, B.C., et al. (2021). Chromatin landscape signals differentially dictate the activities of mSWI/SNF family complexes. Science *373*, 306–315. 10.1126/science.abf8705.

125. Yudkovsky, N., Logie, C., Hahn, S., and Peterson, C.L. (1999). Recruitment of the SWI/SNF chromatin remodeling complex by transcriptional activators. Genes Dev. *13*, 2369–2374.

126. Brenes, A.J., Lamond, A.I., and Cantrell, D.A. (2023). The Immunological Proteome Resource. Nat. Immunol. *24*, 731–731. 10.1038/s41590-023-01483-4.

127. Marchingo, J.M., Sinclair, L.V., Howden, A.J., and Cantrell, D.A. (2020). Quantitative analysis of how Myc controls T cell proteomes and metabolic pathways during T cell activation. eLife *9*, e53725. 10.7554/eLife.53725.

128. Roberts, D.J., and Miyamoto, S. (2015). Hexokinase II integrates energy metabolism and cellular protection: Akting on mitochondria and TORCing to autophagy. Cell Death Differ. *22*, 248–257. 10.1038/cdd.2014.173.

129. Kaech, S.M., Wherry, E.J., and Ahmed, R. (2002). Effector and memory T-cell differentiation: implications for vaccine development. Nat. Rev. Immunol. *2*, 251–262. 10.1038/nri778.

130. Alessandrini, A., Chiaur, D.S., and Pagano, M. (1997). Regulation of the cyclin-dependent kinase inhibitor p27 by degradation and phosphorylation. Leukemia *11*, 342–345. 10.1038/sj.leu.2400581.

131. Pircher, H., Michalopoulos, E.E., Iwamoto, A., Ohashi, P.S., Baenziger, J., Hengartner, H., Zinkernagel, R.M., and Mak, T.W. (1987). Molecular analysis of the antigen receptor of virus-specific cytotoxic T cells and identification of a new V alpha family. Eur. J. Immunol. *17*, 1843–1846. 10.1002/eji.1830171226.

132. Corces, M.R., Trevino, A.E., Hamilton, E.G., Greenside, P.G., Sinnott-Armstrong, N.A., Vesuna, S., Satpathy, A.T., Rubin, A.J., Montine, K.S., Wu, B., et al. (2017). An improved ATAC-seq protocol reduces background and enables interrogation of frozen tissues. Nat. Methods *14*, 959–962. 10.1038/nmeth.4396.

133. Dobin, A., Davis, C.A., Schlesinger, F., Drenkow, J., Zaleski, C., Jha, S., Batut, P., Chaisson, M., and Gingeras, T.R. (2013). STAR: ultrafast universal RNA-seq aligner. Bioinforma. Oxf. Engl. *29*, 15–21. 10.1093/bioinformatics/bts635.

134. Heinz, S., Benner, C., Spann, N., Bertolino, E., Lin, Y.C., Laslo, P., Cheng, J.X., Murre, C., Singh, H., and Glass, C.K. (2010). Simple combinations of lineage-determining transcription factors prime cis-regulatory elements required for

macrophage and B cell identities. Mol. Cell *38*, 576–589. 10.1016/j.molcel.2010.05.004.

135. Liao, Y., Smyth, G.K., and Shi, W. (2014). featureCounts: an efficient general purpose program for assigning sequence reads to genomic features. Bioinformatics *30*, 923–930. 10.1093/bioinformatics/btt656.

136. Love, M.I., Huber, W., and Anders, S. (2014). Moderated estimation of fold change and dispersion for RNA-seq data with DESeq2. Genome Biol. *15*, 550. 10.1186/s13059-014-0550-8.

137. Ramírez, F., Ryan, D.P., Grüning, B., Bhardwaj, V., Kilpert, F., Richter, A.S., Heyne, S., Dündar, F., and Manke, T. (2016). deepTools2: a next generation web server for deep-sequencing data analysis. Nucleic Acids Res. *44*, W160-165. 10.1093/nar/gkw257.

138. Behr, F.M., Parga-Vidal, L., Kragten, N.A.M., van Dam, T.J.P., Wesselink, T.H., Sheridan, B.S., Arens, R., van Lier, R.A.W., Stark, R., and van Gisbergen, K.P.J.M. (2020). Tissue-resident memory CD8+ T cells shape local and systemic secondary T cell responses. Nat. Immunol. *21*, 1070–1081. 10.1038/s41590-020-0723-4.

139. Buenrostro, J.D., Giresi, P.G., Zaba, L.C., Chang, H.Y., and Greenleaf, W.J. (2013). Transposition of native chromatin for fast and sensitive epigenomic profiling of open chromatin, DNA-binding proteins and nucleosome position. Nat. Methods *10*, 1213–1218. 10.1038/nmeth.2688.

140. Skene, P.J., and Henikoff, S. (2017). An efficient targeted nuclease strategy for high-resolution mapping of DNA binding sites. eLife *6*, e21856. 10.7554/eLife.21856.

141. Corces, M.R., Buenrostro, J.D., Wu, B., Greenside, P.G., Chan, S.M., Koenig, J.L., Snyder, M.P., Pritchard, J.K., Kundaje, A., Greenleaf, W.J., et al. (2016). Lineage-specific and single-cell chromatin accessibility charts human hematopoiesis and leukemia evolution. Nat. Genet. *48*, 1193–1203. 10.1038/ng.3646.

142. Yu, B., Zhang, K., Milner, J.J., Toma, C., Chen, R., Scott-Browne, J.P., Pereira, R.M., Crotty, S., Chang, J.T., Pipkin, M.E., et al. (2017). Epigenetic landscapes reveal transcription factors that regulate CD8+ T cell differentiation. Nat. Immunol. *18*, 573–582. 10.1038/ni.3706.

143. Kurachi, M., Barnitz, R.A., Yosef, N., Odorizzi, P.M., DiIorio, M.A., Lemieux, M.E., Yates, K., Godec, J., Klatt, M.G., Regev, A., et al. (2014). The transcription factor BATF operates as an essential differentiation checkpoint in early effector CD8+ T cells. Nat. Immunol. *15*, 373–383. 10.1038/ni.2834.

144. Tsao, H.-W., Kaminski, J., Kurachi, M., Barnitz, R.A., DiIorio, M.A., LaFleur, M.W., Ise, W., Kurosaki, T., Wherry, E.J., Haining, W.N., et al. (2022). Batf-mediated

epigenetic control of effector CD8+ T cell differentiation. Sci. Immunol. *7*, eabi4919. 10.1126/sciimmunol.abi4919.

145. Zhong, Y., Walker, S.K., Pritykin, Y., Leslie, C.S., Rudensky, A.Y., and van der Veeken, J. (2022). Hierarchical regulation of the resting and activated T cell epigenome by major transcription factor families. Nat. Immunol. *23*, 122–134. 10.1038/s41590-021-01086-x.

146. Subramanian, A., Tamayo, P., Mootha, V.K., Mukherjee, S., Ebert, B.L., Gillette, M.A., Paulovich, A., Pomeroy, S.L., Golub, T.R., Lander, E.S., et al. (2005). Gene set enrichment analysis: a knowledge-based approach for interpreting genome-wide expression profiles. Proc. Natl. Acad. Sci. U. S. A. *102*, 15545–15550. 10.1073/pnas.0506580102.

147. Dominguez, C.X., Amezquita, R.A., Guan, T., Marshall, H.D., Joshi, N.S., Kleinstein, S.H., and Kaech, S.M. (2015). The transcription factors ZEB2 and T-bet cooperate to program cytotoxic T cell terminal differentiation in response to LCMV viral infection. J. Exp. Med. *212*, 2041–2056. 10.1084/jem.20150186.

148. Prier, J.E., Li, J., Gearing, L.J., Olshansky, M., Sng, X.Y.X., Hertzog, P.J., and Turner, S.J. (2019). Early T-BET Expression Ensures an Appropriate CD8+ Lineage-Specific Transcriptional Landscape after Influenza A Virus Infection. J. Immunol. Baltim. Md 1950 *203*, 1044–1054. 10.4049/jimmunol.1801431.

149. Shan, Q., Zeng, Z., Xing, S., Li, F., Hartwig, S.M., Gullicksrud, J.A., Kurup, S.P., Van Braeckel-Budimir, N., Su, Y., Martin, M.D., et al. (2017). The transcription factor Runx3 guards cytotoxic CD8+ effector T cells against deviation towards follicular helper T cell lineage. Nat. Immunol. *18*, 931–939. 10.1038/ni.3773.

150. Farnaby, W., Koegl, M., Roy, M.J., Whitworth, C., Diers, E., Trainor, N., Zollman, D., Steurer, S., Karolyi-Oezguer, J., Riedmueller, C., et al. (2019). BAF complex vulnerabilities in cancer demonstrated via structure-based PROTAC design. Nat. Chem. Biol. *15*, 672–680. 10.1038/s41589-019-0294-6.

151. Papillon, J.P.N., Nakajima, K., Adair, C.D., Hempel, J., Jouk, A.O., Karki, R.G., Mathieu, S., Möbitz, H., Ntaganda, R., Smith, T., et al. (2018). Discovery of Orally Active Inhibitors of Brahma Homolog (BRM)/SMARCA2 ATPase Activity for the Treatment of Brahma Related Gene 1 (BRG1)/SMARCA4-Mutant Cancers. J. Med. Chem. *61*, 10155–10172. 10.1021/acs.jmedchem.8b01318.

152. Zhang, K., Wang, M., Zhao, Y., and Wang, W. (2019). Taiji: System-level identification of key transcription factors reveals transcriptional waves in mouse embryonic development. Sci. Adv. *5*, eaav3262. 10.1126/sciadv.aav3262.

153. Milner, J.J., Nguyen, H., Omilusik, K., Reina-Campos, M., Tsai, M., Toma, C., Delpoux, A., Boland, B.S., Hedrick, S.M., Chang, J.T., et al. (2020). Delineation of a molecularly distinct terminally differentiated memory CD8 T cell population. Proc. Natl. Acad. Sci. U. S. A. *117*, 25667–25678. 10.1073/pnas.2008571117.

154. Wu, J., Madi, A., Mieg, A., Hotz-Wagenblatt, A., Weisshaar, N., Ma, S., Mohr, K., Schlimbach, T., Hering, M., Borgers, H., et al. (2020). T Cell Factor 1 Suppresses CD103+ Lung Tissue-Resident Memory T Cell Development. Cell Rep. *31*, 107484. 10.1016/j.celrep.2020.03.048.

155. Youngblood, B., Hale, J.S., Kissick, H.T., Ahn, E., Xu, X., Wieland, A., Araki, K., West, E.E., Ghoneim, H.E., Fan, Y., et al. (2017). Effector CD8 T cells dedifferentiate into long-lived memory cells. Nature *552*, 404–409. 10.1038/nature25144.

156. Braun, S.M.G., Kirkland, J.G., Chory, E.J., Husmann, D., Calarco, J.P., and Crabtree, G.R. (2017). Rapid and reversible epigenome editing by endogenous chromatin regulators. Nat. Commun. *8*, 560. 10.1038/s41467-017-00644-y.

157. Ho, L., Miller, E.L., Ronan, J.L., Ho, W., Jothi, R., and Crabtree, G.R. (2011). esBAF Facilitates Pluripotency by Conditioning the Genome for LIF/STAT3Signalingand by Regulating Polycomb Function. Nat. Cell Biol. *13*, 903–913. 10.1038/ncb2285.

158. Kadoch, C., Williams, R.T., Calarco, J.P., Miller, E.L., Weber, C.M., Braun, S.M.G., Pulice, J.L., Chory, E.J., and Crabtree, G.R. (2017). Dynamics of BAF-Polycomb complex opposition on heterochromatin in normal and oncogenic states. Nat. Genet. *49*, 213–222. 10.1038/ng.3734.

159. Nakayama, R.T., Pulice, J.L., Valencia, A.M., McBride, M.J., McKenzie, Z.M., Gillespie, M.A., Ku, W.L., Teng, M., Cui, K., Williams, R.T., et al. (2017). SMARCB1 is required for widespread BAF complex-mediated activation of enhancers and bivalent promoters. Nat. Genet. *49*, 1613–1623. 10.1038/ng.3958.

160. Stanton, B.Z., Hodges, C., Calarco, J.P., Braun, S.M.G., Ku, W.L., Kadoch, C., Zhao, K., and Crabtree, G.R. (2017). Smarca4 ATPase mutations disrupt direct eviction of PRC1 from chromatin. Nat. Genet. *49*, 282–288. 10.1038/ng.3735.

161. Weber, C.M., Hafner, A., Kirkland, J.G., Braun, S.M.G., Stanton, B.Z., Boettiger, A.N., and Crabtree, G.R. (2021). mSWI/SNF promotes Polycomb repression both directly and through genome-wide redistribution. Nat. Struct. Mol. Biol. *28*, 501–511. 10.1038/s41594-021-00604-7.

162. Pace, L., Goudot, C., Zueva, E., Gueguen, P., Burgdorf, N., Waterfall, J.J., Quivy, J.-P., Almouzni, G., and Amigorena, S. (2018). The epigenetic control of stemness in CD8+ T cell fate commitment. Science *359*, 177–186. 10.1126/science.aah6499.

163. Oestreich, K.J., and Weinmann, A.S. (2012). T-bet employs diverse regulatory mechanisms to repress transcription. Trends Immunol. *33*, 78–83. 10.1016/j.it.2011.10.005.

164. Omilusik, K.D., Best, J.A., Yu, B., Goossens, S., Weidemann, A., Nguyen, J.V., Seuntjens, E., Stryjewska, A., Zweier, C., Roychoudhuri, R., et al. (2015).

Transcriptional repressor ZEB2 promotes terminal differentiation of CD8+ effector and memory T cell populations during infection. J. Exp. Med. *212*, 2027–2039. 10.1084/jem.20150194.

165. Rutishauser, R.L., Martins, G.A., Kalachikov, S., Chandele, A., Parish, I.A., Meffre, E., Jacob, J., Calame, K., and Kaech, S.M. (2009). Transcriptional repressor Blimp-1 promotes CD8(+) T cell terminal differentiation and represses the acquisition of central memory T cell properties. Immunity *31*, 296–308. 10.1016/j.immuni.2009.05.014.

166. Iurlaro, M., Stadler, M.B., Masoni, F., Jagani, Z., Galli, G.G., and Schübeler, D. (2021). Mammalian SWI/SNF continuously restores local accessibility to chromatin. Nat. Genet. *53*, 279–287. 10.1038/s41588-020-00768-w.

167. Schick, S., Grosche, S., Kohl, K.E., Drpic, D., Jaeger, M.G., Marella, N.C., Imrichova, H., Lin, J.-M.G., Hofstätter, G., Schuster, M., et al. (2021). Acute BAF perturbation causes immediate changes in chromatin accessibility. Nat. Genet. *53*, 269–278. 10.1038/s41588-021-00777-3.

168. Zhang, N., and Bevan, M.J. (2013). Transforming growth factor-β signaling controls the formation and maintenance of gut-resident memory T cells by regulating migration and retention. Immunity *39*, 687–696. 10.1016/j.immuni.2013.08.019.

169. Schenkel, J.M., and Masopust, D. (2014). Tissue-Resident Memory T Cells. Immunity *41*, 886–897. 10.1016/j.immuni.2014.12.007.

170. Amsen, D., van Gisbergen, K.P.J.M., Hombrink, P., and van Lier, R.A.W. (2018). Tissue-resident memory T cells at the center of immunity to solid tumors. Nat. Immunol. *19*, 538–546. 10.1038/s41590-018-0114-2.

171. Okła, K., Farber, D.L., and Zou, W. (2021). Tissue-resident memory T cells in tumor immunity and immunotherapy. J. Exp. Med. *218*, e20201605. 10.1084/jem.20201605.

172. Long, L., Wei, J., Lim, S.A., Raynor, J.L., Shi, H., Connelly, J.P., Wang, H., Guy, C., Xie, B., Chapman, N.M., et al. (2021). CRISPR screens unveil signal hubs for nutrient licensing of T cell immunity. Nature *600*, 308–313. 10.1038/s41586-021-04109-7.

173. Loo, C.-S., Gatchalian, J., Liang, Y., Leblanc, M., Xie, M., Ho, J., Venkatraghavan, B., Hargreaves, D.C., and Zheng, Y. (2020). A Genome-wide CRISPR Screen Reveals a Role for the Non-canonical Nucleosome-Remodeling BAF Complex in Foxp3 Expression and Regulatory T Cell Function. Immunity *53*, 143-157.e8. 10.1016/j.immuni.2020.06.011.

174. Corradin, O., and Scacheri, P.C. (2014). Enhancer variants: evaluating functions in common disease. Genome Med. *6*, 85. 10.1186/s13073-014-0085-3.

175. WANG, X., NAGL, N.G., JR, WILSKER, D., VAN SCOY, M., PACCHIONE, S., YACIUK, P., DALLAS, P.B., and MORAN, E. (2004). Two related ARID family proteins are alternative subunits of human SWI/SNF complexes. Biochem. J. *383*, 319–325. 10.1042/BJ20040524.

176. Wu, J.N., and Roberts, C.W.M. (2013). ARID1A Mutations in Cancer: Another Epigenetic Tumor Suppressor? Cancer Discov. *3*, 35–43. 10.1158/2159-8290.CD-12-0361.

177. Heng, T.S.P., Painter, M.W., and Immunological Genome Project Consortium (2008). The Immunological Genome Project: networks of gene expression in immune cells. Nat. Immunol. *9*, 1091–1094. 10.1038/ni1008-1091.

178. van der Sluijs, P.J., Jansen, S., Vergano, S.A., Adachi-Fukuda, M., Alanay, Y., AlKindy, A., Baban, A., Bayat, A., Beck-Wödl, S., Berry, K., et al. (2019). The ARID1B spectrum in 143 patients: from nonsyndromic intellectual disability to Coffin–Siris syndrome. Genet. Med. *21*, 1295–1307. 10.1038/s41436-018-0330-z.

179. Moffat, J.J., Jung, E.-M., Ka, M., Jeon, B.T., Lee, H., and Kim, W.-Y. (2021). Differential roles of ARID1B in excitatory and inhibitory neural progenitors in the developing cortex. Sci. Rep. *11*, 3856. 10.1038/s41598-021-82974-y.

180. Pagliaroli, L., Porazzi, P., Curtis, A.T., Scopa, C., Mikkers, H.M.M., Freund, C., Daxinger, L., Deliard, S., Welsh, S.A., Offley, S., et al. (2021). Inability to switch from ARID1A-BAF to ARID1B-BAF impairs exit from pluripotency and commitment towards neural crest formation in ARID1B-related neurodevelopmental disorders. Nat. Commun. *12*, 6469. 10.1038/s41467-021-26810-x.

181. Madan, V., Shyamsunder, P., Dakle, P., Teoh, W.W., Han, L., Cao, Z., Mohd Nordin, H., Jizhong, S., Mr, Shuizhou, Y., Hossain, M.Z., et al. (2023). Dissecting the role of SWI/SNF component ARID1B in steady state hematopoiesis. Blood Adv., bloodadvances.2023009946. 10.1182/bloodadvances.2023009946.

182. Schick, S., Rendeiro, A.F., Runggatscher, K., Ringler, A., Boidol, B., Hinkel, M., Májek, P., Vulliard, L., Penz, T., Parapatics, K., et al. (2019). Systematic characterization of BAF mutations provides insights into intracomplex synthetic lethalities in human cancers. Nat. Genet. *51*, 1399–1410. 10.1038/s41588-019-0477-9.

183. Wayne, N.L., Duarte-Vogel, S., Kraemer, S., and Rager, J.D. (2019). Exposure assessment of laboratory workers to hazardous waste from mice treated with tamoxifen and bromodeoxyuridine. J. Chem. Health Saf. *26*, 2–8. 10.1016/j.jchas.2018.08.003.